Gas Turbine Power Generators
Innovative Adaptive Sliding Mode Load Controller

Alessandro Palmieri

Electrical, Electronic, Telecommunications Engineering and Naval Architecture Departement

University of Genoa

A thesis submitted for the degree of

Doctor of Philosophy

Genoa 2021

Abstract

This thesis deals with the design of an innovative load controller for heavy-duty gas turbine power generators and with its practical implementation on real industrial power plants. A robust controller based on the Sliding Mode control technique is designed, in order to improve the performance of the gas turbine system with respect to the traditional Proportional-Integral-Derivative based regulation currently employed. As a matter of fact, such regulation encounters many difficulties when the system operates in off-design conditions, which is the most frequent situation, leading to a deterioration of the gas turbine performance. This work is developed in collaboration with Ansaldo Energia S.p.A., which is one of the most important heavy-duty gas turbines manufacturing company in the world. The interaction with the industrial partner represents one of the key points of this thesis since the proposed controller could be implemented on real industrial microprocessors and it was possible to validate its performance in a Real Time Simulation environment in the Ansaldo Energia R&D laboratories. The controller validation, performed in a Hardware-In-the-Loop set-up, showed highly satisfactory results and important improvements in comparison with the traditional regulation of the GT power generator.

Contents

1. Introduction

The power generation industry is today a patchwork of many diverse energy sources, each one exploiting different physical phenomena to generate electricity [1]. The variety of available energy sources has allowed to increase the global power generation efficiency, above all, thanks to Renewable Energy Sources (RES), which has envisaged an extremely rapid growth in the last two decades [2, 3]. However, the aggressive penetration of RES has deeply changed the electrical system operating mode, giving rise to significant challenges [4, 5]. One of the main problems is given by the stochastic fluctuation of the electrical power generated by RES, which has to be compensated in order to preserve the electrical system stability, but also the power generation reduced inertia [6] makes the entire system more vulnerable to contingency such as faults. Different solutions and different technologies are employed to solve these still open problems. In particular, Gas Turbines (GTs), being dispatchable and able to regulate power faster than any other conventional energy source, represent a valid tool in this scenario. What makes interesting these components is also their wide scalability range and the possibility of being installed in hybrid power plants, such as conventional combined-cycle (steam power plants) or more innovative configurations (fuel cells) [7]. In this situation it appears that improving the performance of GT power generators is a matter of vital importance in order to satisfactorily meet the new and more stringent electrical system requirements. However, reducing the power generation response time for heavy duty GTs (given their high Combustion Chamber Temperature (CCT)) may lead to strongly undesired consequences. Indeed, unwanted phenomena may arise in the combustion chamber (CC), deriving from CCT high gradients, resulting in a lifetime reduction of the GT itself (high CCT peaks, humming [8] etc.). In addition, CCT measurement of heavy-duty GTs is an impossible task to perform (no measuring sensors are nowadays technologically able to withstand the extreme physical conditions in the CC), therefore, no real-time logics can be designed to protect the machine. The current common practice, far from being optimal, is to monitor the exhaust gas temperature (EGT), which is strongly related to the CCT,

and take protecting actions (reducing the fuel in) as soon as an EGT threshold value is reached. However, such logic being based on the EGT measurement, which suffers from a time-delay whose time constant is roughly about some seconds for technical reasons, is highly inefficient. As a matter of fact, this rather long time-delay filters rapid CCT dynamics and spikes, making this protection logic not particularly effective and causing a de-rating effect on the generated power dynamics due to a drastic fuel reduction.

The controllers employed nowadays on GTs are mainly Proportional Integral Derivative (PID) based. As well known, such controllers can be efficiently designed when linear systems are concerned, while they determine low dynamic performance in case of nonlinear systems. Heavy duty GTs being highly nonlinear systems characterized by strongly coupled dynamics, represent a challenging task for these linear controllers, furthermore, a strong dynamic de-rating effect is imposed by the external protection loop described above [9]. Thus, it seems clear that the operation of GTs must be dynamically improved in order to achieve the fastest power response and avoiding any CCT peaks at the same time.

Recently some authors focused on the definition of more advanced controllers for GTs. A H_∞ robust controller is designed in [10] for a heavy-duty GT and compared to the performance provided by a model predictive control application developed in [11], while a neuro-fuzzy scheme is proposed in [12] for a GT in a biomass-based electric power plant. However, the works just mentioned rely all on the well-known linear GT model proposed by Rowen [13], which cannot accurately represents the strong nonlinear dynamic behaviours of the real system. A nonlinear GT model (i.e. a more realistic model) is rarely considered for the control system design, especially as far as heavy-duty GTs are concerned, giving rise to rather simplified controllers in general not able to meet the desired performance. In addition, some approaches focus on the speed regulation such as [14], however GTs installed in large-scale electrical grids are bound to follow a desired power profile which is generated by an external controller dedicated to the grid frequency regulation and economic dispatch.

This thesis wants to represent the continuation and conclusion of a project begun with my Master thesis and developed in collaboration with Ansaldo Energia S.P.A., which is one of the most important heavy-duty GT manufacturing company in the world. The figure of the industrial partner represents one of the key points of this thesis, indeed the work could assume a significant industrial relevance, on one hand thanks to a constant interaction between us and the Ansaldo Energia engineers, and on the other hand because it comes directly from a need of the industrial world. In

this view, this work aims at establishing a solid basis for the design of an innovative load controller successfully employable on real GT applications. To this end, a robust controller must be designed and, among others, we focused on the Sliding Mode control theory, which is one of the most powerful control technique in terms of both reliability and flexibility [15]. In particular, an advanced version of the first-order SM theory is studied, namely the Adaptive Sliding Mode (ASM) control approach is employed [16]. The ASM technique differs from the traditional one of [17] in the calculation of the uncertainties compensating terms k. In particular, while they are derived through a complex study of the system functions upper bounds in the latter case, they are obtained by means of dynamic adaptive laws in the former one. Then, no knowledge about the entity of the uncertainties is necessary in the ASM case, because k can independently adapt itself to the current system conditions. Therefore, the ASM control appears much more powerful compared to the classical SM in terms of both performance (i.e. no overestimation of k occurs) and implementation simplicity (only a simple adaptive law has to be implemented instead of a combination of complex state-dependent bounds).

On balance, three different steps characterize this thesis project, namely: *(i)* an in-depth study of the ASM control theory and of the GT system model, which was started in the Master thesis and gave rise to a publication on the *IEEE Transactions on Energy Conversion* [18]; *(ii)* the design of a model based ASM controller and its application to a realistic GT model in a Matlab&Simulink simulation environment; *(iii)* implementation of the proposed controller on real industrial microprocessors and its validation in a real-time simulation environment. This last part of the work could not have been possible without the parternship of the company, which made its R&D laboratories available to perform the tests. In particular, the designed controller was implemented on real industrial controllers ABB Symphony Plus HPC800, which are the same systems installed in real plants, and interfaced with a very accurate model of the GT AE94.3A [19] running on a real-time machine.

The final results shown in this thesis are publicated on the Elsevier journal *Energy* in [20].

2. Adaptive Sliding Mode Control Theory

As mentioned in the Introduction, the ASM technique is an improvement of the classical SM control theory, in particular, in this thesis, the Slotine approach described in [17] is taken as reference. In this chapter, firstly such theory is described reporting the most significant concepts the technique is based on, then its adaptive version is shown, focusing on the key elements which make it suitable for in field real applications.

2.1 Sliding Control

The SM control is one of the most powerful nonlinear control techniques, characterized by strong robustness to system uncertainties and high reliability. From a control point of view, modeling inaccuracies can be classified into two major categories:

- structured (or parametric) uncertainties;
- unstructured uncertainties (or unmodeled dynamics).

The former refer to a non-exact knowledge of the system parameters values, while the latter concern unmodeled or neglected dyamics during the system modeling. As a matter of fact, when dealing with the control of real systems, both of them are always present and can strongly deteriorate its performance, even leading to the control system failure. Therefore, robust control techniques become more and more attractive on one hand to handle systems parametric uncertainties, on the other hand to design model based controllers relying on simplified and more manageable system models.

In this view, the SM technique is based on the remark that it is much easier to control 1^{st}-order systems (i.e., systems described by 1^{st}-order differential equations), be they nonlinear or uncertain, than it is to control general i^{th}-order systems (i.e., systems described by i^{th}-order differential equations). Accordingly, a notational simplification is introduced, which, in effect, allows n^{th}-order problems to be replaced by

equivalent 1^{st}-order problems. Several control theories derive from the classical SM technique illustrated in [15], [17], [21], [22]. Among others, the Higher Order Sliding Mode (HOSM) theory gained particular importance in the last decades [23]. Indeed, the HOSM techniques aim at solving or at least mitigating the so-called *chattering* phenomenon, which is discussed later in the next sections, by designing suitable control laws [24], [25], [26]. This theory allows the use of different type of algorithms, among which the *super twisting* algorithm is one of the most spread and exploited [27], which is commonly developed together with adaptive control strategies [28], [29].

Please note that from now on the analysis for Single-Input Single-Output systems is reported, then it will be easily extended for Multi-Input Multi-Output systems later.

2.1.1 The Sliding Variable - Definition of the equivalent control problem

Consider the following nonlinear system of the form

$$\begin{cases} x^{(n)} = f(\underline{x}) + g(\underline{x})u \\ y = x \end{cases} \tag{2.1}$$

where $\underline{x} = [x, \dot{x}, \ddot{x}, ..., x^{n-1}]$ is the n-dimensional state vector, y and u are the system scalar output and input respectively, while f and g are scalar functions. Please observe that system (2.1) can then be seen as a perturbed chain of integrators. Let us introduce

$$e = x - x_d \tag{2.2}$$

as the tracking error of system (2.1), where x_d is the state reference. As a matter of fact, the control objective is to steer the tracking error (2.2) to zero, which means leading the state x to its reference x_d in a finite time.

To reduce the n-dimensional control problem to a first order equivalent problem, the sliding variable definition is introduced as follows

$$\sigma = \left(\lambda_2 \frac{d}{dt} + \lambda_1\right)^{n-1} e \tag{2.3}$$

using the notation in [17], while λ_1 and λ_2 are positive constant terms. Now, given the tracking error (2.2) and the sliding variable definition in (2.3), system (2.1) can be transformed in

$$\dot{\sigma} = \frac{d}{dt}\left[\left(\lambda_2 \frac{d}{dt} + \lambda_1\right)^{n-1} (x - x_d)\right] \tag{2.4}$$

By expressing (2.3) through the Newton binomial, (2.4) becomes

$$\dot{\sigma} = \lambda_2^{n-1}(x^{(n)} - x_d^{(n)}) + x_q^{(n)} \tag{2.5}$$

where

$$x_q^{(n)} = \sum_{k=1}^{n} \binom{n}{k} \frac{d^{n-k}e}{dt^{n-k}} \lambda_2^{n-k} \lambda_1^k \tag{2.6}$$

Looking at equation (2.5) and taking into account (2.1), one can observe that $\dot{\sigma}$ directly depends on the control variable u. Focusing on the sliding variable definition in (2.3), it can be noted that the tracking error e and the sliding variable σ are related by a linear dynamics of order $(n-1)$. In particular, their relation can be seen as a $(n-1)$ series of transfer fuctions as follows.

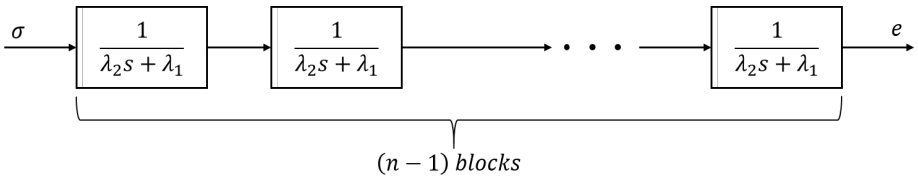

Figure 2.1: Sliding variable and tracking error relation.

Hence, once σ is steered to zero, the tracking error e will be led to zero with a $(n-1)^{th}$ dynamics determined by λ_1 and λ_2.

On balance, the sliding variable definition in (2.3) and its dynamic equation in (2.4) define a 1^{st}-dimensional control problem equivalent to the original n-dimensional one.

2.1.2 Discontinuous Control Law

From the previous subsection, it is clear that the control objective for the equivalent control problem is to steer the sliding variable σ to zero in finite time, so that the tracking error e, which is the control objective of the original problem, will nullify after a transient described by a $(n-1)^{th}$ order dynamics.
Therefore, the control input u must be designed to achieve $\sigma = 0$ in finite time, then one possible solution is [17]:

$$u = u_0 + u_a \tag{2.7}$$

where u_0 is the so-called nominal part of the command law of the form

$$u_0 = \frac{1}{g}\left[x_d^{(n)} - x_q^{(n)} - f\right] \tag{2.8}$$

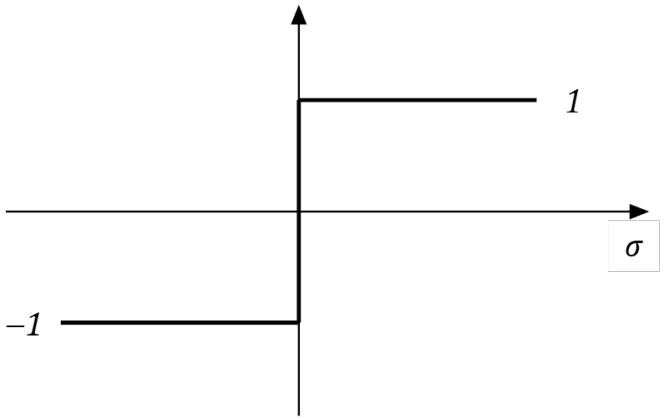

Figure 2.2: Sign function.

while u_a is the adaptive part of the command law, namely, the part able to dominate all the modelling uncertainties, which can be written as

$$u_a = \frac{1}{g}\left[-k\ sgn(\sigma)\right] \tag{2.9}$$

in which $k > 0$ is the SM control gain and $sgn(\sigma)$ is the function illustrated in Fig. 2.2. It is demonstrated that given system (2.1), the tracking error (2.2), the sliding

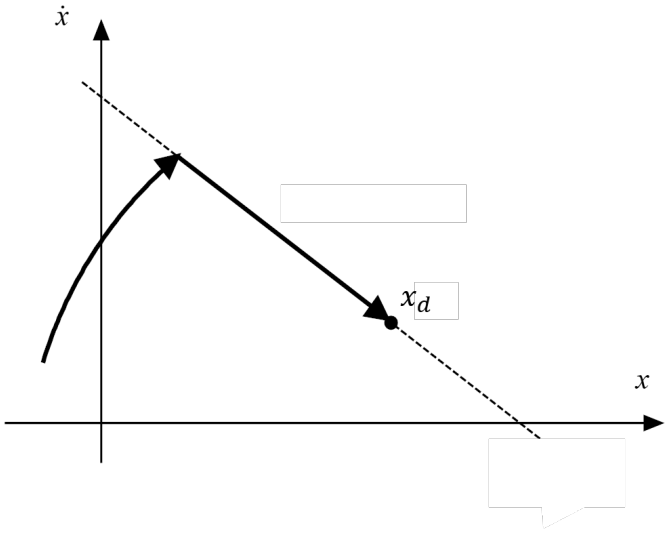

Figure 2.3: System trajectory in sliding mode.

variable definition (2.3) and the control law (2.7), by choosing a suitable value for the gain k, the original control problem is solved and the tracking error e is steered to zero in finite time [15],[17]. In particular, k must be higher enough to make the sliding surface $\sigma = 0$ an invariant set. For clarity's sake, a qualitative graphical illustration

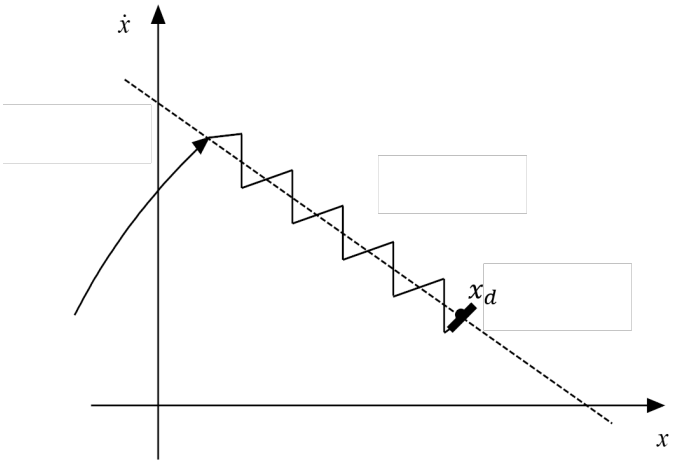

Figure 2.4: Real system trajectory in sliding mode.

of the trajectory of a first order system controlled via a SM approach is shown in Fig. 2.3. Please note that this behaviour is purely theoretical, since it can be achieved only with an infinite control switching frequency. Hence, considering a limited switching frequency, the system behaves as in Fig. 2.4.

This phenomenon is known as *chattering* and it is typical of the SM approaches. The chattering must be mitigated in real applications since it can be disruptive for several systems. This major drawback makes the discontinuous control law (2.7) unappliable for most of real applications.

2.1.3 Continuous Control Law

In this subsection an alternative continuous control law suitable to be applied in real applications is proposed. In particular, the adaptive part (2.9) of the command law (2.8) is modified as follows:

$$u_a = \frac{1}{g}\left[-k\, sat\left(\frac{\sigma}{\phi}\right)\right] \tag{2.10}$$

where ϕ is the halfwidth of some boundary layer surrounding the sliding surface $\sigma = 0$ and $sat(\sigma/\phi)$ is the function reported in Fig. 2.5.
It is clear that for $\phi \to 0$ the $sat(\sigma/\phi)$ function tends to the $sgn(\sigma)$ function, tracing back to the discontiuous control. Intuitively, both the SM gain k and the boundary layer halfwidth ϕ play a role in the chattering alleviation and in particular their ratio k/ϕ. In this case, the SM gain must be higher enough to make the boundary layer an invariant set, namely so that the sliding variable σ is led into the boundary layer and kept inside it indefinetely. with command law (2.10) the convergence is guaranteed

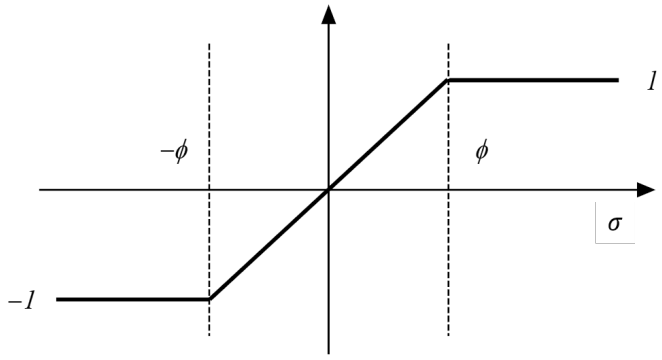

Figure 2.5: Saturation function.

in finite time to the boundary layer, however at the price that the robustness features could be lost.

Using (2.10) instead of (2.9) means that the sliding variable σ is not led to zero anymore, but it is upper bounded by the boundary layer halfwidth ϕ. Therefore, also the tracking error (2.2) cannot be nullify, but it is upper bounded too. Looking at the sliding variable definition (2.3), the upper bound for e can be obtained as

$$|e(t)| \leq \frac{\phi}{\lambda_1^{n-1}} \qquad for\ t \to \infty \tag{2.11}$$

Hence, it is intuitive that a trade-off between the accuracy of the tracking and the dynamic behaviour of the controller must be considered during the design. As a matter of fact, avoiding the chattering phenomenon in real applications is vital for preserving the system lifetime, therefore in some cases the accuracy obtainable with the approach described above might not be enough for the control purpose.

In order to overcome this problem, the following slight modification of the sliding variable definition is proposed

$$\sigma = c_I \int e\, dt + \left(\lambda_2 \frac{d}{dt} + \lambda_1\right)^{n-1} e \tag{2.12}$$

where c_I is a positive constant term. Such sliding variable definition can be trace back in literature as the *Integral Sliding Mode* [30],[31],[32].

With this new sliding variable definition, one can note that a whatever steady-state for σ implies the zeroing of the tracking error e, which is the control objective.

Finally, by applying the continuous command law (2.8),(2.10) with the new sliding variable definition (2.12) and a suitbale value for the SM gain k, the tracking error e is led to zero asymptotically [33].

2.1.4 Adaptive law

In this section an innovative method for the calculation of the SM controller gain is presented. The choice of k is a key point for the controller effectiveness, indeed on one hand its value has to be higher enough to be able to steer the sliding variable inside the boundary layer, but on the other hand it must be kept the lower possible to avoid the insurgency of the chattering phenomenon.

To this end, an automatic adaptive law for the SM controller gain can be introduced [34], [35]. In contrast with other ASM theories [36], [37], the proposed adaptive law is based on an innovative dual boundary layer mechanism, which is defined as follows:

$$\dot{k} = \begin{cases} \omega \dfrac{|\sigma| - \phi}{\phi} & for\ |\sigma| > \phi \\ 0 & for\ \psi \leq |\sigma| \leq \phi \\ -\theta \dfrac{\psi - |\sigma|}{\psi} & for\ |\sigma| < \psi \end{cases} \tag{2.13}$$

where ω and θ are some positive gains to tune the adaptive law time-response, while ψ is an inner boundary layer. For clarity's sake, the adaptive law scheme is depicted in Fig. 2.6. The main logic standing behind this adaptive law is that if the sliding

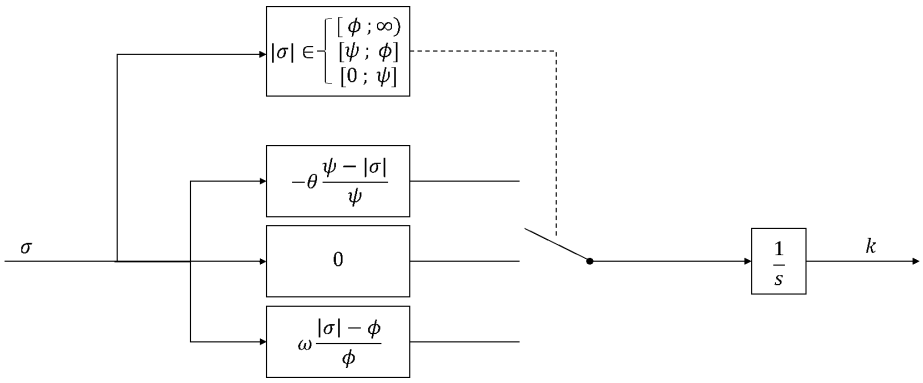

Figure 2.6: Adaptive law scheme.

variable is out of the outer boundary, the controller is not properly compensating the system uncertainties, thus the gain needs to increase. It will increase until the sliding variable enters the outer boundary layer again. At this point, two scenarios may arise: the sliding variable settles between the two boundary layers or it settles inside the inner one. In this latter case it means that the control gain has increased more than necessary, therefore a reduction law is introduced in order to avoid the insurgence of chattering phenomena. Thanks to this algorithm, the controller gains are not

overestimated, with consequently benefits in terms of system stability and chattering phenomena avoidance. A qualitative example of the sliding variable time evolution and of the consequent adaptive gain regulation according to (2.13) is reported in Fig. 2.7.

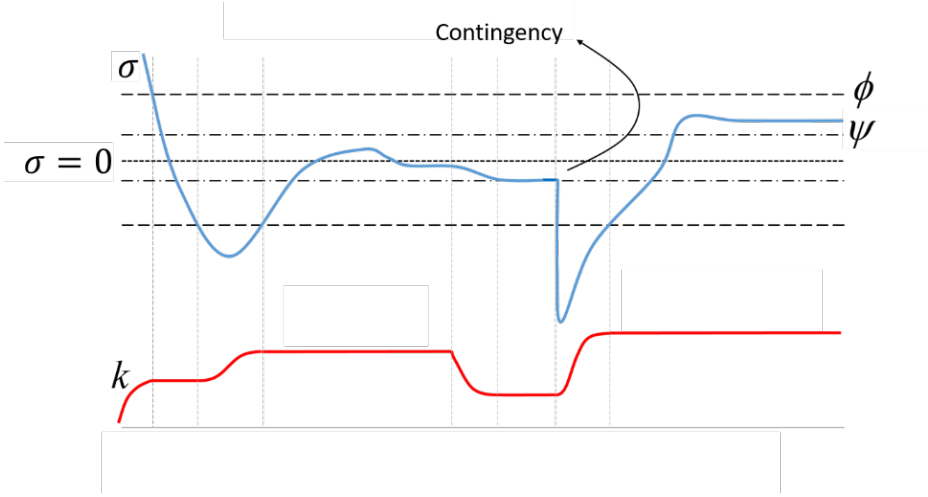

Figure 2.7: Sliding variable and gain behaviours due to the adaptive law regulation.

2.1.5 Extension to Multi-Input-Multi-Output systems

The extension of the proposed control technique from SISO to MIMO systems is straightforward. For the sake of simplicity, an example for a n^{th}-order nonlinear system with only two inputs and two outputs is considered. Then, the following MIMO system is taken into account

$$\begin{bmatrix} x_1^{(r_1)} \\ x_2^{(r_2)} \end{bmatrix} = \begin{bmatrix} f_1(\underline{x}) \\ f_2(\underline{x}) \end{bmatrix} + \begin{bmatrix} b_{11}(\underline{x}) & b_{12}(\underline{x}) \\ b_{21}(\underline{x}) & b_{22}(\underline{x}) \end{bmatrix} \begin{bmatrix} u_1 \\ u_2 \end{bmatrix} \tag{2.14}$$

$$\begin{bmatrix} y_1 \\ y_2 \end{bmatrix} = \begin{bmatrix} x_1 \\ x_2 \end{bmatrix} \tag{2.15}$$

where r_1 and r_2 are the relative degrees of the two outputs with respect to the system inputs, $\underline{x} = [x_1, \dot{x}_1, \ldots, x_1^{(r_1)}, x_2, \dot{x}_2, \ldots, x_2^{(r_2)}]$ is the n-dimensional state vector, y is the 2×1 output vector, u is the 2×1 input vector, while f_1, f_2, b_{11}, b_{12}, b_{21}, b_{22} are scalar functions of the state vector $\underline{x}$.

Then, analogous quantities for the tracking error (2.2) and for the sliding variable (2.12) can be defined for each system output, namely:

$$\begin{cases} e_1 = x_1 - x_{1d} \\ e_2 = x_2 - x_{2d} \end{cases} \tag{2.16}$$

$$\begin{cases} \sigma_1 = c_{I,1} \int e_1 \, dt \; + \left(\lambda_{2,1} \frac{d}{dt} + \lambda_{1,1}\right)^{r_1 - 1} e_1 \\ \sigma_2 = c_{I,2} \int e_2 \, dt \; + \left(\lambda_{2,2} \frac{d}{dt} + \lambda_{1,2}\right)^{r_2 - 1} e_2 \end{cases} \tag{2.17}$$

Also in the MIMO case, a nominal and an adaptive part of the commmand law can be defined, leading to the following control laws:

$$\underline{u} = \underline{u}_0 + \underline{u}_a \tag{2.18}$$

where

$$\underline{u}_0 = \boldsymbol{B}^{-1} \begin{bmatrix} x_{1,d}^{(r_1)} - x_{1,q}^{(r_1)} - f_1 \\ x_{2,d}^{(r_2)} - x_{2,q}^{(r_2)} - f_2 \end{bmatrix} \tag{2.19}$$

$$\underline{u}_a = -\boldsymbol{B}^{-1} \begin{bmatrix} sat\,(\sigma_1/\phi_1) & 0 \\ 0 & sat\,(\sigma_2/\phi_2) \end{bmatrix} \begin{bmatrix} k_1 \\ k_2 \end{bmatrix} \tag{2.20}$$

in which the symbols assume the same meanings as in the SISO case and $\boldsymbol{B}$ is the gain matrix

$$\boldsymbol{B} = \begin{bmatrix} b_{11}(\underline{x}) & b_{12}(\underline{x}) \\ b_{21}(\underline{x}) & b_{22}(\underline{x}) \end{bmatrix} \tag{2.21}$$

which must be an invertible matrix at least in the system domain.

Furthermore, the control gains are obtained by the following adaptive laws.

$$\dot{k}_{1(2)} = \begin{cases} \omega_{1(2)} \dfrac{|\sigma_{1(2)}| - \phi_{1(2)}}{\phi_{1(2)}} & for \; |\sigma_{1(2)}| > \phi_{1(2)} \\ 0 & for \; \psi_{1(2)} \leq |\sigma_{1(2)}| \leq \phi_{1(2)} \\ -\theta_{1(2)} \dfrac{\psi_{1(2)} - |\sigma_{1(2)}|}{\psi_{1(2)}} & for \; |\sigma_{1(2)}| < \psi_{1(2)} \end{cases} \tag{2.22}$$

The example with 2 inputs and 2 outputs shows that 2 sliding controllers must be designed, one per each control channel, while the coupling between the channels is realized by the gain matrix $\boldsymbol{B}$. Therefore, for m inputs and m ouputs, m sliding controllers have to be designed, and the $m \times m$ gain matrix will be the coupling element between them.

3. Gas Turbine System Overview

A schematic representation of a heavy-duty GT is depicted in Fig. 3.1. The machine is composed by three macro components: the compressor, the CC and the turbine. The GT operation can be divided into three phases: *(i)* the Inlet Guide Vanes (IGV) let the air enter the compressor, which lead the pressurised air flow into the CC; *(ii)* the intake valves inject the fuel in the CC for the combustion to happen; *(iii)* the high temperature pressurised fluid expands in the turbine, generating mechanical power at the generator shaft [38]. In a classical combined-cycle configuration, the

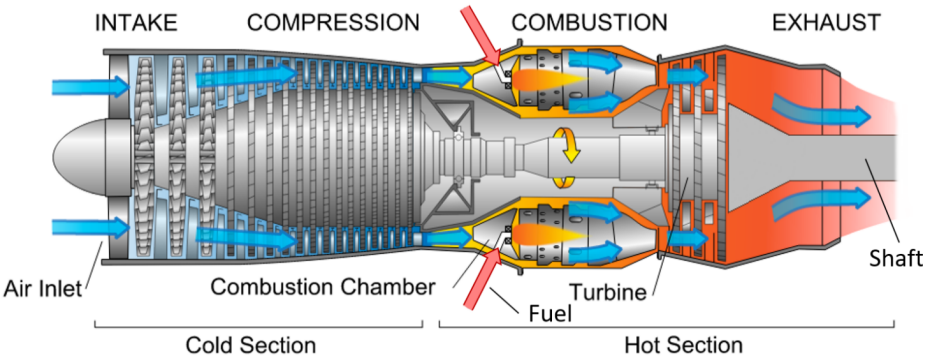

Figure 3.1: Gas turbine system.

exhaust gas exiting the turbine stages are sent to a heat recovery steam generator. From an operational point of view, a heavy-duty GT has two alternative controllers (i.e. the speed control and the load controller operating) working nested in several protection systems. The speed control is of limited interest since it is only used for the machine connection to the grid with not relevant performance requirements. The load controller, object of the present project, is in charge to follow the electric power request provided by external regulating loops (primary, secondary and tertiary regulation) when the system is operating connected to the electricity grid. Moreover, it has also to cope with the control of the EGT, which in general needs to be constant, thus making much harder for the CCT to give rise to unwanted spikes, especially during fast load increase operations.

For clarity's sake, the following table summarizes all the quantities and variables included in the GT mathematical model.

Table 3.1: GT model nomenclature

Symbol	Description	Unit
$\dot{m}_a$	Air, fuel flow	kg/s
$\dot{m}_f$	Fuel flow	kg/s
m_e	Exhaust gas flow	kg/s
V_{cc}	Volume of the combustion chamber	m^3
ρ_{cc}	Air density expressed	kg/m^3
p_{cc}	Combustion chamber pressure	Pa
T_{cc}	Combustion chamber temperature	K
R_e	Exhaust gases constant	J/kgK
c_{pa}	Air specific heat at constant pressure	J/kgK
T_a	Air temperature entering the combustion chamber	K
H_f	Fuel lower heating value	J/kg
H_e	Enthalpy of the exhaust gas at the combustion chamber outlet	J/kg
U	Internal energy of the control volume	J/kg
T_{amb}	Ambient temperature	K
p_{amb}	Ambient pressure	Pa
H_c	Rated adiabatic efficiency of the compressor	-
R_a	Air ideal gas constant	J/kgK
M_{a0}	Rated air flow of the compressor	kg/s
p_{ccN}	Rated pressure of the combustion chamber	Pa
T_{ccN}	Rated temperature at the exit of the combustion chamber	K
$\dot{m}_a^*$	Air requests expressed	kg/s
$\dot{m}_f^*$	Fuel requests expressed	kg/s
K_{igv}	Static gain of the air intake channel	p.u.
K_{at}	Static gains of the fuel intake channel	p.u.
τ_{igv}	Air intake channel equivalent time constant	s
τ_{at}	Fuel intake channel equivalent time constant	s
T_{exh}	Temperature of exhaust gases exiting the turbine	K
η_T	Turbine efficiency	-
T_{exhm}	Measure of the exhaust gases temperature	K
τ_{tc}	Temperature measurement time constant	s
P_{GT}	Power produced by the gas generating unit	W
η_{el}	Mechanical to electrical conversion efficiency	-

3.1 Gas Turbine Mathematical Model

The mathematical model of the GT system used for the controller design is presented in this section. In order to obtain a mathematical model suitable for the ASM

controller design, some simplifying hypothesis are carrried out, namely:

- the CC is considered as a single control volume and its state variables (temperature and pressure) describe the thermodynamic characteristics of the fluid;
- the gas inside the CC is considered to be ideal;
- the actuations of air and fuel are modelled with a linear, first order transfer function;
- the output power is described by an empirical simplified formulation, function of the CC temperature and pressure only.

In the following, the modelling of the CC, of the actuators dynamics and of the system outputs are presented in detail.

3.1.1 Combustion Chamber Modelling

Considering the CC volume, it is possible to write the mass balance equation as

$$\dot{m}_a + \dot{m}_f - \dot{m}_e = V_{cc} \left(\frac{d\rho_{cc}(t)}{dt} \right) \tag{3.1}$$

being $\dot{m}_a$, $\dot{m}_f$ and $\dot{m}_e$ the air, fuel and high temperature exhaust gas flows in kg/s respectively, V_{cc} is the volume of the CC in m^3 and ρ_{cc} is the air density in kg/m^3. Recalling the fundamental law of ideal gases, it is possible to write the air density inside the CC as

$$\rho_{cc}(t) = \frac{p_{cc}(t)}{R_e \, T_{cc}(t)} \tag{3.2}$$

where p_{cc} is the CC pressure in Pa, T_{cc} is the CC temperature in K and R_e is the exhaust gas constant in J/kgK. Differentiating (3.2) with respect to time and considering (3.1) one obtains

$$\dot{m}_a + \dot{m}_f - \dot{m}_e = V_{cc} \left(\frac{1}{R_e \, T_{cc}(t)} \frac{dp_{cc}(t)}{dt} - \frac{p_{cc}(t)}{R_e \, T_{cc}^2(t)} \frac{dT_{cc}(t)}{dt} \right) \tag{3.3}$$

Then, by applying the energy balance equation to the CC one can write

$$\dot{m}_a c_{pa} T_a + \dot{m}_f H_f - \dot{m}_e H_e = \frac{d}{dt} \left(V_{cc} \rho_{cc}(t) U(t) \right) \tag{3.4}$$

where c_{pa} is the air specific heat at constant pressure in J/kgK, T_a is the air temperature entering the CC in K, H_f is the fuel lower heating value in J/kg, H_e is the enthalpy of the exhaust gas at the CC outlet in J/kg and U is the internal energy

of the control volume in J/kg. Under the hypothesis of ideal gas, it is possible to express the internal energy as

$$U(t) = H_e - R_e T_{cc}(t) = (c_{pe} - R_e)\, T_{cc}(t) \tag{3.5}$$

where c_{pe} is the exhaust gas specific heat at constant pressure in J/kgK.

Now, substituting (3.5) in (3.4), and recalling (3.2), one obtains

$$\frac{d}{dt}\left(V_{cc}\,\rho_{cc}(t)U(t)\right) = (c_{pe} - R_e)\, T_{cc}(t) V_{cc} \frac{d\rho_{cc}(t)}{dt} + \frac{dT_{cc}(t)}{dt} \frac{p_{cc}(t) V_{cc}}{R_e T_{cc}(t)} (c_{pe} - R_e) \tag{3.6}$$

From (3.6) and considering (3.1)-(3.4), the differential equation for the CC temperature is obtained

$$\begin{aligned} \frac{dT_{cc}(t)}{dt} = \frac{T_{cc}(t)\, R_e}{V_{cc}\,(c_{pe} - R_e)\, p_{cc}(t)} \{ & [(R_e - c_{pe})\, T_{cc}(t) + c_{pa} T_a]\, \dot{m}_a + \\ & [(R_e - c_{pe})\, T_{cc}(t) + H_f]\, \dot{m}_f - R_e T_{cc}(t) \dot{m}_e \} \end{aligned} \tag{3.7}$$

Then, recalling (3.3) and considering (3.7), one can write the differential equation for the CC pressure as

$$\frac{dp_{cc}(t)}{dt} = \frac{R_e}{V_{cc}\,(c_{pe} - R_e)} (\dot{m}_a c_{pa} T_a + \dot{m}_f H_f - \dot{m}_e c_{pe} T_{cc}(t)) \tag{3.8}$$

To complete the CC modelling, the air temperature T_a and the exhaust gas flow $\dot{m}_e$ have to be defined as functions of the two state variables p_{cc} and T_{cc}. Considering the air compression as an adiabitc process with constant efficiency, the air temperature can be defined

$$T_a(t) = \frac{T_{amb}}{\eta_c} \left[\left(\frac{p_{cc}(t)}{p_{amb}} \right)^{\frac{R_a}{c_{pa}}} + \eta_c - 1 \right] \tag{3.9}$$

being T_{amb} and p_{amb} the ambient temperature in K and pressure in Pa respectively, η_c the rated adiabatic efficiency of the compressor while R_a is the air ideal gas constant in J/kgK. Finally, the exhaust gas flow can be expressed by the following nonlinear relation [39]

$$\dot{m}_e = M_{a0} \frac{\sqrt{T_{ccN}}}{p_{ccN}} \frac{p_{cc}(t)}{\sqrt{T_{cc}(t)}} \tag{3.10}$$

where M_{a0} is the rated air flow of the compressor in kg/s while p_{ccN} and T_{ccN} are the CC rated pressure in Pa and temperature in K.

3.1.2 Air and Fuel Inlet Systems Modelling

Now, the modelling of the air and fuel inlet systems is taken into account. The air flow regulation is performed by the so-called Inlet Guide Vanes (IGV), which can vary the air flow from its rated value to almost the 60% of it. On the other hand, fuel intake is achieved by means of a system of valves which allow producing a uniform distribution of the flame inside the CC. For the sake of simplicity, these two actuation systems are modeled here as first order linear dynamics, namely

$$\begin{cases} \frac{d\dot{m}_a}{dt} = \frac{K_{igv}}{\tau_{igv}}\,\dot{m}_a^* - \frac{1}{\tau_{igv}}\,\dot{m}_a \\ \frac{d\dot{m}_f}{dt} = \frac{K_{at}}{\tau_{at}}\,\dot{m}_f^* - \frac{1}{\tau_{at}}\,\dot{m}_f \end{cases} \tag{3.11}$$

where $\dot{m}_a^*$ and $\dot{m}_f^*$ are the air and fuel requests expressed in kg/s, K_{igv} and K_{at} are the static gains of the two intake channels while τ_{igv} and τ_{at} are the corresponding time constants in s. Even if linear first order dynamics are quite simple, the real fuel flow actuator dynamic behaviour is well represented by the second equation of (3.11), in contrast, IGV dynamics is characterized by a nonlinear behaviour caused by a limit on the maximum speed they can move (limit provided by the motor actuator and by the relevant inertia of the blades). This aspect is neglected here in order to make the system model be manageable during the model based controller design.

3.1.3 Definition of the Gas Turbine System Outputs

According to the control objectives, the electrical power generated and the exhaust gas temperature are defined as system outputs. In particular, as previous mentioned, the power P_{GT} is expressed as function of the two CC state variables:

$$P_{GT} = \eta_{el}\left[\alpha\big(T_{cc}(t)\,p_{cc}(t)\big)^{\beta} + \gamma\right] \tag{3.12}$$

where α, β and γ are constant terms and η_{el} is the electric generator efficiency. Please observe that relation (3.12) was provided by Ansaldo Energia R&D division, and it relies on documented references in literature (see [38]). Then, the temperature of exhaust gases exiting the turbine (T_{ex}) can be calculated referring once again (as for the compressor) to an adiabatic process, namely

$$T_{ex} = T_{cc}(t)\,\eta_T\left[\left(\frac{p_{amb}}{p_{cc}(t)}\right)^{\frac{R_e}{c_{pe}}} + \frac{1}{\eta_T} - 1\right] \tag{3.13}$$

From a practical point of view T_{ex} needs to be measured by means of a temperature sensor. Usually pressure, temperature and power meters dynamics are neglected since

they are characterized by time responses much faster than the dynamic evolution of the system. Nevertheless, this assumption is not valid for the measurement of the air temperature exiting the turbine, since the airflow is characterized by a relevant speed and quite high temperature (almost 580 °C). In this highly stressed environment, it is necessary to use special temperature meters, which are characterized by very slow dynamic behaviours. For this reason it is not possible to neglect the time delay generated by the output temperature measurement, therefore an additional quantity is introduced, namely the T_{exm}, which is the temperature meausurement provided by the slow dynamic sensor. Hence, this quantity represents the second system output, and its differential equation can be written as

$$\frac{dT_{exm}}{dt} = \frac{1}{\tau_{tc}} \left(T_{ex} - T_{exm}\right) \tag{3.14}$$

By putting (3.13) into (3.14), the differential equation for T_{exm} can be expressed as function of the other state variables, namely

$$\frac{dT_{exm}}{dt} = \frac{1}{\tau_{tc}} \left\{ T_{cc}(t)\, \eta_T \left[\left(\frac{p_{amb}}{p_{cc}(t)} \right)^{\frac{R_e}{c_{pe}}} + \frac{1}{\eta_T} - 1 \right] - T_{exm} \right\} \tag{3.15}$$

3.1.4 Final Fifth Order Mathematical Model

On balance, the final 5$^{\text{th}}$ order model in state space form of the GT system can be written as

$$\begin{cases} \dot{\underline{x}} = \underline{f}(\underline{x}) + \boldsymbol{G}(\underline{x})\underline{u} \\ \underline{y} = \underline{h}(\underline{x}) \end{cases} \tag{3.16}$$

where $\underline{x}$ is the 5×1 state vector, $\underline{u}$ is the 2×1 input vector and $\underline{y}$ is the 2×1 output vector, respectively defined as

$$\underline{x} = \left[p_{cc} \;\; T_{cc} \;\; \dot{m}_a \;\; \dot{m}_f \;\; T_{exm} \right]^T \tag{3.17}$$

$$\underline{u} = \left[\dot{m}_a^* \;\; \dot{m}_f^* \right]^T \tag{3.18}$$

$$\underline{y} = \left[P_{GT} \;\; T_{exm} \right]^T \tag{3.19}$$

while $\underline{f}$ is a 5×1 vector field whose components are defined as

$$f_1(\underline{x}) = \frac{R_e}{V_{cc}\left(c_{pe} - R_e\right)} \left\{ x_3 \frac{c_{pa} T_{amb}}{\eta_c} \left[\left(\frac{x_1}{p_{amb}} \right)^{\frac{R_a}{c_{pa}}} + \eta_c - 1 \right] + x_4 H_f - c_{pe} M_{a0} \frac{\sqrt{T_{ccN}}}{p_{ccN}} x_2 \frac{x_1}{\sqrt{x_2}} \right\} \tag{3.20}$$

$$f_2(\underline{x}) = \frac{x_2\, R_e}{V_{cc}\,(c_{pe} - R_e)\, x_1}\Bigg\{\Bigg\{\,(R_e - c_{pe})\, x_2 + c_{pa}\frac{T_{amb}}{\eta_c}\left[\left(\frac{x_1}{p_{amb}}\right)^{\frac{R_a}{c_{pa}}} + \eta_c - 1\right]\Bigg\}x_3 + \left[\,(R_e - c_{pe})\, x_2 + H_f\right]x_4 - R_e x_2 M_{a0}\frac{\sqrt{T_{ccN}}}{p_{ccN}}\frac{x_1}{\sqrt{x_2}}\Bigg\} \quad (3.21)$$

$$f_3(\underline{x}) = -\frac{1}{\tau_{igv}}x_3 \quad (3.22)$$

$$f_4(\underline{x}) = -\frac{1}{\tau_{at}}x_4 \quad (3.23)$$

$$f_5(\underline{x}) = \frac{1}{\tau_{tc}}\left\{x_2\,\eta_T\left[\left(\frac{p_{amb}}{x_1}\right)^{\frac{R_e}{c_{pe}}} + \frac{1}{\eta_T} - 1\right] - x_5\right\} \quad (3.24)$$

$\boldsymbol{G}$ is a 5×2 matrix written as

$$\boldsymbol{G}(\underline{x}) = \left[\underline{g}_1(\underline{x})\;\; \underline{g}_2(\underline{x})\right] = \begin{bmatrix} 0 & 0 \\ 0 & 0 \\ \frac{1}{\tau_{igv}} & 0 \\ 0 & \frac{1}{\tau_{at}} \\ 0 & 0 \end{bmatrix} \quad (3.25)$$

while $\underline{h}$ is a 2×1 vector field expressed as

$$\underline{h}(\underline{x}) = \begin{bmatrix} \eta_{el}\left[\alpha(x_1 x_2)^{\beta} + \gamma\right] \\ x_5 \end{bmatrix} \quad (3.26)$$

The model described above, which will be called "Fifth order GT model" from now on, is used for the design of the first version of the ASM controller which will be shown later. As a general comment, the complexity of the system, in terms of both system functions and system dynamic order, makes the design of the model based controller be rather complicated, especially from an implementation point of view. This aspect will be more clear looking at the controller design procedure, developed in the following chapters. For these reasons, an approximated second order GT system model is presented in the next section, which is obtained by applying some further simplifications to the fifth order model (3.16).

3.1.5 Approximate Second Order System Model

Starting from the fifth order GT model (3.16) some approximations are introduced to make the system model more manageable during the controller design and implementation. In particular, the following aspects are considered:

– the dynamics of the air and fuel intake systems are neglected (i.e. $\dot{m}_a \equiv \dot{m}_a^*$ and $\dot{m}_f \equiv \dot{m}_f^*$);

– the dynamics of the EGT meausurement sensor is neglected (i.e. $T_{ex} \equiv T_{exm}$);

– some approximations in the CC dynamics are introduced, namely

$$\dot{m}_e = M_{a0}\frac{\sqrt{T_{ccN}}}{p_{ccN}}\frac{p_{cc}(t)}{\sqrt{T_{cc}(t)}} \simeq M_{a0}\frac{T_{ccN}}{p_{ccN}}\frac{p_{cc}(t)}{T_{cc}(t)} \tag{3.27}$$

$$R_e T_{cc}\left[H_f - T_{cc}\left(c_{pe} - R_e\right)\right] \simeq R_e T_{cc} H_f \tag{3.28}$$

In conclusion, the following 2$^{\text{nd}}$ order model is derived:

$$\begin{cases} \dot{\underline{\hat{x}}} = \underline{\hat{f}}(\underline{\hat{x}}) + \hat{\boldsymbol{G}}(\underline{\hat{x}})\underline{\hat{u}} \\ \underline{\hat{y}} = \underline{\hat{h}}(\underline{\hat{x}}) \end{cases} \tag{3.29}$$

where $\underline{\hat{x}}$ is the 2×1 state vector, while $\underline{\hat{u}}$ and $\underline{\hat{y}}$ are 2×1 input and output vectors respectively defined as:

$$\underline{\hat{x}} = \left[p_{cc} \;\; T_{cc}\right]^T \tag{3.30}$$

$$\underline{\hat{u}} = \left[\dot{m}_a \;\; \dot{m}_f\right]^T \tag{3.31}$$

$$\underline{\hat{y}} = \left[P_{GT} \;\; T_{ex}\right]^T \tag{3.32}$$

Then, $\underline{\hat{f}}$ is a 2×1 vector field defined as:

$$\underline{\hat{f}}(\underline{\hat{x}}) = \begin{bmatrix} A_1\hat{x}_1 \\ B_1\hat{x}_2 \end{bmatrix} \tag{3.33}$$

and $\hat{\boldsymbol{G}}$ is a 2×2 matrix which can be written as:

$$\hat{\boldsymbol{G}}(\underline{\hat{x}}) = \left[\underline{\hat{g}}_1(\underline{\hat{x}}) \;\; \underline{\hat{g}}_2(\underline{\hat{x}})\right] = \begin{bmatrix} A_2(D_1 + D_2\hat{x}_1^{k_a}) & A_3 \\ \frac{\hat{x}_2}{\hat{x}_1}\left[B_2\hat{x}_2 + A_2(D_1 + D_2\hat{x}_1^{k_a})\right] & A_3\frac{\hat{x}_2}{\hat{x}_1} \end{bmatrix} \tag{3.34}$$

while the 2×1 vector field $\underline{\hat{h}}$ is:

$$\underline{\hat{h}}(\underline{\hat{x}}) = \begin{bmatrix} \eta_{el}[\alpha(x_1x_2)^\beta + \gamma] \\ x_2\left(C_2 + C_3x_1^{-k_e}\right) \end{bmatrix} \tag{3.35}$$

where the constant terms are defined as:

$$\begin{cases} A_1 = -\frac{R_e}{V_{cc}(c_{pe}-R_e)}k_1c_{pe} \\ A_2 = \frac{R_e}{V_{cc}(c_{pe}-R_e)}c_{pa} \\ A_3 = \frac{R_e}{V_{cc}(c_{pe}-R_e)}H_f \end{cases} \tag{3.36}$$

$$\begin{cases} B_1 = -\frac{R_e^2}{V_{cc}(c_{pe}-R_e)} k_1 \\ B_2 = -\frac{R_e}{V_{cc}} \end{cases} \tag{3.37}$$

$$\begin{cases} C_1 = -\eta_T \, k_e \, p_{amb}^{k_e} \\ C_2 = 1 - \eta_T \\ C_3 = \eta_T \, p_{amb}^{k_e} \end{cases} \tag{3.38}$$

$$\begin{cases} D_1 = T_{amb}(1 - \frac{1}{\eta_C}) \\ D_2 = \frac{T_{amb}}{\eta_C \, p_{amb}^{k_a}} \end{cases} \tag{3.39}$$

$$\begin{cases} k_a = \frac{R_a}{c_{pa}} \\ k_e = \frac{R_e}{c_{pe}} \\ k_1 = M_{a0} \frac{T_{ccN}}{p_{ccN}} \end{cases} \tag{3.40}$$

Please note that the values of the parameters appearing both in the 5^{th}-order GT model and in the approximate one are classified data, therefore they will be omitted in this work.

4. Adaptive Sliding Mode controller design

In this chapter the adaptive sliding mode controller design procedure is presented. In particular, two ASM controller versions are developed, the first one is based on the full 5^{th} order GT model, while the second one considers the approximated 2^{nd} order model.

For clarity's sake, they will be referred as *ASM controller full* and *ASM controller approx* respectively.

4.1 Adaptive Sliding Mode controller full design

As previous mentioned, this controller is designed considering the 5^{th} order mathematical model developed for the GT system. Looking at the model (3.16)-(3.26), one can note that a state-space transformation is required to make it suitable for the controller sythesis. In ther words, an input-state linearization procedure is needed to derive the so-called Companion Form (CF) the controller design requires [17].

4.1.1 State transformation

The CF is defined as:

$$y_i^{r_i} = f_{i,CF}(\underline{x}) + \sum_{j=1}^{m} b_{ij}(\underline{x})u_j \quad i = 1, ..., m \tag{4.1}$$

where m is the number of controlled outputs (equal to the number of the inputs), r_i is the dynamic order (or relative degree) of the output y_i, while $f_{i,CF}(\underline{x})$ and $b_{ij}(\underline{x})$ are scalar functions of the state variables.

Let define the 1^{st} order Lie derivative of a scalar function $p : \mathbb{R}^n \to \mathbb{R}$ along the vector field $\underline{q} : \mathbb{R}^n \to \mathbb{R}^n$ as follows [17]:

$$L_q p(z_1, z_2, ..., z_n) = \frac{\partial p}{\partial z_1} q_1 + \frac{\partial p}{\partial z_2} q_2 + ... + \frac{\partial p}{\partial z_n} q_n \tag{4.2}$$

The i$^{\text{th}}$ Lie derivative can be obtained recursively:

$$L_q^i p(z_1, z_2, ..., z_n) = \frac{\partial L_q^{i-1} p}{\partial z_1} q_1 + \frac{\partial L_q^{i-1} p}{\partial z_2} q_2 + ... + \frac{\partial L_q^{i-1} p}{\partial z_n} q_n \tag{4.3}$$

Definitions (4.2), (4.3) allow to define the CF functions for the considered GT model, namely:

$$\begin{aligned} \dot{y}_1 &= L_f h_1(\underline{x}) \\ \ddot{y}_1 &= L_f^2 h_1(\underline{x}) + L_{g_1} L_f h_1(\underline{x}) u_1 + L_{g_2} L_f h_1(\underline{x}) u_2 \end{aligned} \tag{4.4}$$

Focusing on the temperature channel and repeating the same procedure as above, one obtains:

$$\begin{aligned} \dot{y}_2 &= L_f h_2(\underline{x}) \\ \ddot{y}_2 &= L_f^2 h_2(\underline{x}) \\ \dddot{y}_2 &= L_f^3 h_2(\underline{x}) + L_{g_1} L_f^2 h_2(\underline{x}) u_1 + L_{g_2} L_f^2 h_2(\underline{x}) u_2 \end{aligned} \tag{4.5}$$

On balance, the two outputs have relative degree $r_P = 2$ and $r_T = 3$ respectively. In addition, the global relative degree $r = r_P + r_T = 5$ is equal to the dynamic order of the original system, which implies the absence of internal dynamics [17].

Finally, the transformed system can be written as:

$$\begin{bmatrix} \ddot{y}_1 \\ \dddot{y}_2 \end{bmatrix} = \begin{bmatrix} \ddot{P}_{GT} \\ \dddot{T}_{exm} \end{bmatrix} = \begin{bmatrix} f_{1,CF}(\underline{x}) \\ f_{2,CF}(\underline{x}) \end{bmatrix} + \begin{bmatrix} b_{11}(\underline{x}) & b_{12}(\underline{x}) \\ b_{21}(\underline{x}) & b_{22}(\underline{x}) \end{bmatrix} \begin{bmatrix} u_1 \\ u_2 \end{bmatrix} \tag{4.6}$$

where

$$\begin{bmatrix} f_{1,CF}(\underline{x}) \\ f_{2,CF}(\underline{x}) \end{bmatrix} = \begin{bmatrix} L_f^2 h_1(\underline{x}) \\ L_f^3 h_2(\underline{x}) \end{bmatrix} \tag{4.7}$$

and

$$\begin{bmatrix} b_{11}(\underline{x}) & b_{12}(\underline{x}) \\ b_{21}(\underline{x}) & b_{22}(\underline{x}) \end{bmatrix} = \begin{bmatrix} L_{g_1} L_f h_1(\underline{x}) & L_{g_2} L_f h_1(\underline{x}) \\ L_{g_1} L_f^2 h_2(\underline{x}) & L_{g_2} L_f^2 h_2(\underline{x}) \end{bmatrix} \tag{4.8}$$

System (4.6) is now suitable for the controller design. Recalling the sliding variable definition (2.17), the sliding variables for the GT power and EGT control channels can be respectively written as:

$$\begin{aligned} \sigma_P &= c_{I,P} \int e_P \, dt \, + \left(\lambda_{2,P} \frac{d}{dt} + \lambda_{1,P} \right)^{r_P - 1} e_P \\ &= c_{I,P} \int e_P \, dt \, + \lambda_{1,P} \, e_P + \lambda_{2,P} \, \dot{e}_P \end{aligned} \tag{4.9}$$

$$\begin{aligned} \sigma_T &= c_{I,T} \int e_T \, dt \, + \left(\lambda_{2,T} \frac{d}{dt} + \lambda_{1,T} \right)^{r_T - 1} e_T \\ &= c_{I,T} \int e_T \, dt \, + \lambda_{1,T}^2 \, e_T + 2 \lambda_{1,T} \lambda_{2,T} \, \dot{e}_T + \lambda_{2,T}^2 \, \ddot{e}_T \end{aligned} \tag{4.10}$$

where $e_P = y_1 - y_{1,d}$ and $e_T = y_2 - y_{2,d}$ are the tracking errors of the two control channels, while $y_{1,d}$ and $y_{2,d}$ are the reference signals for the two controlled variables. Then, considering the command laws defined for MIMO systems in (2.18)-(2.22), the following control laws are obtained:

$$\begin{bmatrix} u_1 \\ u_2 \end{bmatrix} = \begin{bmatrix} \dot{m}_a^* \\ \dot{m}_f^* \end{bmatrix} = \begin{bmatrix} u_{0,1} \\ u_{0,2} \end{bmatrix} + \begin{bmatrix} u_{a,1} \\ u_{a,2} \end{bmatrix} \tag{4.11}$$

where

$$\begin{bmatrix} u_{0,1} \\ u_{0,2} \end{bmatrix} = \begin{bmatrix} L_{g_1} L_f h_1(\underline{x}) & L_{g_2} L_f h_1(\underline{x}) \\ L_{g_1} L_f^2 h_2(\underline{x}) & L_{g_2} L_f^2 h_2(\underline{x}) \end{bmatrix}^{-1} \begin{bmatrix} \lambda_{1,P}\, \dot{e}_P + \lambda_{2,P}\, \ddot{y}_{1,d} - L_f^2 h_1(\hat{\underline{x}}) \\ \lambda_{1,T}^2\, \dot{e}_T + 2\lambda_{1,T}\lambda_{2,T}\, \ddot{e}_T + \lambda_{2,T}^2\, \dddot{y}_{2,d} - L_f^3 h_2(\hat{\underline{x}}) \end{bmatrix} \tag{4.12}$$

$$\begin{bmatrix} u_{a,1} \\ u_{a,2} \end{bmatrix} = \begin{bmatrix} L_{g_1} L_f h_1(\underline{x}) & L_{g_2} L_f h_1(\underline{x}) \\ L_{g_1} L_f^2 h_2(\underline{x}) & L_{g_2} L_f^2 h_2(\underline{x}) \end{bmatrix}^{-1} \begin{bmatrix} sat\,(\sigma_P/\phi_P) & 0 \\ 0 & sat\,(\sigma_T/\phi_T) \end{bmatrix} \begin{bmatrix} k_P \\ k_T \end{bmatrix} \tag{4.13}$$

and

$$\dot{k}_{P(T)} = \begin{cases} \omega_{P(T)} \dfrac{|\sigma_{P(T)}| - \phi_{P(T)}}{\phi_{P(T)}} & for\ |\sigma_{P(T)}| > \phi_{P(T)} \\ 0 & for\ \psi_{P(T)} \le |\sigma_{P(T)}| \le \phi_{P(T)} \\ -\theta_{P(T)} \dfrac{\psi_{P(T)} - |\sigma_{P(T)}|}{\psi_{P(T)}} & for\ |\sigma_{P(T)}| < \psi_{P(T)} \end{cases} \tag{4.14}$$

The controller proposed above is very accurate from a modelling point of view, however it is clear from the complexity of the functions involved that it is quite expensive from a computational perspective considering the computational capability of industrial controllers. Another aspect to keep in mind is the calculation of the time derivatives of the error signals. As a matter of fact they can be obtained by means of robust differentiators, e.g. Levant differentiators [40] or Super Twisting Algorithm based differentiators [41], however obtaining very accurate results is not always possible.

In addition, please note that these control laws need all the state measurements to calculate the Lie functions, but they are not fully available unfortunately. Indeed, the combustion chamber temperature measurement is not technically obtainable as explained in the previous chapters, then some CCT estimate must be provided. A possible estimate can be derived from the measurements of the CC pressure and the GT power, by inverting the following formula

$$P_{GT} = \eta_{el} \left[\alpha (p_{cc} T_{cc})^{\beta} + \gamma \right] \tag{4.15}$$

one can obtain

$$T_{cc} = \frac{1}{p_{cc}} \left[\frac{P_{GT}/\eta_{el} - \gamma}{\alpha} \right]^{\frac{1}{\beta}} \tag{4.16}$$

It is intuitive that the accuracy of such controller is deteriorated by the approximations and uncertainties introduced by the CCT estimation, which affect almost all the functions involved in the control laws calculation.

These considerations lead to the developing of an alternative controller based on a much simpler GT model with the aim to design more manageable command laws to be implemented in real microprocessors.

4.2 Adaptive Sliding Mode controller approx design

As mentioned above, this controller is based on the approximate 2nd order GT model developed in section 3.1.5. The controller design follows the procedure already presented for the *ASM full* controller in the previous section.

The state transformation applied to system (3.29)-(3.39) leads to the following dynamic system.

$$\begin{bmatrix}\dot{\hat{y}}_1\\ \dot{\hat{y}}_2\end{bmatrix} = \begin{bmatrix}\dot{P}_{GT}\\ \dot{T}_{ex}\end{bmatrix} = \begin{bmatrix}\hat{f}_{1,CF}(\underline{\hat{f}})\\ \hat{f}_{2,CF}(\underline{\hat{x}})\end{bmatrix} + \begin{bmatrix}\hat{b}_{11}(\underline{\hat{x}}) & \hat{b}_{12}(\underline{\hat{x}})\\ \hat{b}_{21}(\underline{\hat{x}}) & \hat{b}_{22}(\underline{\hat{x}})\end{bmatrix}\begin{bmatrix}\hat{u}_1\\ \hat{u}_2\end{bmatrix} \tag{4.17}$$

where

$$\begin{bmatrix}\hat{f}_{1,CF}(\underline{\hat{x}})\\ \hat{f}_{2,CF}(\underline{\hat{x}})\end{bmatrix} = \begin{bmatrix}L_{\hat{f}}\hat{h}_1(\underline{x})\\ L_{\hat{f}}\hat{h}_2(\underline{x})\end{bmatrix} \tag{4.18}$$

and

$$\begin{bmatrix}\hat{b}_{11}(\underline{\hat{x}}) & \hat{b}_{12}(\underline{\hat{x}})\\ \hat{b}_{21}(\underline{\hat{x}}) & \hat{b}_{22}(\underline{\hat{x}})\end{bmatrix} = \begin{bmatrix}L_{\hat{g}_1}\hat{h}_1(\underline{\hat{x}}) & L_{\hat{g}_2}\hat{h}_1(\underline{\hat{x}})\\ L_{\hat{g}_1}\hat{h}_2(\underline{\hat{x}}) & L_{\hat{g}_2}\hat{h}_2(\underline{\hat{x}})\end{bmatrix} \tag{4.19}$$

Then, the sliding variables can be defined as:

$$\hat{\sigma}_P = c_{I,P}\int e_P\,dt\; + e_P \tag{4.20}$$

$$\hat{\sigma}_T = c_{I,T}\int e_T\,dt\; + e_T \tag{4.21}$$

Finally the command laws can be written as follows

$$\begin{bmatrix}\hat{u}_1\\ \hat{u}_2\end{bmatrix} = \begin{bmatrix}\dot{m}_a\\ \dot{m}_f\end{bmatrix} = \begin{bmatrix}\hat{u}_{0,1}\\ \hat{u}_{0,2}\end{bmatrix} + \begin{bmatrix}\hat{u}_{a,1}\\ \hat{u}_{a,2}\end{bmatrix} \tag{4.22}$$

where

$$\begin{bmatrix}\hat{u}_{0,1}\\ \hat{u}_{0,2}\end{bmatrix} = \begin{bmatrix}L_{\hat{g}_1}\hat{h}_1(\underline{\hat{x}}) & L_{\hat{g}_2}\hat{h}_1(\underline{\hat{x}})\\ L_{\hat{g}_1}\hat{h}_2(\underline{\hat{x}}) & L_{\hat{g}_2}\hat{h}_2(\underline{\hat{x}})\end{bmatrix}^{-1}\begin{bmatrix}\dot{y}_{1,d} - L_{\hat{f}}\hat{h}_1(\underline{\hat{x}})\\ \dot{y}_{2,d} - L_{\hat{f}}\hat{h}_2(\underline{\hat{x}})\end{bmatrix} \tag{4.23}$$

$$\begin{bmatrix}\hat{u}_{a,1}\\ \hat{u}_{a,2}\end{bmatrix} = \begin{bmatrix}L_{\hat{g}_1}\hat{h}_1(\underline{\hat{x}}) & L_{\hat{g}_2}\hat{h}_1(\underline{\hat{x}})\\ L_{\hat{g}_1}\hat{h}_2(\underline{\hat{x}}) & L_{\hat{g}_2}\hat{h}_2(\underline{\hat{x}})\end{bmatrix}^{-1}\begin{bmatrix}sat\,(\hat{\sigma}_P/\phi_P) & 0\\ 0 & sat\,(\hat{\sigma}_T/\phi_T)\end{bmatrix}\begin{bmatrix}k_P\\ k_T\end{bmatrix} \tag{4.24}$$

and

$$\dot{k}_{P(T)} = \begin{cases}\omega_{P(T)}\,\dfrac{|\hat{\sigma}_{P(T)}| - \phi_{P(T)}}{\phi_{P(T)}} & for\ |\hat{\sigma}_{P(T)}| > \phi_{P(T)}\\ 0 & for\ \psi_{P(T)} \le |\hat{\sigma}_{P(T)}| \le \phi_{P(T)}\\ -\theta_{P(T)}\,\dfrac{\psi_{P(T)} - |\hat{\sigma}_{P(T)}|}{\psi_{P(T)}} & for\ |\hat{\sigma}_{P(T)}| < \psi_{P(T)}\end{cases} \tag{4.25}$$

4.3 Controller Parameters Tuning

In this section some guidelines for a suitable controller tuning are provided. It is clear that the following considerations have to be considered as general hints, indeed, as a matter of fact, a fine tuning is always needed to achieve the desired system perfomance, depending on the specific application.

The controller parameters are listed in Table 4.1.

Table 4.1: Controller Parameters

Symbol	Description
c_I	Integral coefficient of the sliding variable
λ_1	Proportional coefficient of the sliding variable
λ_2	Derivative coefficient of the sliding variable
ϕ	Boundary layer halfwidth for the sliding variable
ψ	Inner boundary layer halfwidth for the sliding variable
ω	Increasing coefficient of the controller gain
θ	Decreasing coefficient of the controller gain

Two major aspects must be considered during the controller tuning:

- The controller must be powerful enough to achieve the control objectives with desired performance.

- The chattering phenomenon must be avoided.

To this end, a suitable controller tuning must be performed considering the tuning parameters listed above, each one playing a specific role in the system performance. Furthermore, the system channels coupling must be considered, indeed a parameter change related to a channel inevitably influences the behaviour of the others.
The tuning parameters can be divided into two macro groups: the sliding variable parameters and the control gain parameters.

The *control gain parameters* regulate the adaptive law behaviour. The aim of the adaptive law is to adapt the control gain k to keep the sliding variable σ inside the boundary layer ϕ and to avoid chattering phenomenon at the same time. To this end, the control gain is increased and decreased according to the adaptive law (2.13) to keep the sliding variable between ψ and ϕ. In particular, the ω influences the increase rate of k while θ influences its decrease rate. In addition, ω plays an important role during transient, while θ is fundamental in steady state, to keep the control gain value as lower as possible in order to avoid the chattering. However, high values of θ

are not recommended, because k could decrease too much, hence making σ exit the boundary layer ϕ. High values of ω must be avoided as well, to avoid an excessive increase of the control gain, leading to chattering. The adaptation of the gains is necessary for the good operation of the system, indeed in this way they are optimized in every system working points. As final consideration, we can say that k and ϕ play an opposite role as regards the chattering. What is important is their ratio. To put it simple, higher values of k/ϕ mean more chattering and vice versa.

In the following subsection this aspect is deeply investigated by means of a simple example on a 1$^{\text{st}}$-order MIMO nonlinear system. In particular, an analysis developed with the application of the bifurcation theory [42] is reported, showing the effect of the controller parameters on the controlled system behaviour.

4.3.1 Controller Tuning: a Simple Demonstrative Example

This section aims at showing the effect of the controller parameters on the controlled system. For the sake of simplicity's a simple nonlinear system is taken into account, namely the Buck-Boost circuit of Fig. 4.1 is considered. A state space average model

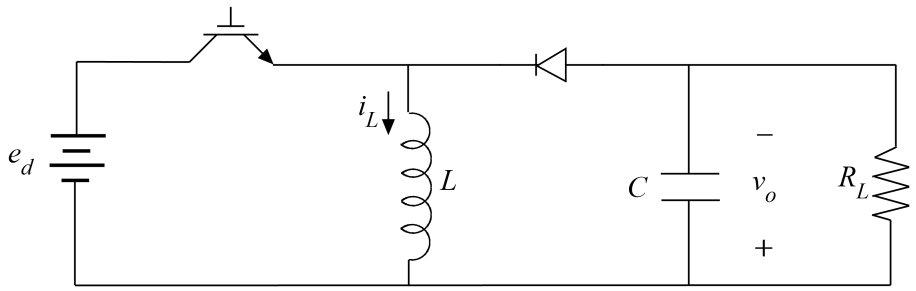

Figure 4.1: Buck-Boost system scheme.

of the BB converter can be written as follows:

$$\begin{bmatrix} \dot{x_1} \\ \dot{x_2} \end{bmatrix} = \begin{bmatrix} \frac{-x_2}{L} \\ \frac{R_L x_1 - x_2}{R_L C} \end{bmatrix} + \begin{bmatrix} \frac{E+x_2}{L} \\ \frac{-x_1}{C} \end{bmatrix} u \tag{4.26}$$

$$y = x_2 \tag{4.27}$$

where $\underline{x} = [x_1, x_2]^T = [i_L, v_o]^T$ is the system state vector in which i_L is the inductor current and v_o is the capacitor voltage, $u = \delta$ is the duty cycle system input, L, R and C are the values of inductance in H, load resistance in Ω and capacitance in F respectively, while E is the DC power supply rated voltage in V.

In order to investigate the roles of the controller parameters on the qualitative behaviour of the system, a bifurcation study can be carried out by means of dedicated tools, such as brute-force methods (purely numerical search of the stationary and oscillatory solutions) or continuation methods (based on the implicit function theorem, also known as Dini's theorem) [43].

The sensitivity analysis is carried out on the BB system (4.26) controlled via the command law (2.10) with the sliding variable (2.12). In order to apply the continuation method, which deals with smooth functions only, a slight approximation to (2.10) is introduced, considering the *tanh* function instead of the *sat* one. By means of the software MATCONT [44], a bifurcation analysis is developed taking into account the control parameters k, ϕ, λ_1 and c_I (please observe that λ_2 does not appear in this case). The study revealed that in the k-ϕ plane, a straight line which divides it into a stable half-plane and an unstable one exists (see Fig. 4.2). In

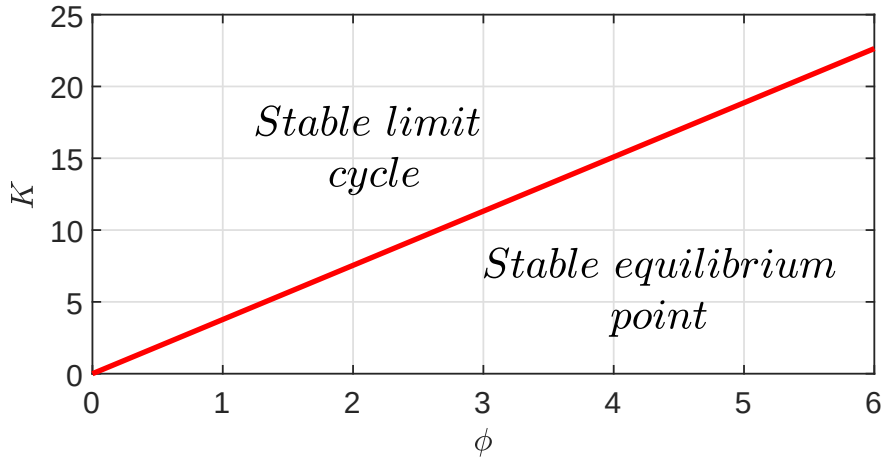

Figure 4.2: Hopf Bifurcation curve in the K-ϕ plane.

particular, the red line in Fig. 4.2 represents Hopf bifurcation points, which can be defined as follows [43].

Definition. The Hopf bifurcation is a local bifurcation in which an equilibrium point of a dynamical system loses stability, as a pair of complex conjugate eigenvalues, of the Jacobian matrix associated to the equilibrium point, crosses the complex plane imaginary axis. As a consequence, a small-amplitude limit cycle branches from the equilibrium point.

This result confirms that the significant information is contained in the ratio k/ϕ. Therefore, the rest of the analysis was developed considering λ_1 and c_I at fixed k/ϕ values, obtaining the results reported in Fig. 4.3. The graphic shows Hopf bifurcation

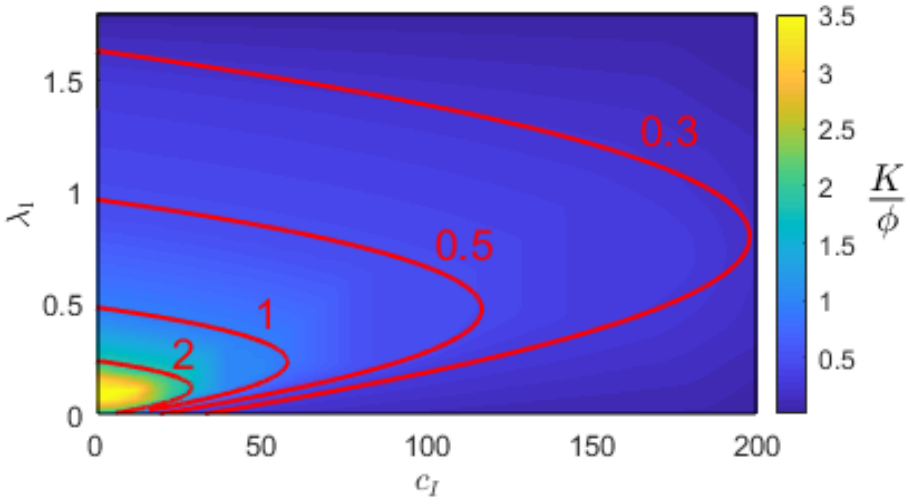

Figure 4.3: Hopf Bifurcation diagram of the Buck-Boost system controlled via the proposed solution.

curves (red lines) in the c_I-λ_1 plane, parameterized by the ratio k/ϕ.

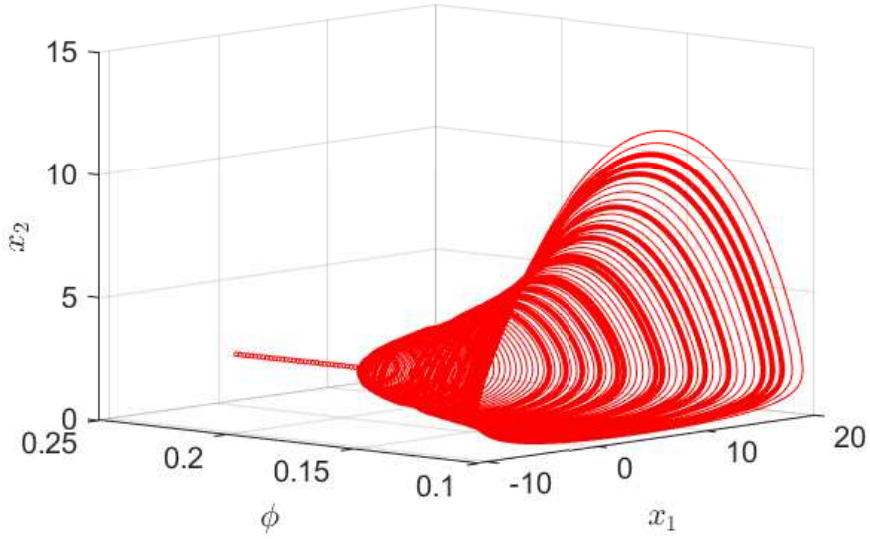

Figure 4.4: Steady-state system trajectories depending on the parameter ϕ.

Looking at Fig. 4.3, it is possible to identify sets of the design parameters to ensure stable equilibrium points, namely the areas enclosed by the red curves.

To prove the validity of the results obtained by the continuation method, the brute-force approach is exploited. Fig. 4.4 and Fig. 4.5 show steady-state solutions of the considered system as functions of the parameter ϕ and c_I respectively, keeping the others constant. As a matter of fact, one can note how increasing ϕ in the former

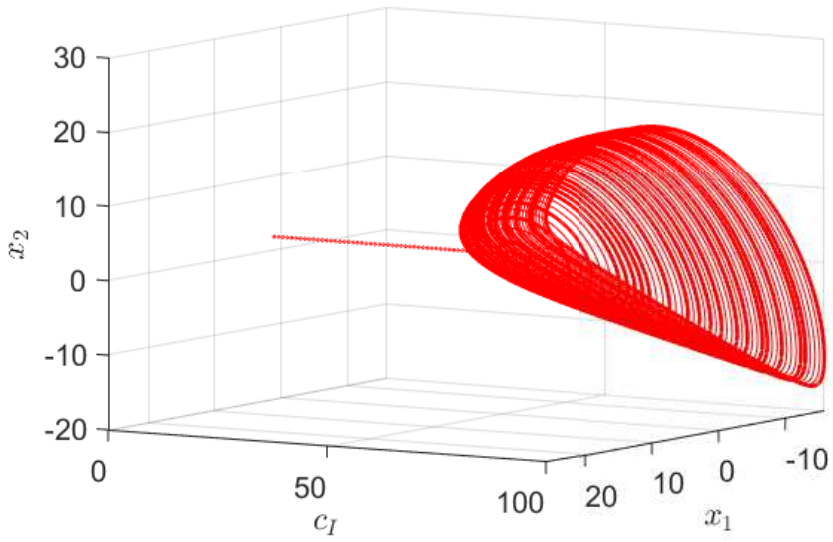

Figure 4.5: Steady-state system trajectories depending on the parameter c_I.

case and decreasing c_I in the latter one, allows to eliminate periodic solutions, in other words avoiding chattering phenomena.

5. Implementation in the Matlab & Simulink simulation environment

The ASM controller designed on the most accurate GT system model was implemented in the Matlab & Simulink simulation environment. The GT model used in these tests refers to the GT AE94.3A owned by Ansaldo Energia, which is a 250 MW rated power gas turbine [19].

Two simulations tests are reported, the first one aims to check the correct application of the control theory and to show the different aspects of the proposed controller, while the second one wants to stress the controller by introducing some realistic uncertainties.

Please observe that, as per the GT model parameters, the ASM controller parameters cannot be divulgated as well, since they are ownership of the company.

The simulations were performed considering the system scheme depicted in Figure 5.1, where P^*_{GT} and T^*_{exm} are the GT power and exhaust gas temperature references respectively.

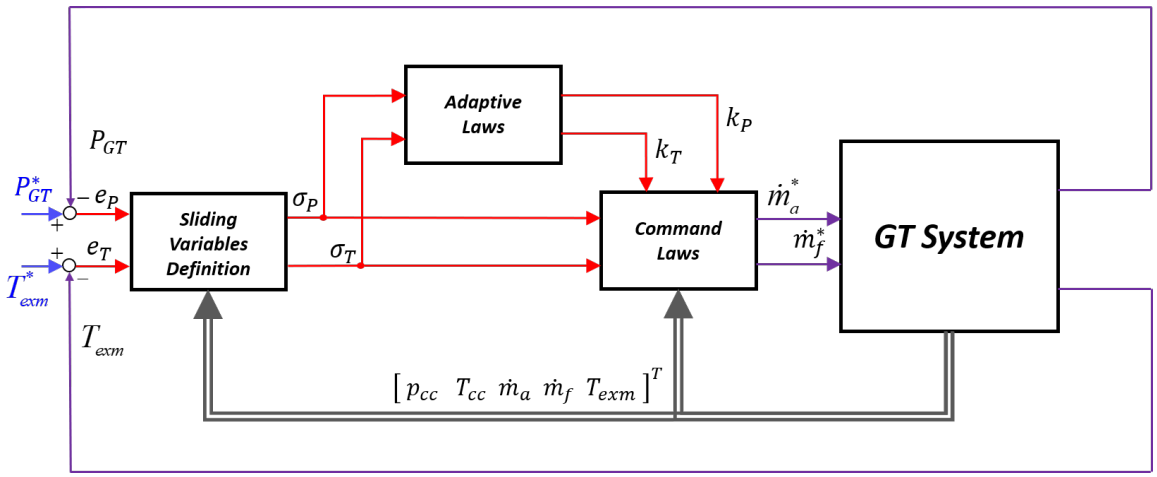

Figure 5.1: Control system scheme.

5.1 Simulation Results

5.1.1 Test 1

In this first test the *ASM controller full* is applied to the 5^{th} order GT model described in section 3.1.4. Therefore, as previous mentioned, this test aims at proving

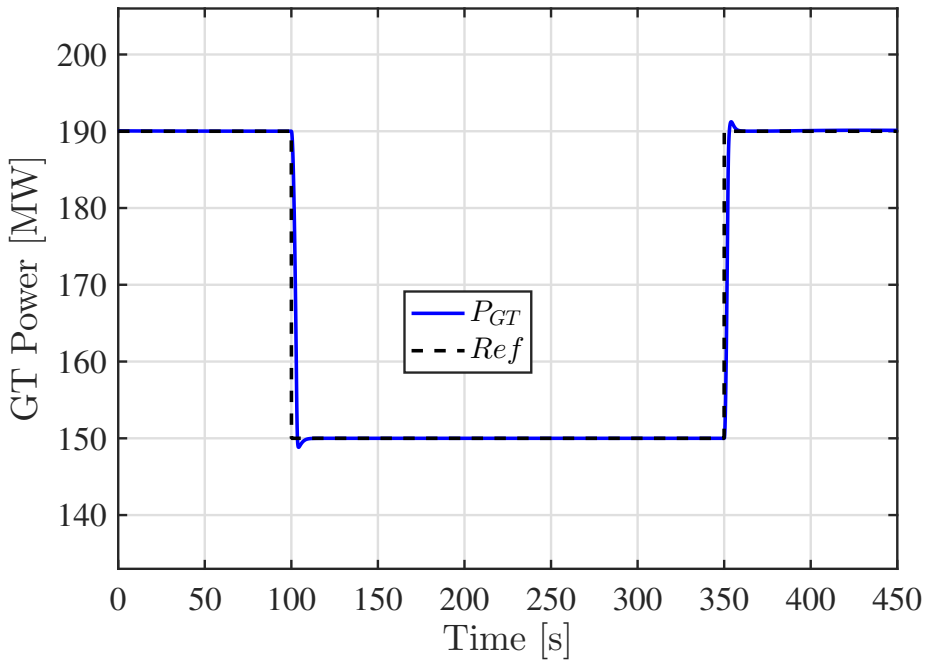

Figure 5.2: GT Power time profile.

the correctness of the employed control technique. A GT power reference change is provided at $t = 100s$ from an initial value of 190 MW to 150 MW, then a step change brings back the GT power reference to 190 MW at $t = 350s$. In Fig. 5.2 the GT power tracking is reported, the ASM controller proves good performance as shown in Fig. 5.3 and 5.4. Please note that such transients are unrealistic, however they are considered here only to check the controller performance under stressful conditions. Despite a very fast response of the power channel, the controller is able to keep the exhaust gas temperature close to the constant reference of 570 °C as shown in Fig. 5.5.

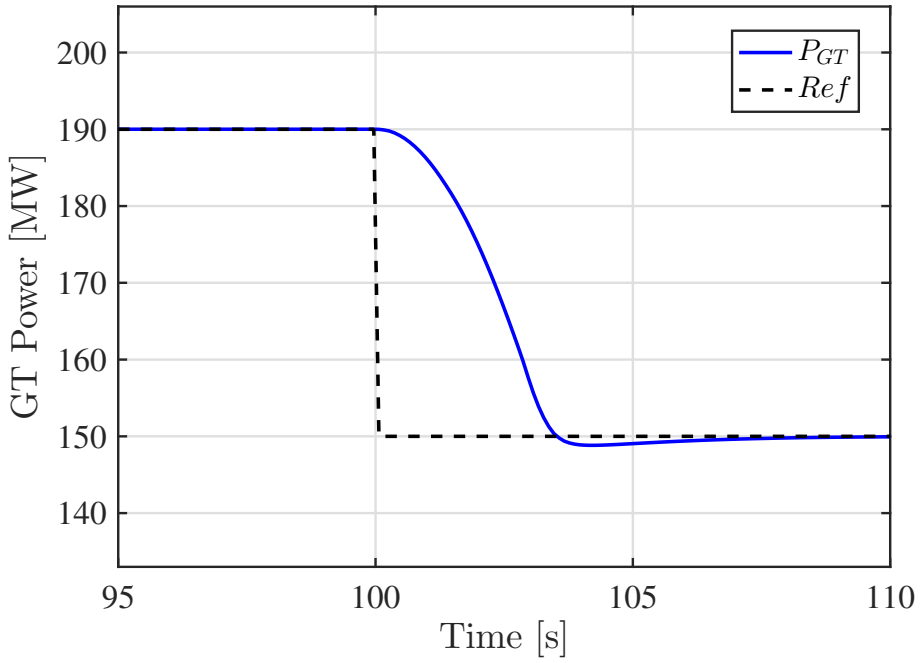

Figure 5.3: GT Power time profile - transient zoom.

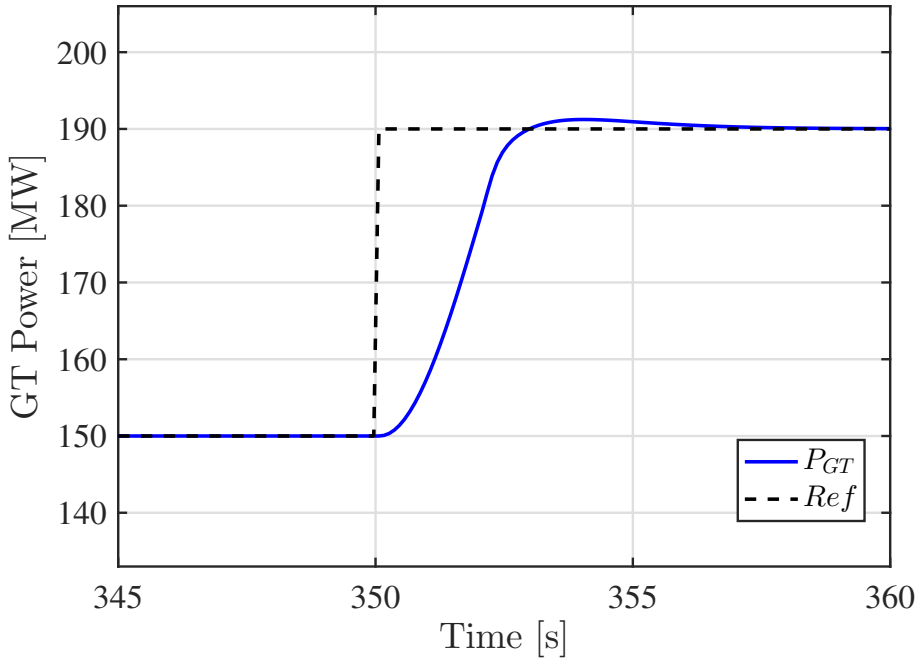

Figure 5.4: GT Power time profile - transient zoom 2.

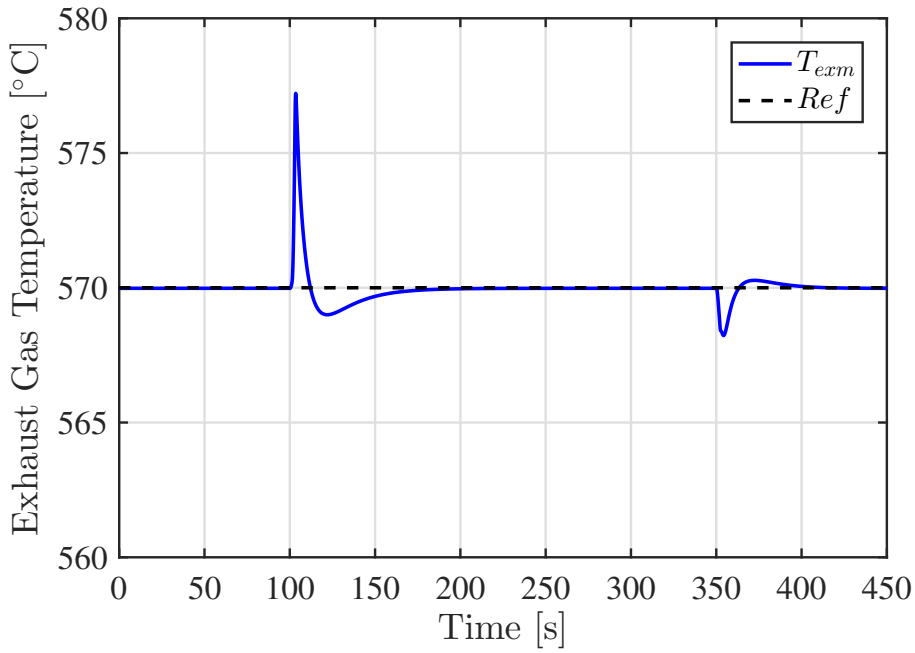

Figure 5.5: Exhaust gas temperature time profile.

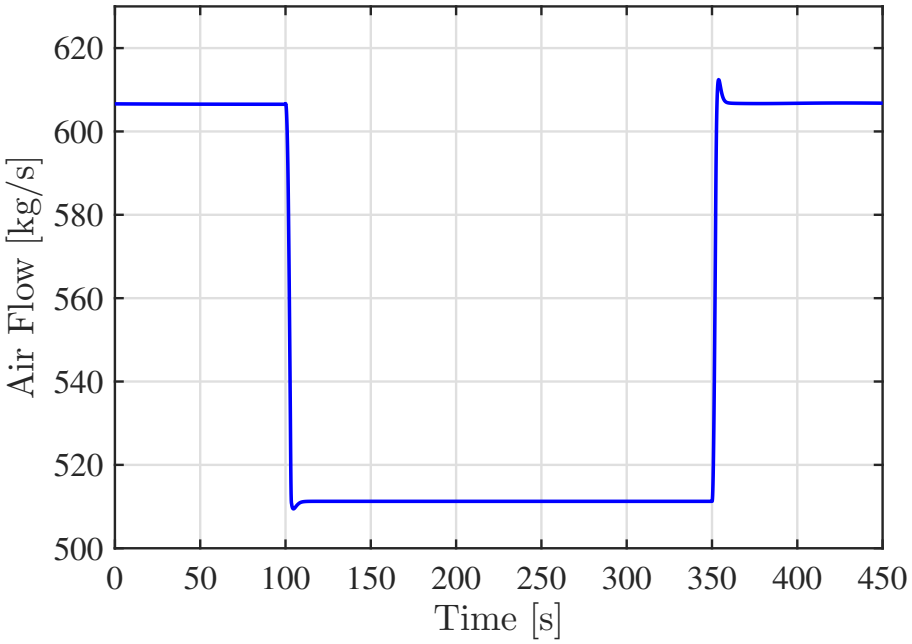

Figure 5.6: Air flow time profile.

Then, the other state variables are reported in Fig.5.6-5.9. In particular, from Fig.5.9 one can note that the combustion chamber temperature profile does not present dangerous spikes.

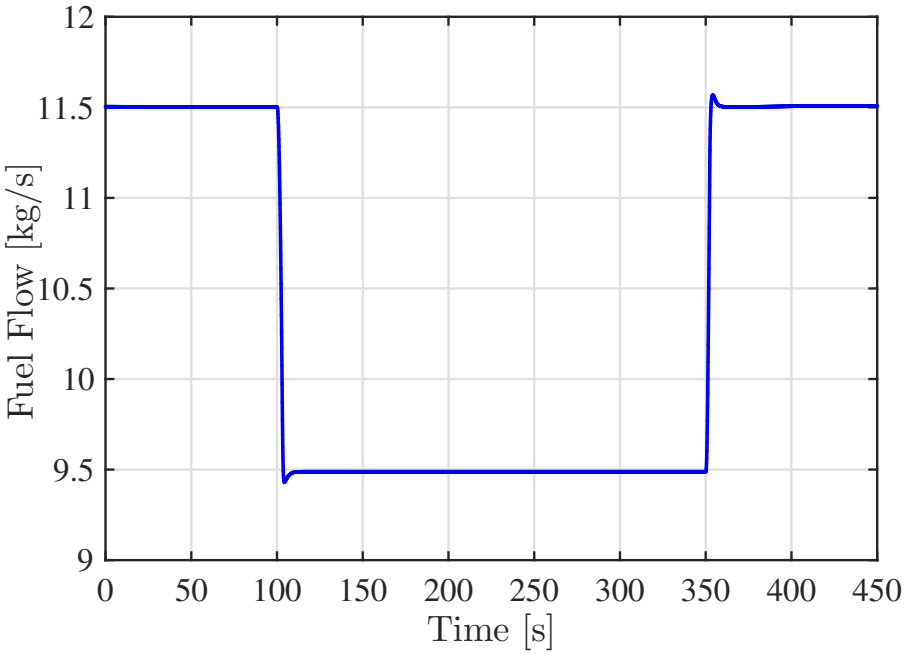

Figure 5.7: Fuel flow time profile.

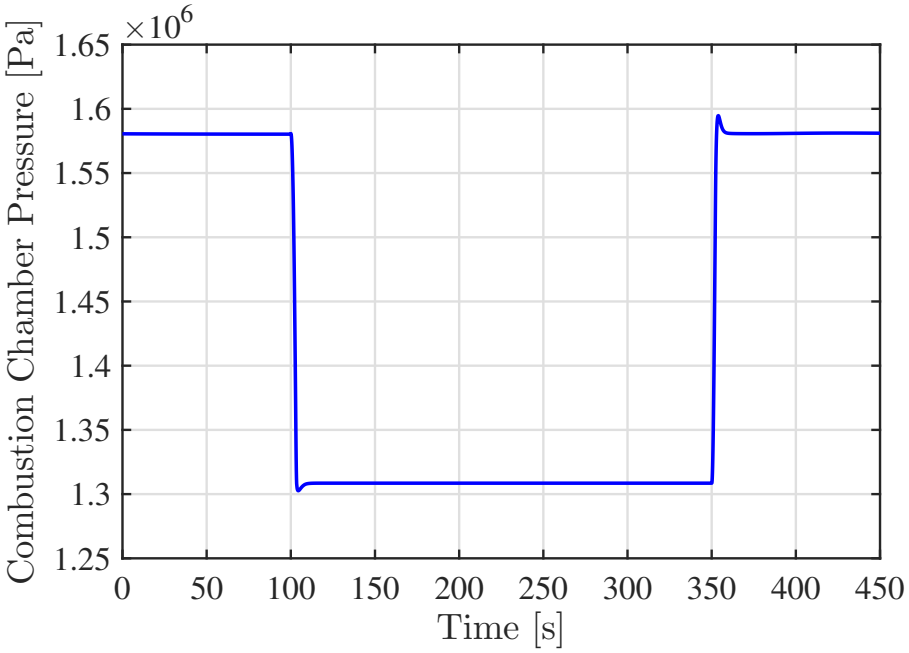

Figure 5.8: Combustion chamber pressure time profile.

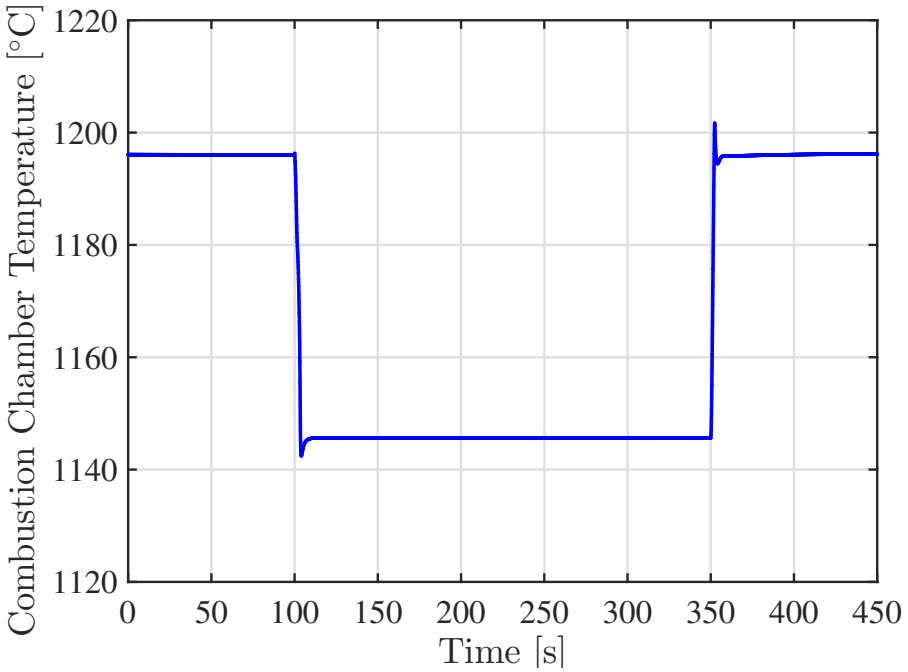

Figure 5.9: Combustion chamber temperature time profile.

This simulation allows to appreciate the controller operations having a look to the graphics related to the controller variables. In Fig.5.10 and Fig.5.11 the sliding variable for the GT power and the related control gain are reported. From this figures,

one can observe the behaviour of these variables regulated by the proposed adaptive laws, which are effectively able to achieve the control objective. In particular, the gain k_P increases once σ_P exits the boundary layer ϕ_P, then it decreases once σ_P is inside the inner boundary layer ψ_P.

Please note, that for practical reasons, a lower bound for the control gains are introduced.

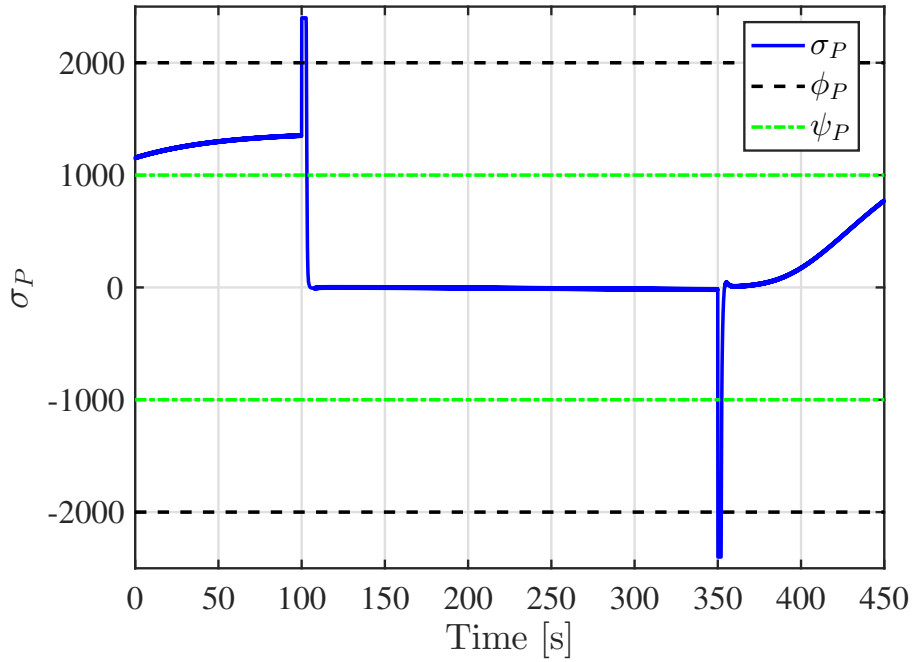

Figure 5.10: Sliding variable for the GT power.

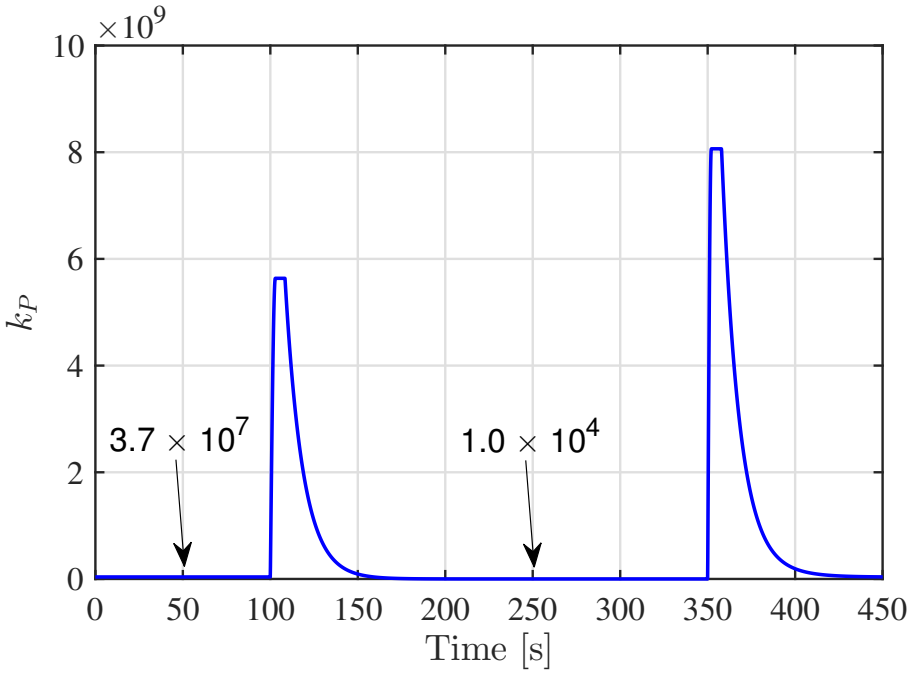

Figure 5.11: ASM gain for the GT power channel.

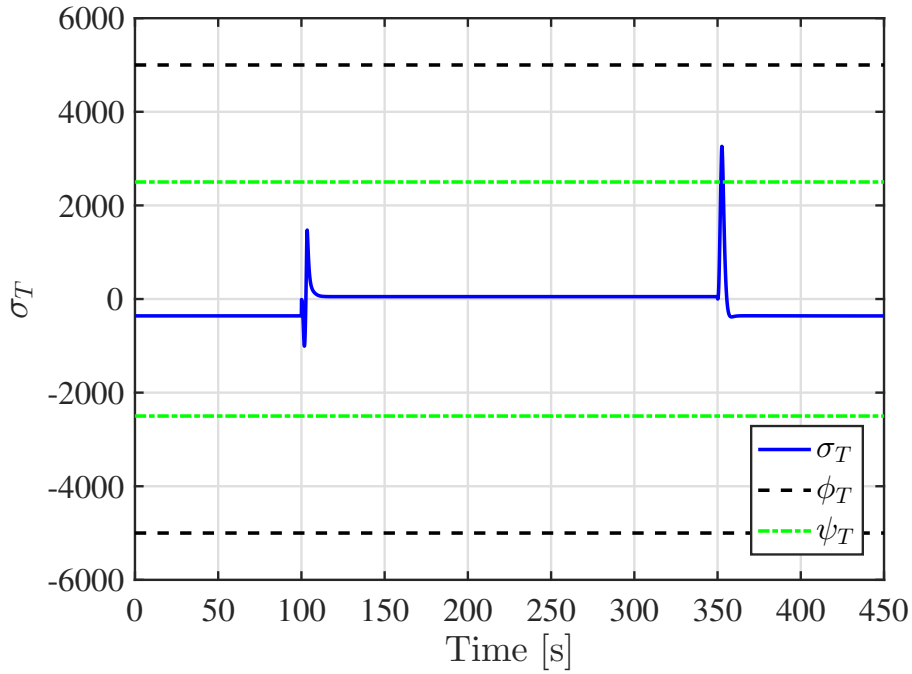

Figure 5.12: Sliding variable for the exhaust gas temperature.

For k_T, instead, any change is observed in Fig.5.13, since the sliding variable σ_T is always kept inside the boundary layer. Therefore, the control gain keeps its lower value all over the transient.

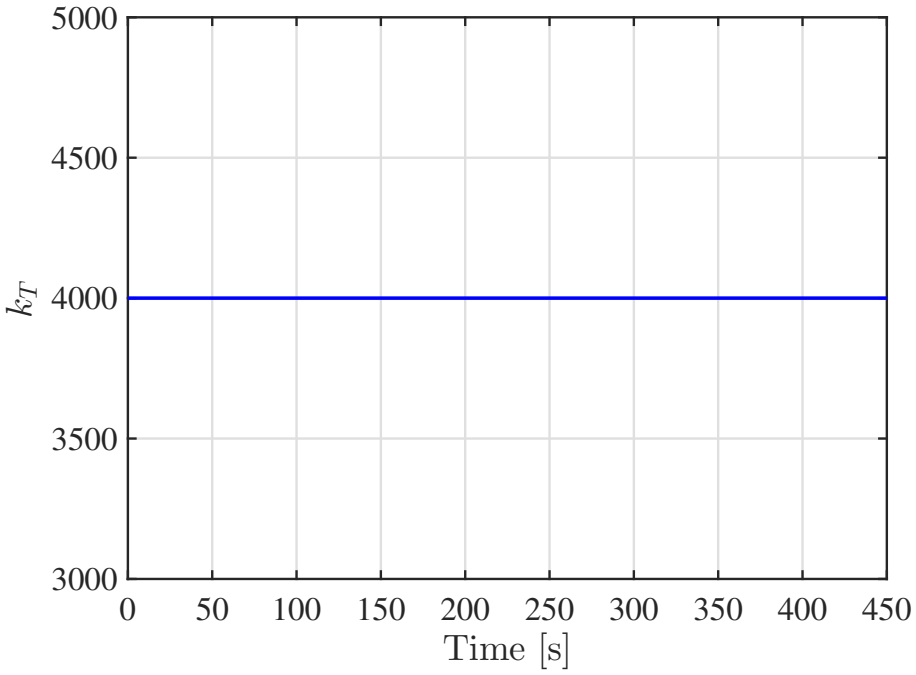

Figure 5.13: ASM gain for the exhaust gas temperature channel.

5.1.2 Test 2

The second test is a robustness test, in order to prove the capability of the proposed controller to handle with different types of uncertainties. The uncertainties considered in this test can be summarized as follows:

- Introduction of a sample time of $20ms$, which is a realistic assumption for an industrial controller employed in this application field.

- Introduction of a white noise affecting the electrical power. Again, this is a realistic condition, since the electrical power measured on the main grid is often affected by a huge amount of harmonics.

- Introduction of a deviation of 5% of some parameters (i.e. c_{pa} c_{pe}, η_T, η_C) used to calculate the controller function. Indeed, such parameters usually change in time and vary depending on the system operating point.

The same transient as the previous test is considered here and the simulation results are shown in the following. From the reported figures, one can note that the controller is able to keep substantially the same performace shown in the previous test also in this robustness test.

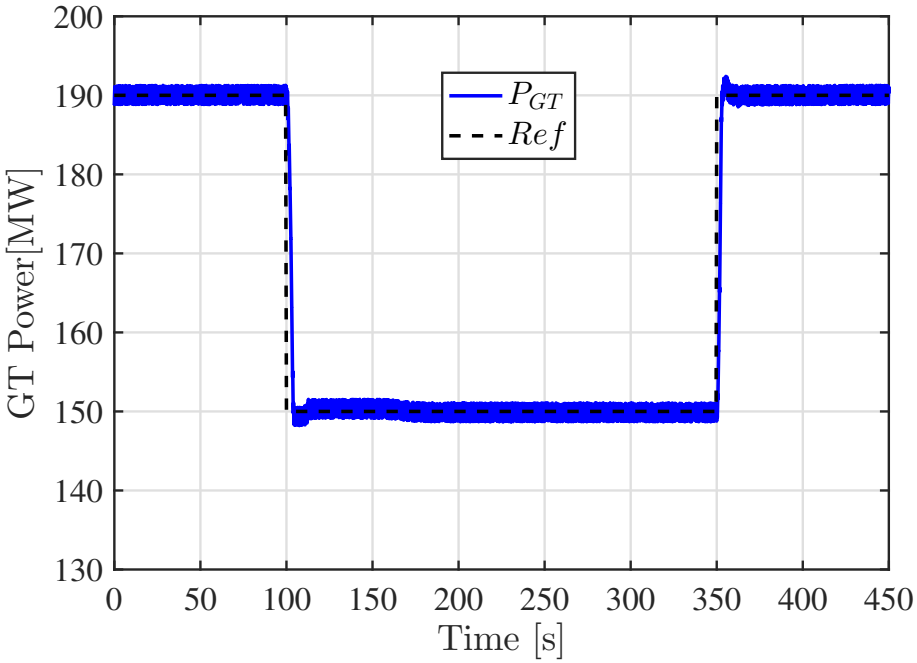

Figure 5.14: GT Power time profile.

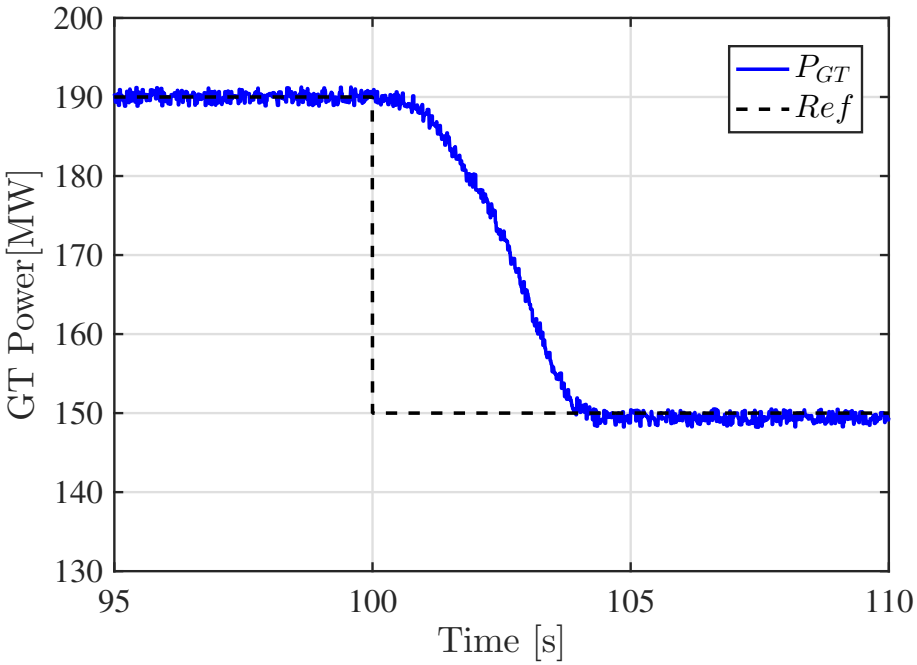

Figure 5.15: GT Power time profile - transient zoom.

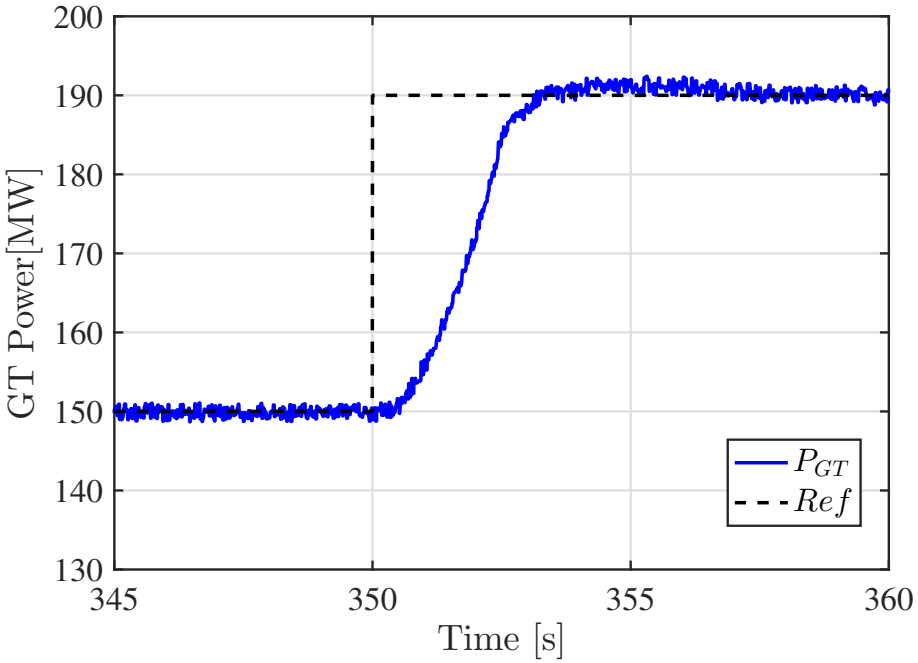

Figure 5.16: GT Power time profile - transient zoom 2.

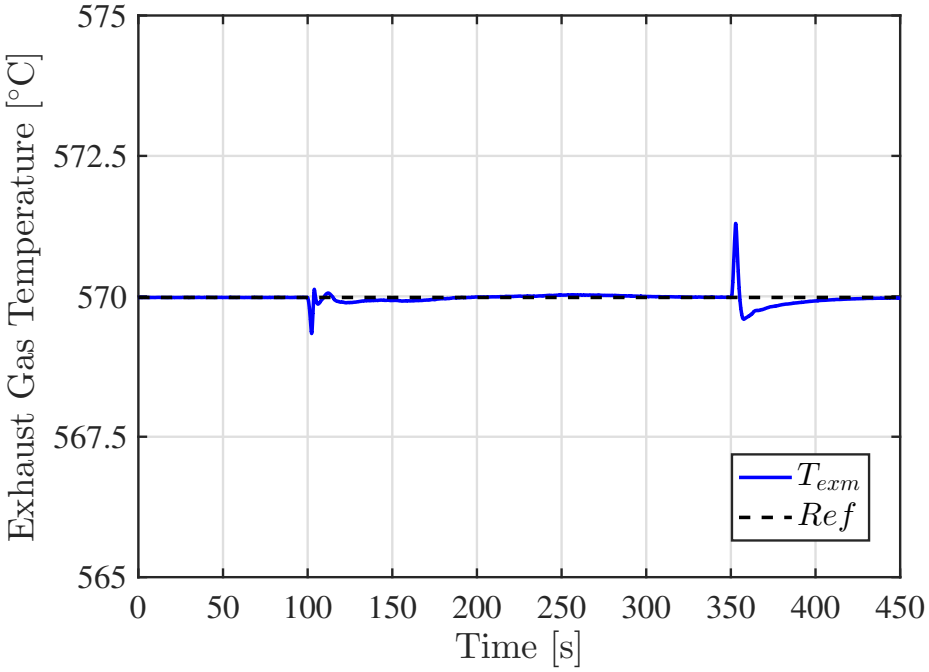

Figure 5.17: Exhaust gas temperature time profile.

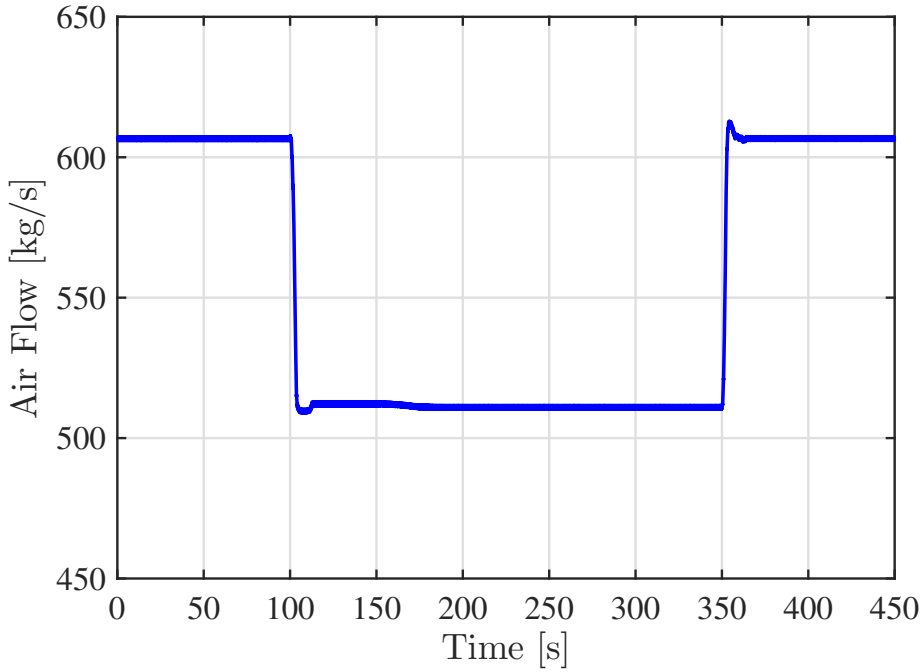

Figure 5.18: Air flow time profile.

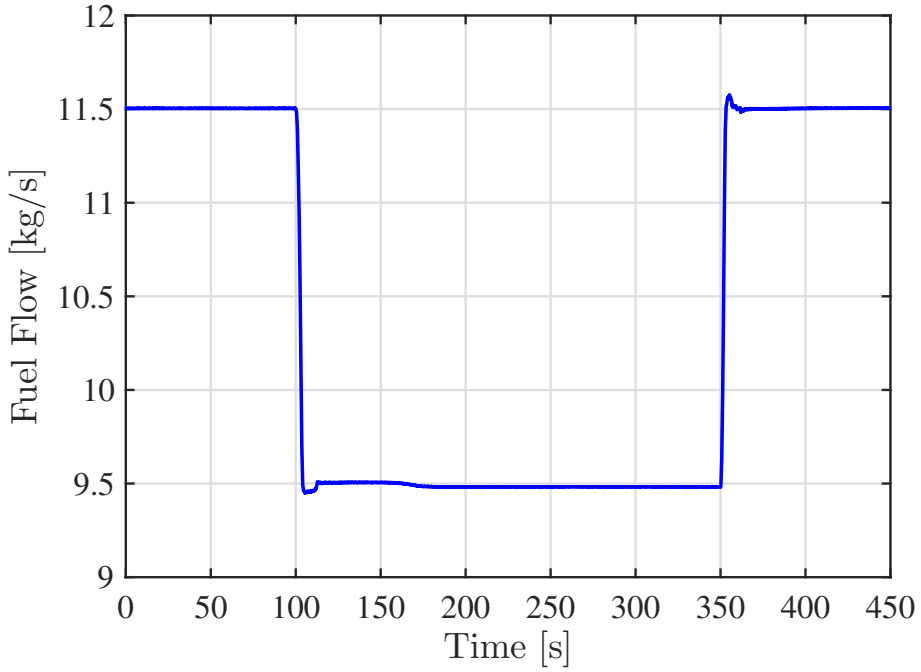

Figure 5.19: Fuel flow time profile.

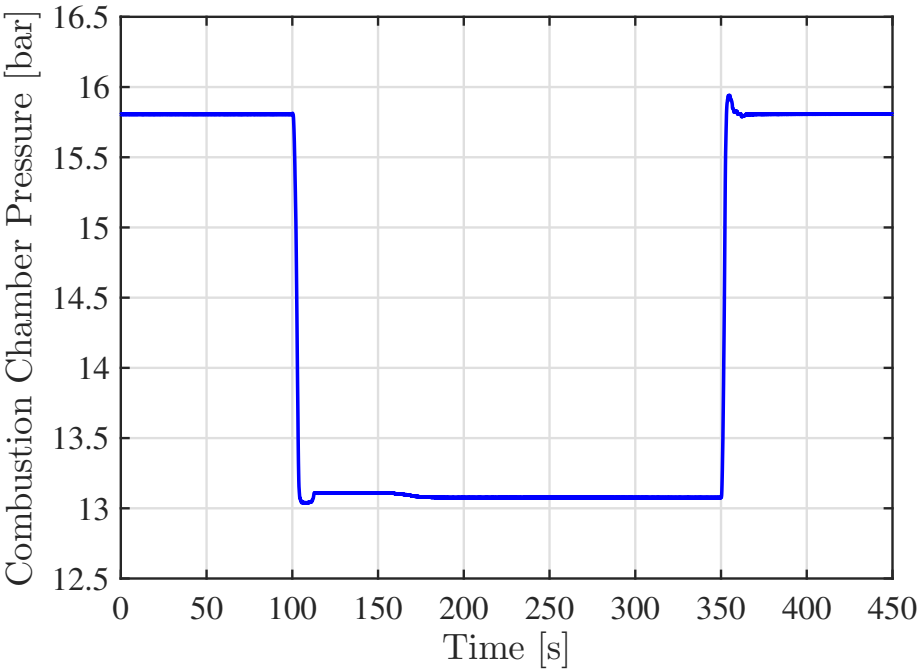

Figure 5.20: Combustion chamber pressure time profile.

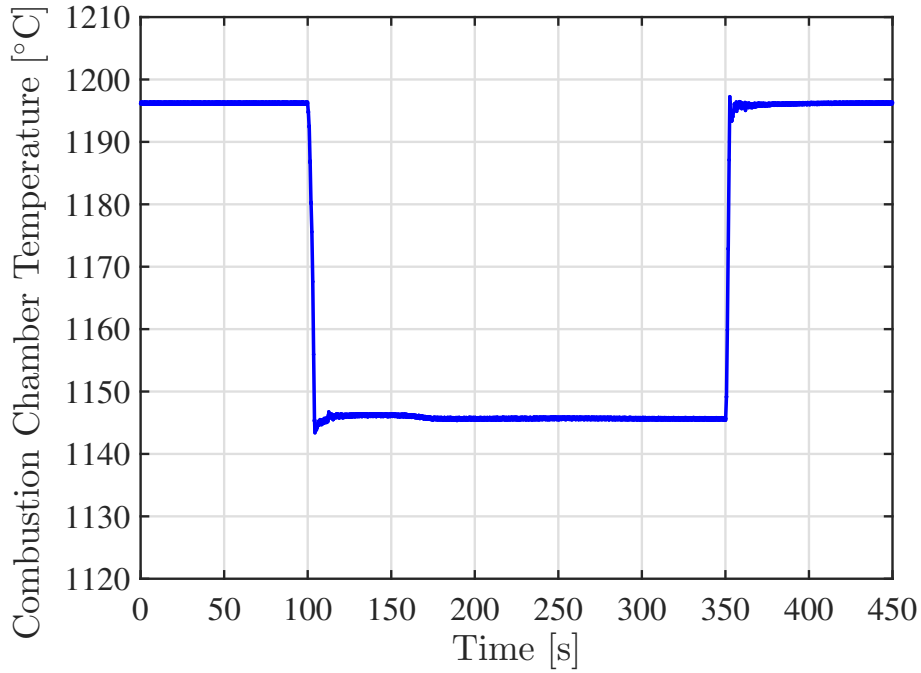

Figure 5.21: Combustion chamber temperature time profile.

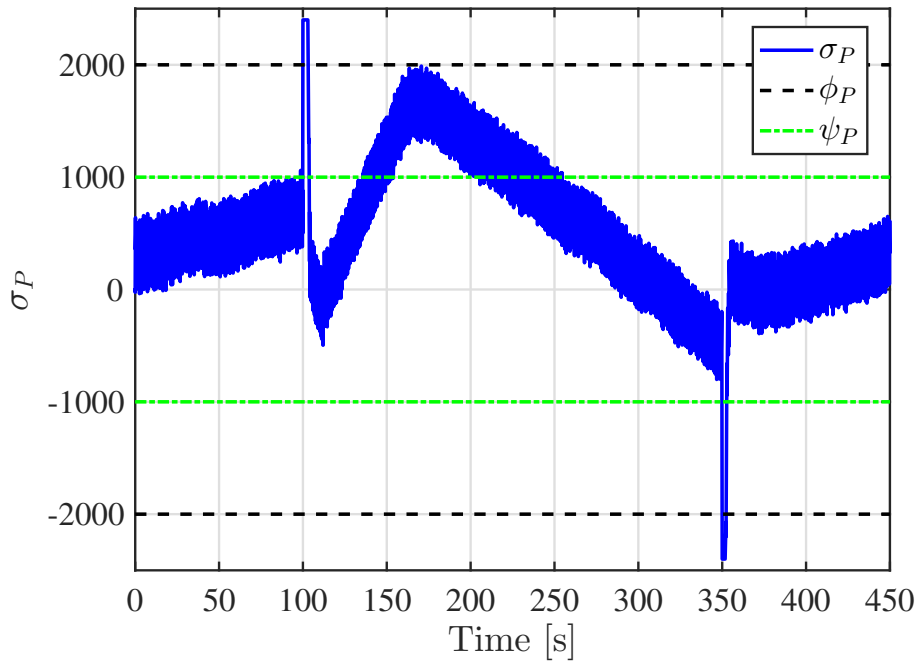

Figure 5.22: Sliding variable for the GT power.

Some differences can be observed looking at the figures depicting the controller quantities. Indeed, from Fig.5.22 and 5.23, higher values for the controller gain k_P can be noted, related to the introduction of additional system uncertainties. Such

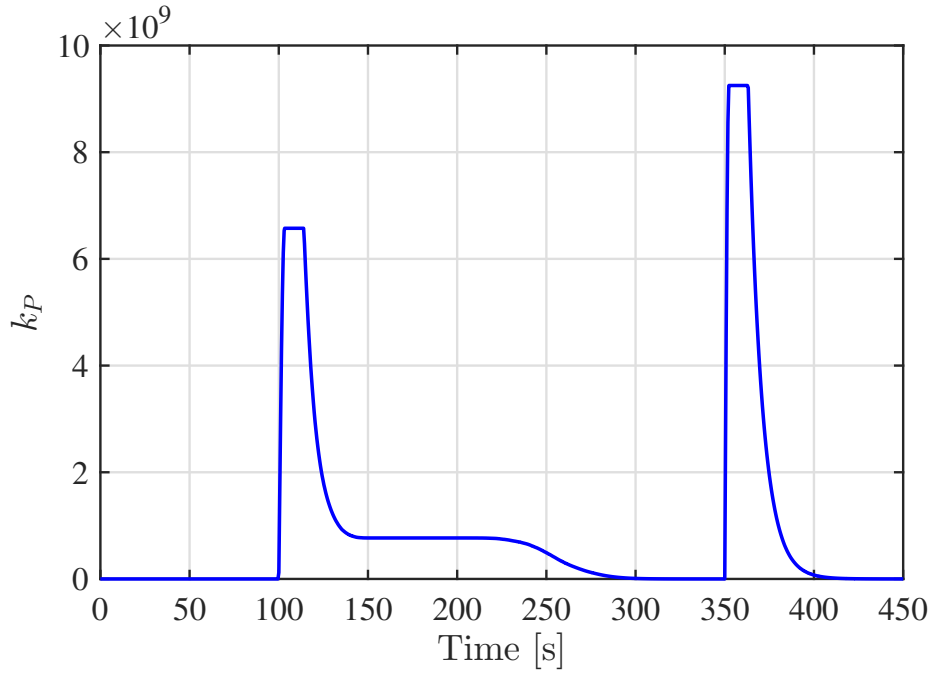

Figure 5.23: ASM gain for the GT power channel.

uncertainties does not affect instead the temperature channel, which keep analogous behaviours as in the previous test (Fig.5.24 and Fig.5.25).

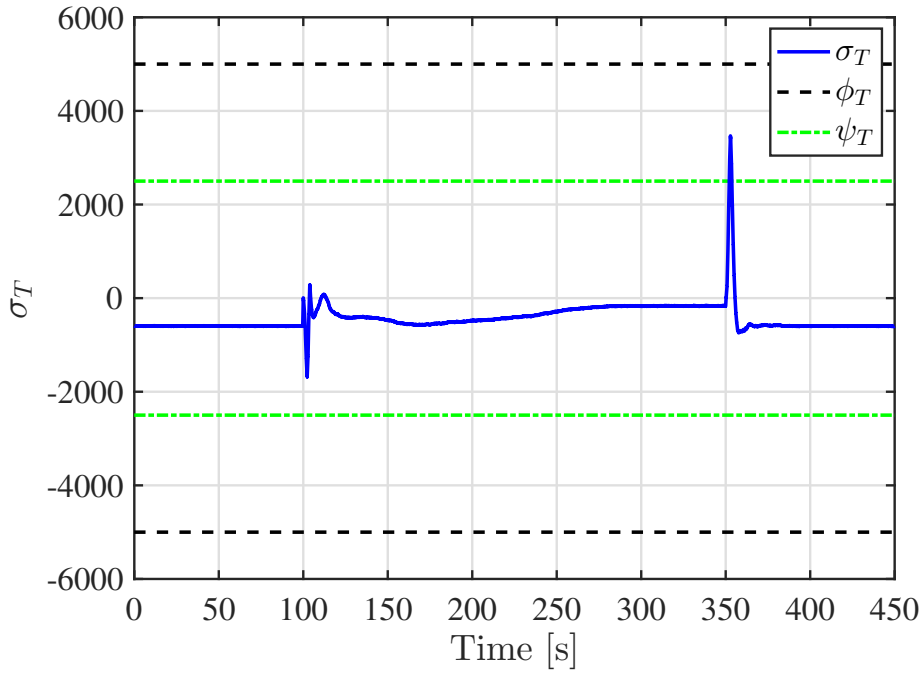

Figure 5.24: Sliding variable for the exhaust gas temperature.

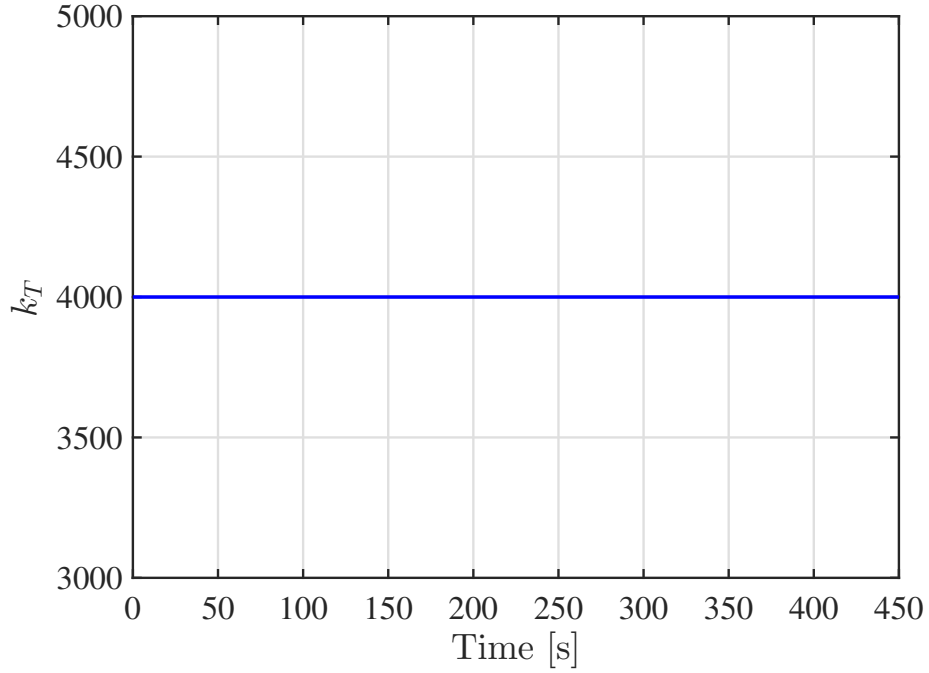

Figure 5.25: ASM gain for the exhaust gas temperature channel.

On balance, from these two tests the ASM controller proved to be capable to achieve the control objective with good performance even in presence of structured and unstructured uncertainties. Nevertheless, in the next chapter it will be shown

how such controller needs to be further adjusted and simplified in order to be suitable for an in-field implementation.

6. Experimental Validation through Real-Time Simulations

The ASM controller implementation and the validation tests were performed in the Ansaldo Energia S.p.A. laboratories.

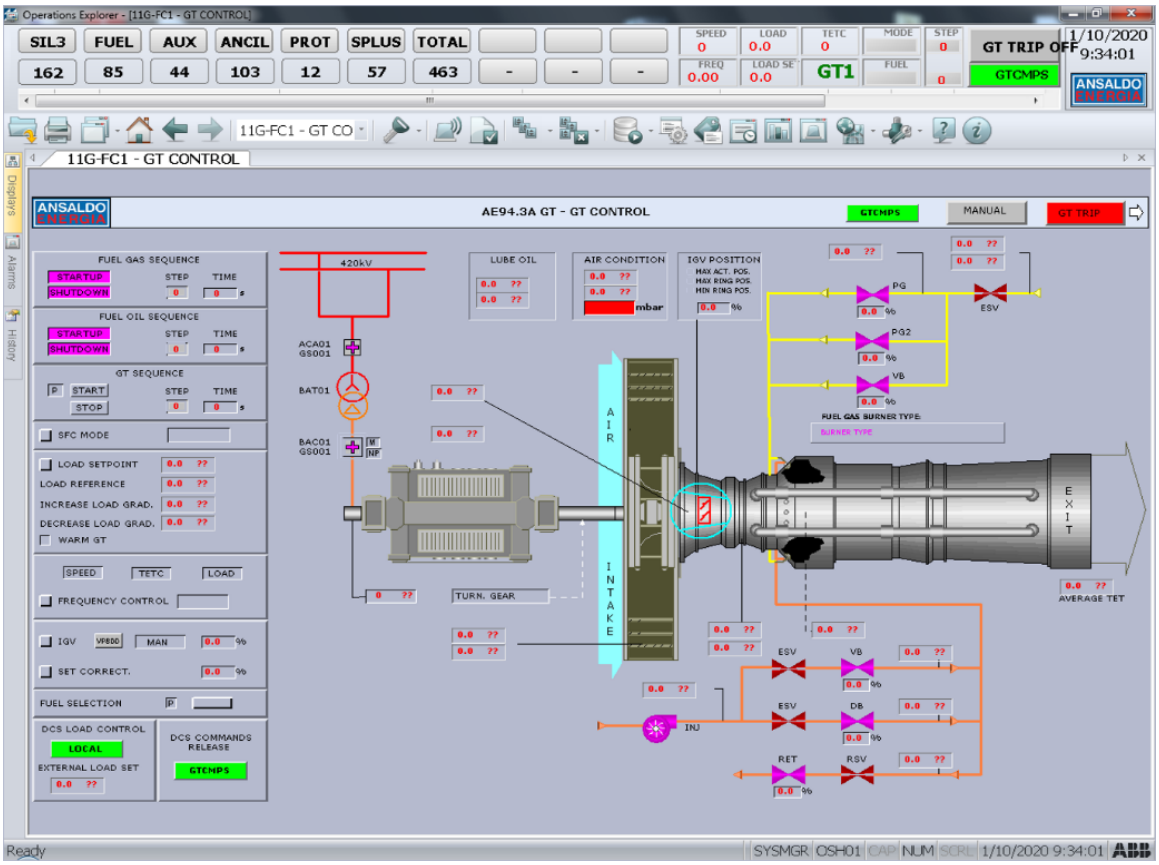

Figure 6.1: HMI of AE94.3A GT.

Due to the impossibility of using a real-scale heavy duty GT, the standard approach used by Ansaldo Energia S.p.A. to test its controller performance before commissioning is via HIL approach. A highly detailed and reliable model of a 250 MW Ansaldo Energia S.p.A. GT (model AE94.3A [19]) together with all auxiliary systems

is implemented on dSPACE Real-Time Simulator. The control part and its Human-Machine Interface (HMI) are hardware components and the very same one used on field by Ansaldo Energia S.p.A. (a screenshot of the HMI is reported in Fig.6.1). The proposed ASM command laws are implemented in an ABB Symphony Plus HPC800 industrial processor. The overall test-bed configuration is depicted in Fig.6.2.

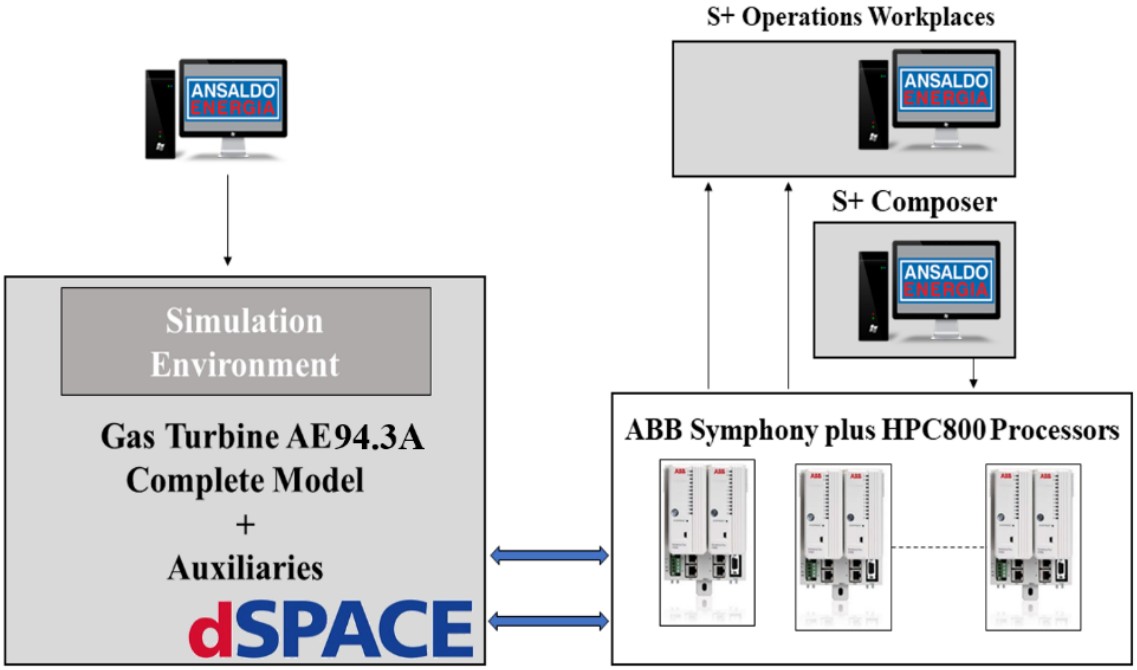

Figure 6.2: Overall real-time HIL simulation test-bed scheme.

Following, specific descriptions of the elements of the HIL set-up are provided.

6.1 Gas Turbine AE94.3A real-time model

In this section some details about the GT model used for the HIL simulation tests are provided. For the sake of clarity, this model is property of Ansaldo Energia S.p.A. and its details are sensible data for the Company and thus they cannot be divulgated. Nevertheless, we will include all the necessary information to clarify the high level of accuracy involved in the model used for experimental validation. A conceptual scheme of the model is reported in Fig.6.3. The main macro components considered in the model are the gas turbine (comprehensive of compressor, plenum, combustion chamber and turbine), the fuel gas and oil inlet systems (FIS), the IGV system and the electric generator.

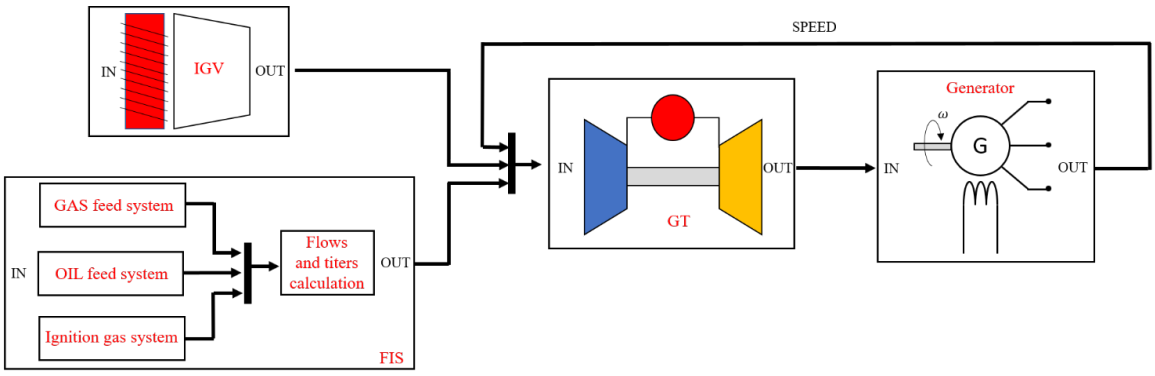

Figure 6.3: Overall real-time HIL simulation test-bed scheme.

The GT system model accounts for three elements, the combustion chamber, the compressor and the turbine. The thermo-fluid dynamic equations related to the accumulation areas are based on the mass-energy conservation principles with concentrated parameters for open fluid systems.

The structure of the dynamic equations describing the combustion chamber are the same used in section 3.1.4, but critical parameters such as the air and exhaust gas specific heats, compressor and turbine efficiencies and exhaust gas composition (assumed as constants in section 3.1.4) are time varying according to 3D dynamic maps defined thanks to measurements recorded by the industrial partner on real power plants.

The electric generator model consists of the power balance equation together with the swing equation, whereas electrical dynamics are neglected due to their small time constants with respect to the GT's ones. The IGV and FIS dynamics are characterized by suitable dynamic function mapped on the real actuators dynamics. Please note that in this model, since it accurately describes the GT real system, the air and fuel

flows are not the actual control inputs anymore, indeed they are replaced by the IGV position and the PRMX valve position respectively, which are the real actuators of the GT. Nevertheless, both of them have a one to one relationship with the quantities considered in the models presented in Chapter 3, hence nothing changes from a control point of view.

The overall real-time model was validated by Ansaldo Energia S.p.A. by comparing the outputs of the real-time simulator with the measurements acquired from the real plant installed all over the world.

6.2 ABB Symphony Plus HPC800 Processor

The SD Series HPC800 controller is a high-performance, high-capacity process controller that is used to support the plant overall control requirements, from discrete and continuous, to batch and advanced control applications [45]. The processors are based on a 256 MHz, 32-bit architecture. Even though this processor is quite slow comparing to the recent technology available on the market, this hardware is still a benchmark in terms of reliability and lifetime. By using extreme-temperature rated components (-40° C to 70° C ambient), SD Series products can be installed near field devices and control elements they interface with, without additional climate control systems which are necessary in remote environments.

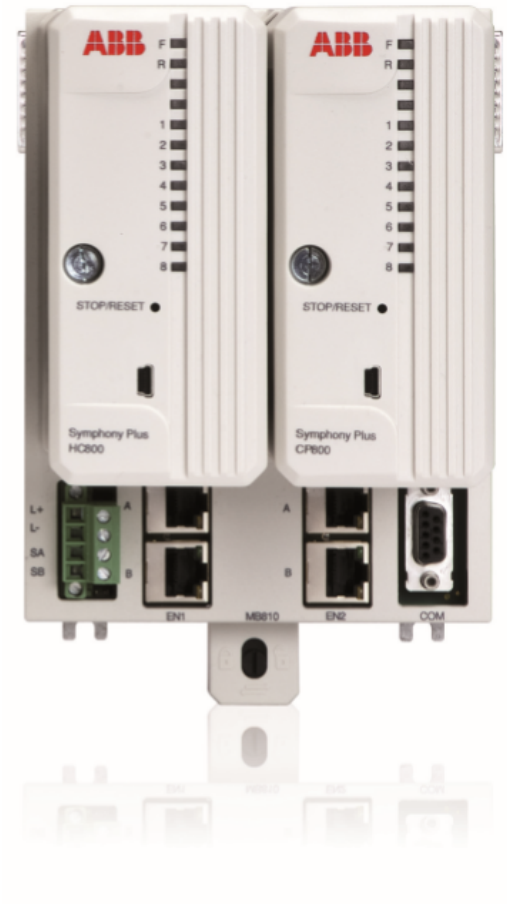

Figure 6.4: ABB SD Series HPC800 processor unit.

The controller embeds two partitions with different cycle times (one cycles at 30 ms and the other cycles at 200 ms). The slowest one could be responsible for the

numerical chattering, as it will be discussed in section 6.3, when the command law is in its original and complicated form. A photo of the processor unit is reported in Fig.6.4.

The controllers are managed thanks to the software S+ Engineering tool [46], provided by ABB, in which all the control logics are implemented. The processors are installed in proper cabinet inside a dedicated room, in which there are the complete boards and all the cables coming from the processor board units, which are connected and interfaced with the real-time simulator. A picture depicting the laboratories' cabinet is reported in Fig.6.5.

Figure 6.5: Cabinets holding the industrial processors and the real-time simulator in the Ansaldo Energia laboratories.

6.3 Definitive Adaptive Sliding Mode controller design

The implementation of complex controllers on industrial microprocessors is a hard task to perform. Indeed, their software structures are not so manageable as the simulation software we can find on Windows platform for instance. Therefore, it is intuitive to understand the difficulty to implement the command laws of the *ASM controller full* used in the simulations executed in Matlab & Simulink.

For these reasons, in order to make the implementation of the proposed controller more manageable, it was decided to implement on the industrial microprocessor the *ASM controller approx* defined in section 4.2.

Nevertheless, even if this controller presents a much lower level of complexity, some further adjustments have to be carried out. As a matter of fact one of the main weaknesses of SM controllers is the production of a high frequency control command, i.e. a control input which is affected by chattering. Most predominantly, chattering is enhanced by an excessively long time-step of the physical controller output (which is due to a slow computational speed and takes the name of *numerical chattering*) and a high SM gain [47]. Therefore, in order to reduce the performance disruption caused by these two factors, the following actions were taken:

- The nominal part $\underline{u}_0$ of the command law is eliminated, since it involved numerous state functions calculations.

- The inverse of the multiplicative matrix $\boldsymbol{B}$ is lower bounded by a constant matrix $\boldsymbol{D}$. In particular, such matrix is termined through the calculation of the state-dependent funcions all over the system state domain.

The elimination of the nominal part of the command law may sound puzzling at first since it is originally conceived as a nonlinear feed-forward action, aiming at improving the controller dynamic performance [15]. However, this remains true as long as the mathematical model which the nominal command law is based on is an accurate description of the physical system, on the contrary, it produces a wrong feed-forward action when modelling uncertainties are significant. Thus, it deteriorates the controller performance and causes the SM gain to reach higher values in order to correct such malfunctioning and leading to chattering.

The multiplicative matrix B has a similar effect if its entries are not a good model of the system, plus such effect is amplified since it directly multiplies the

SM gains. Finally, both actions allow the mathematical backbone of the controller to be "lighter", i.e. most complex calculations are eliminated, obtaining a lower computational effort which in turn allows to avoid computational delays leading to a further chattering alleviation.

On balance, the command laws which will be implemented on the real controller are:

$$\begin{bmatrix} u_1 \\ u_2 \end{bmatrix} = - \begin{bmatrix} d_{11} & d_{12} \\ d_{21} & d_{22} \end{bmatrix} \begin{bmatrix} k_P \; sat\left(\hat{\sigma}_P/\phi_P\right) \\ k_T \; sat\left(\hat{\sigma}_T/\phi_T\right) \end{bmatrix} \tag{6.1}$$

where $d_(ij)$ are the $\boldsymbol{D}$ matrix components. Even if these simplifications appear quite relevant, the carried out simplifications does not compromise the overall system stability [21].

6.4 Plant control system description

The control system implemented on the real processor is briefly described in this section. From Fig.6.6 one can note that several control loops exist. The first one is the Start-up Controller, which acts only in the machine start-up phase. Normal operation controllers are the Speed Controller, which is in charge of keeping the turbine at the correct speed, and the Load Controller, which performs the control of the GT power according to an external reference (the focus of this work). The other controller, namely the Exhaust Gas Temperature Controller (TETC), the pressure rate limiter, the load limiter and the cooling limiter, are protection loops aiming at preserving the machine lifetime. The protective action is implemented by means of a minimum selector that defines the fuel reference to be given to the fuel intake system.

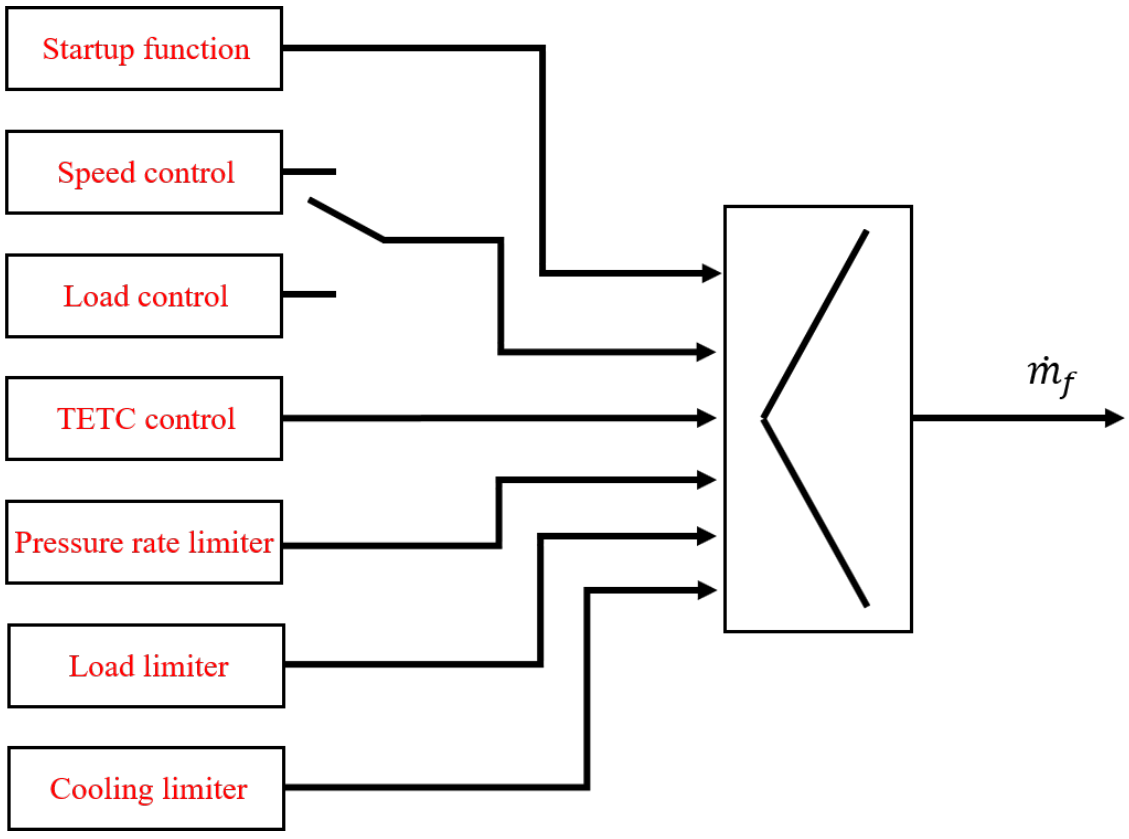

Figure 6.6: Gas Turbine system regulators scheme.

In addition, a control loop related to the EGT regulation exists, which provides the IGV with the desired position in order to make the EGT track its reference signal, generated by internal algorithms aiming at operating the machine in maximum

efficiency conditions. As previously mentioned, the focus of this thesis is the GT power and the EGT control. For this reason, in the following, the conventional control strategy used for the Load Controller and for the EGT regulation is described, pointing out its limits and drawbacks. The standard layout used by Ansaldo Energia is PI-based and depicted in Fig.6.7.

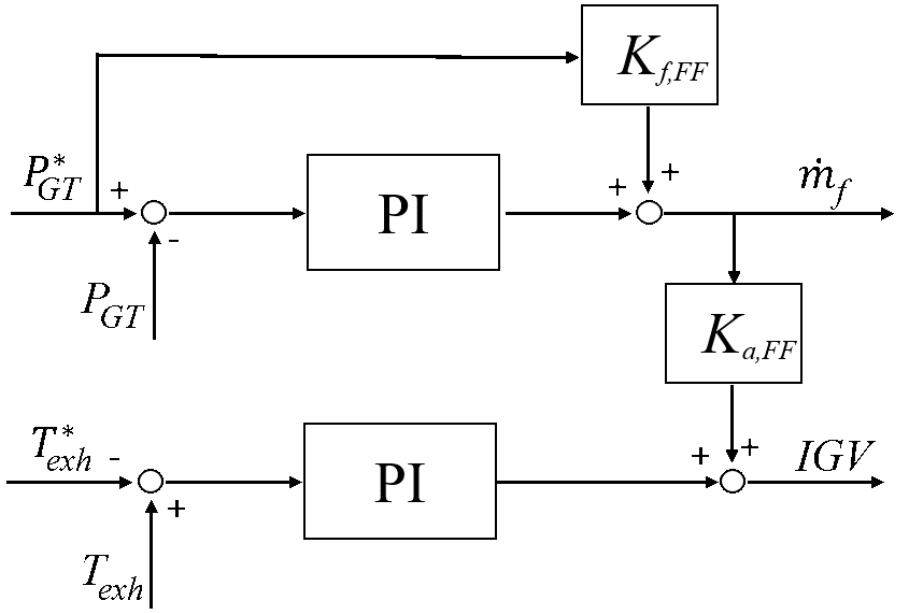

Figure 6.7: Traditional control system scheme.

Two FeedForward (FF) signals, namely $K_{f,FF}$ and $K_{s,FF}$, can be observed in this scheme. They are very important for the correct operations of the GT. In particular, the $K_{f,FF}$ highly influences the GT performance in terms of load control response time, while the FF $K_{a,FF}$ takes into account the coupling between the power channel and temperature channel. Optimally setting these functions is the most critical operation for the control system designer, since the optimum settings change depending on many variables, among which the external environment system boundary conditions. In other words, such strategy cannot perform well while the system operates in off-design conditions, leading to a deterioration of the GT performance.

6.5 Real-Time Simulations Results

In this section the results obtained by the comparison between the innovative ASM controller of section 6.3 and the traditional regulation are reported. Several tests were performed during the controller validation campaign since several transients were considered in different operating conditions (on-design and off-design working conditions). For the sake of conciseness and clarity only the most significant situations are reported and discussed in the following. In particular, three main transients are detailed i.e. *(i)* a load increase in off-designed operating conditions, *(ii)* a load decrease in off-designed operating conditions and *(iii)* a robustness test in presence of noise on the electric power measurement (a very common situation in the real operation of a GT power generator).

As previously stated, all reported simulations are performed in off-design conditions since it represents the most critical system operations. Parameters values are reported in Table 6.1 including off-design values used for the simulation and the design one.

Table 6.1: system Parameters Values

Parameter	Symbol	Design value	Test value
Ambient temperature	T_{amb}	20°C	0°C
Air relative humidity	H_R	40%	90%
Turbine efficiency	η_T	0.934	0.887
Compressor efficiency	η_C	0.871	0.827

6.5.1 Load Increase Test

This simulation considers a load increase from an initial power production of 40 MW to a final value of 250 MW. It is worth noticing that this is the most stressful load increase operation since it starts from the minimum power production and reaches the turbine rated power. In order to carry out a stress test for the controller, the power reference is ramped up with an increase rate of 100 MW/min, which is in general much higher than the one commonly required by TSOs (usually from 20 MW/min to 30 MW/min) [48].

Fig.6.8 provides a comparison between the GT electrical power production achieved by the ASM controller (blue solid line) with the control action provided by the traditional PID controllers (dot-dashed red line). Even though both controllers are able to reach the 250 MW final power production, the reference (dashed black line) dynamic

tracking is quite different. As one can notice, the ASM controller is very close to the reference profile, while the red curve is more distant, especially in the first part of the transient. In order to better highlight the transient performance of the proposed ASM controller, Fig.6.9 provides the plot of the tracking errors determined by both controllers.

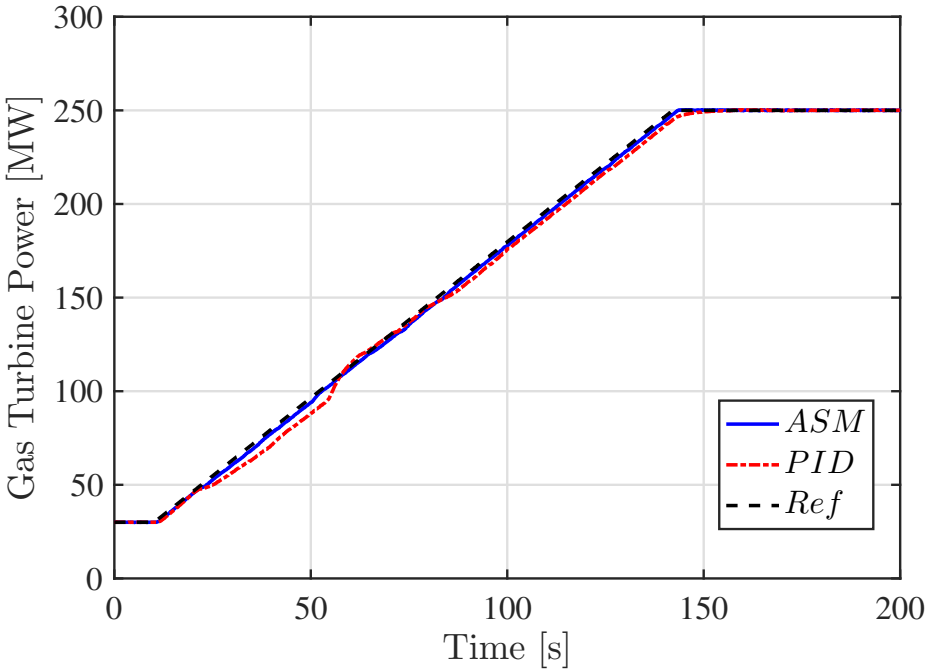

Figure 6.8: Gas turbine power time profile.

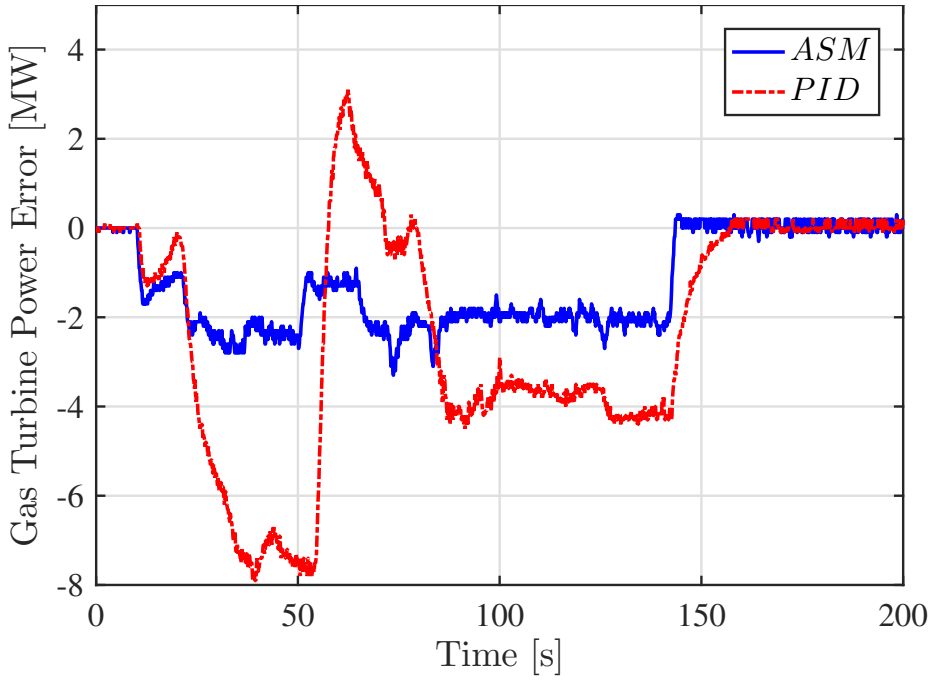

Figure 6.9: Power tracking error time profile.

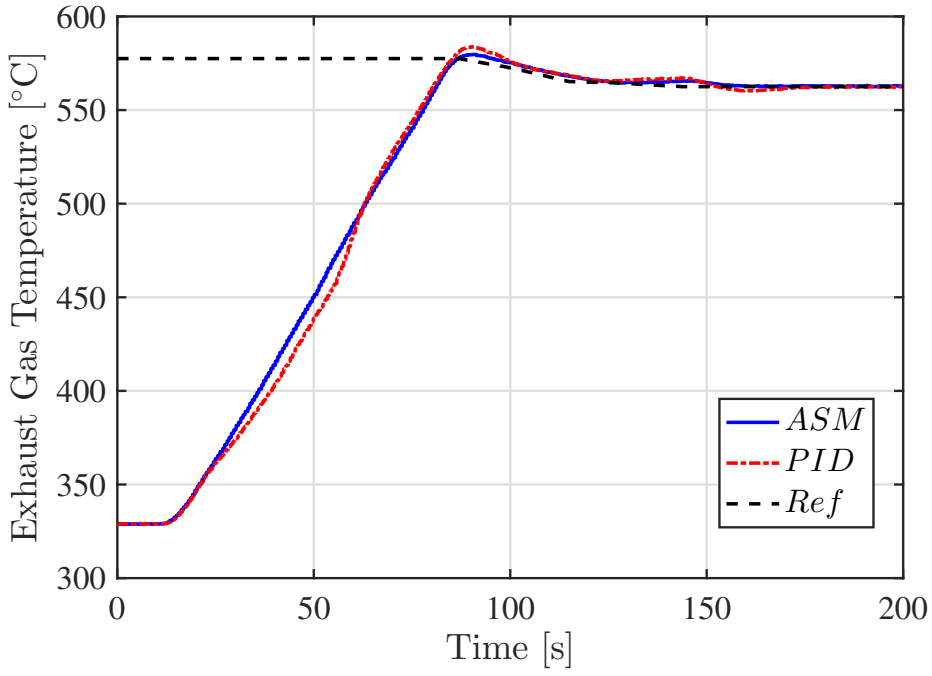

Figure 6.10: Exhaust gas temperature time profile.

It is clear that the machine performance determined by the ASM control are significantly higher than the one obtained thanks to the PID controller. Indeed, the tracking error related to the ASM is far smaller throughout the entire transient

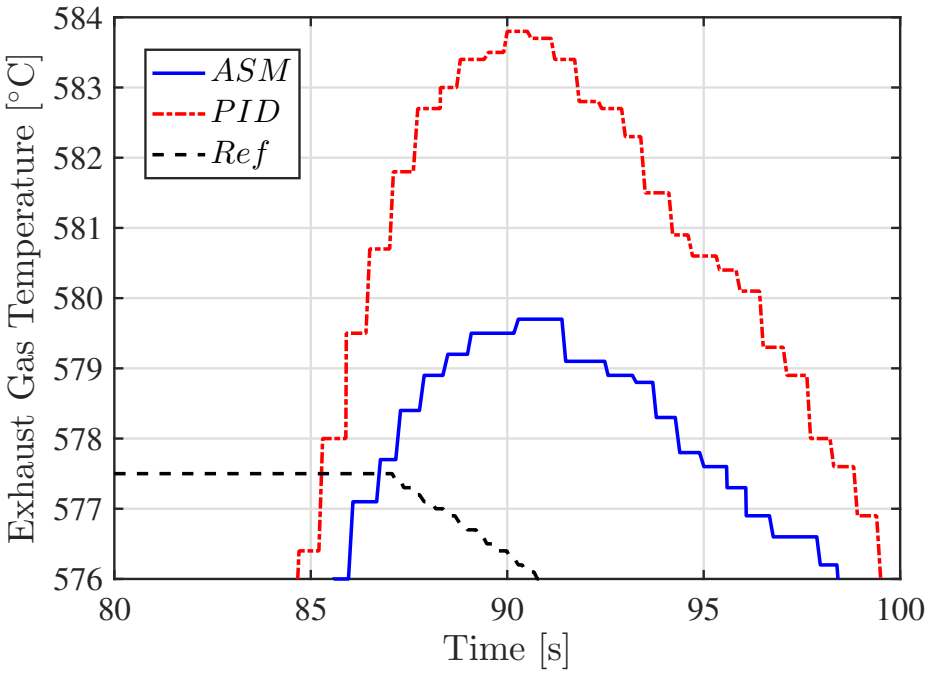

Figure 6.11: Exhaust gas temperature time profile - zoom.

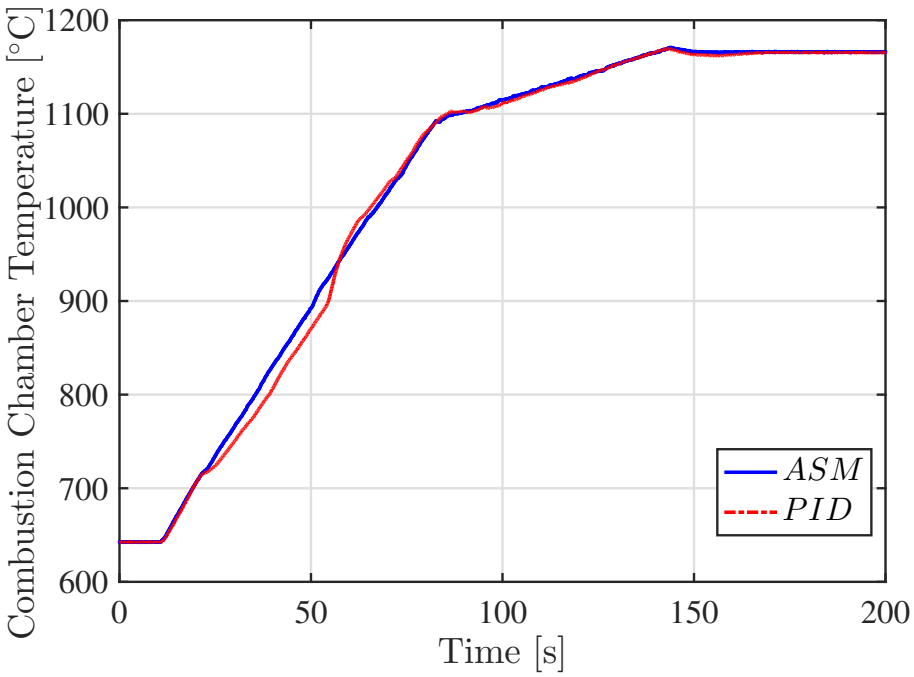

Figure 6.12: Combustion chamber temperature time profile.

compared to the one associated with the PID control, showing a substantial increase in the tracking precision peaking up to a 4 time higher accuracy.

Furthermore, as depicted in Fig.6.11, the ASM controller is capable of limiting the

EGT overshoot (5°C lower with respect to the EGT of the PID controlled system). This condition implies the avoidance of the intervention of the TETC protection loop, unlike the PID case. As one can notice, the EGT reference is not exactly constant, since it is determined by an external calculation that changes it depending on the current operating condition in order to make the GT work as close as possible to its maximum efficiency work point. Despite this fact, the ASM control can efficiently track also this slightly time varying reference determining an even smoother EGT response. In addition, even though the CCT is an unavailable measure in real applications, the internal signal of the real-time simulator can be plotted to verify the absence of undesired behaviours such as dangerous spikes. Indeed, not only is the ASM control able to avoid the intervention of the protection loop, but it is also able to maintain a safe CCT profile as shown in Fig.6.12.

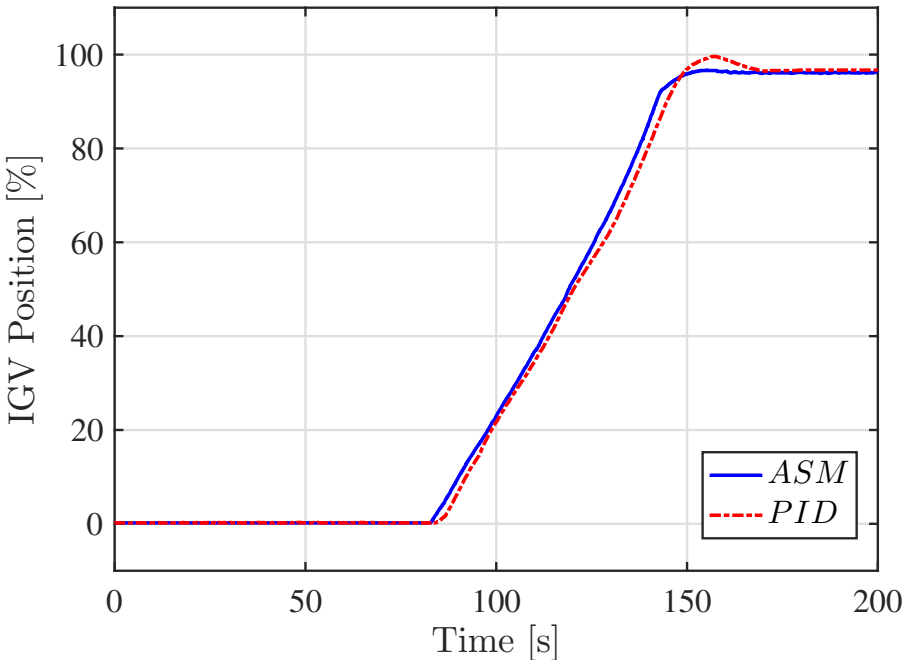

Figure 6.13: IGV position time profile.

Finally, the two control outputs are plotted in Fig.6.13 and Fig.6.14 in order to show their smooth nature. This smooth feature, in contrast with the typical switching control input generated by standard SM controllers, is extremely crucial here, as it allows the physical actuators (IGV and fuel valves) to actually reproduce such profiles. As a general comment, from 6.13 one can observe the transition from the low power operating conditions where IGV are completely closed to the high power operating

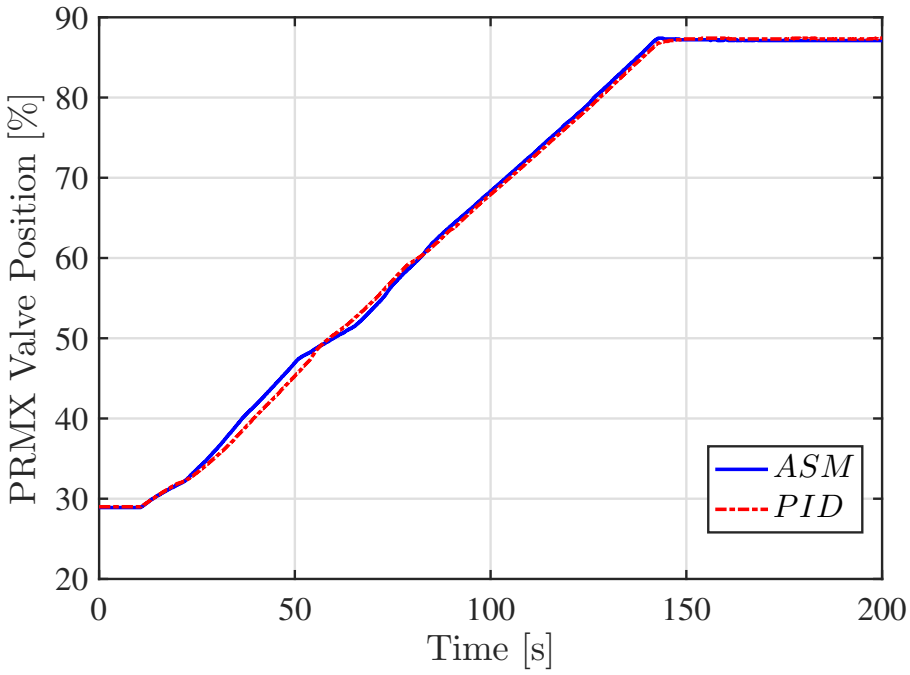

Figure 6.14: PRMX valve position time profile.

conditions where IGV are free to regulate their position according to the control objectives.

6.5.2 Load Decrease Test

In this subsection a load decrease operation is considered, starting from an initial production of 250 MW to a final steady state of 50 MW. Again, the power reference is ramped down with a decrease rate of 100 MW/min. The test power tracking is shown in Fig.6.15 where one can notice that the machine output power controlled by the ASM remains closer to the desired profile compared to the one related to the PID control system. Nevertheless, such improvement can be appreciated more clearly in Fig.6.16 where the power tracking errors are plotted.

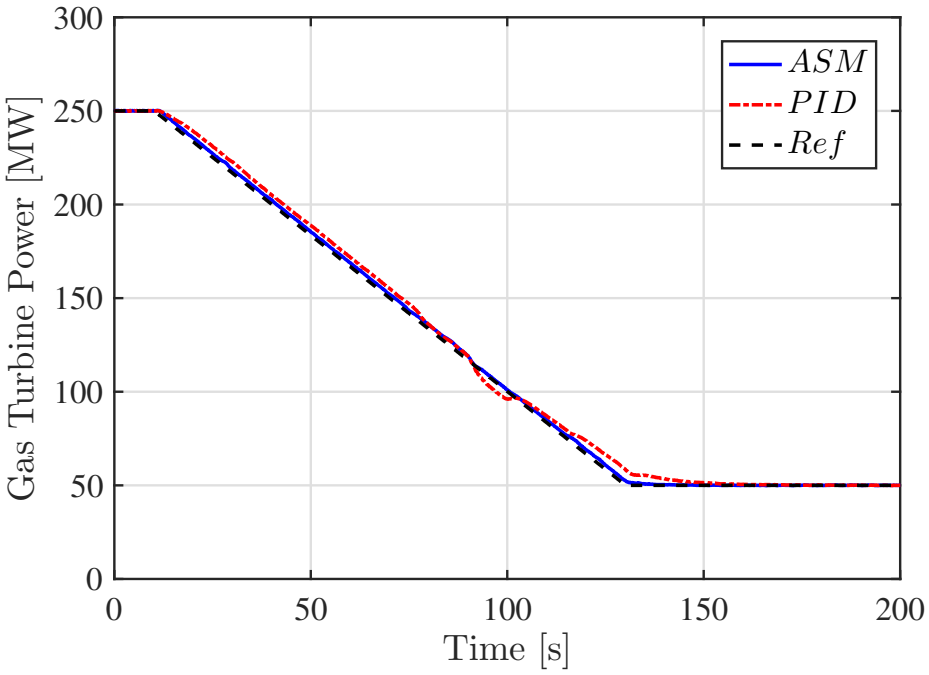

Figure 6.15: Gas turbine power time profile.

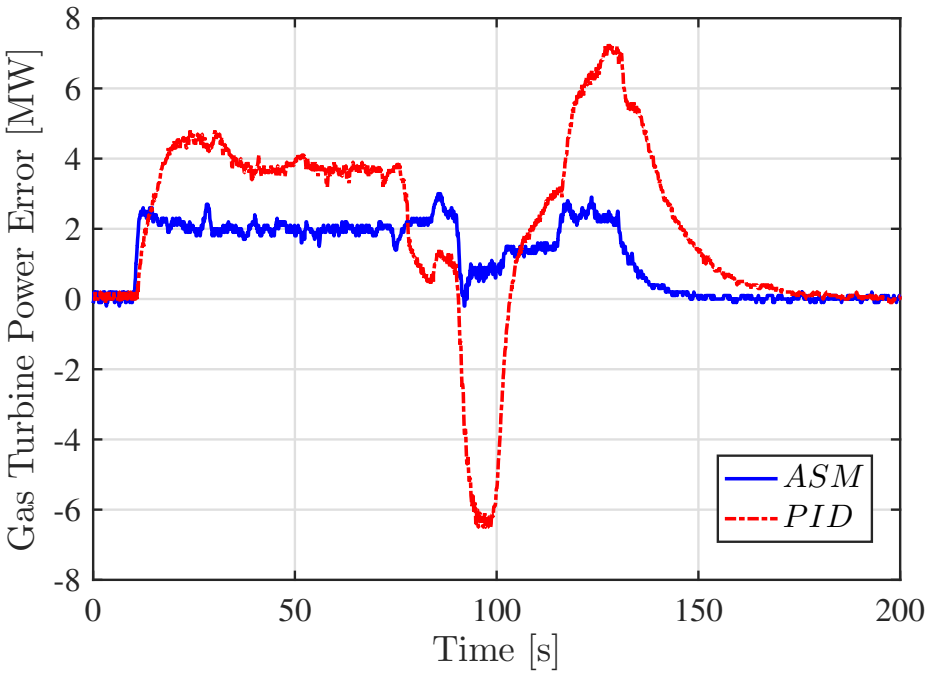

Figure 6.16: Power tracking error time profile.

In Fig.6.17the EGT time profile is reported showing a less stable profile generated by the PID controller. Such undesired fluctuations are caused by the feedforward actions operating in off-design conditions. Besides, these fluctuations are visible also

on the CCT profile, as shown in Fig.6.18. Moreover, one can observe that the EGT

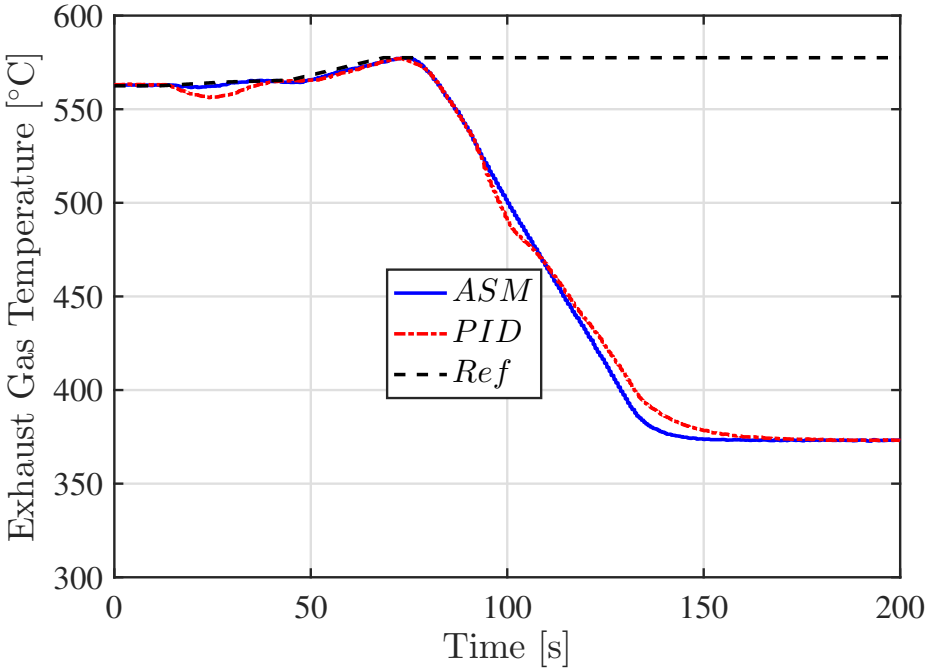

Figure 6.17: Exhaust gas temperature time profile.

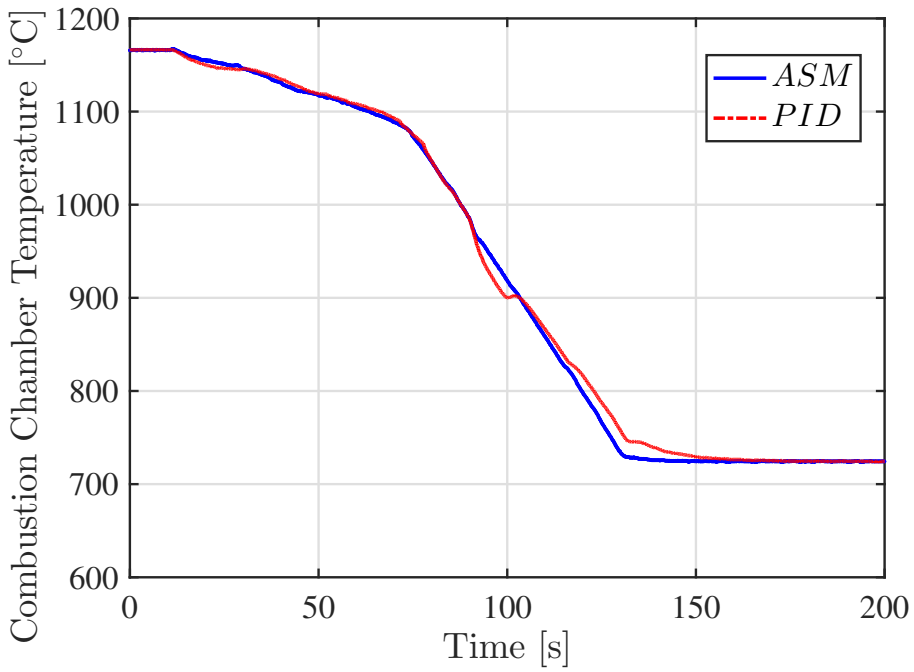

Figure 6.18: Combustion chamber temperature time profile.

regulation is abandoned for low power operating conditions, due to the saturation of

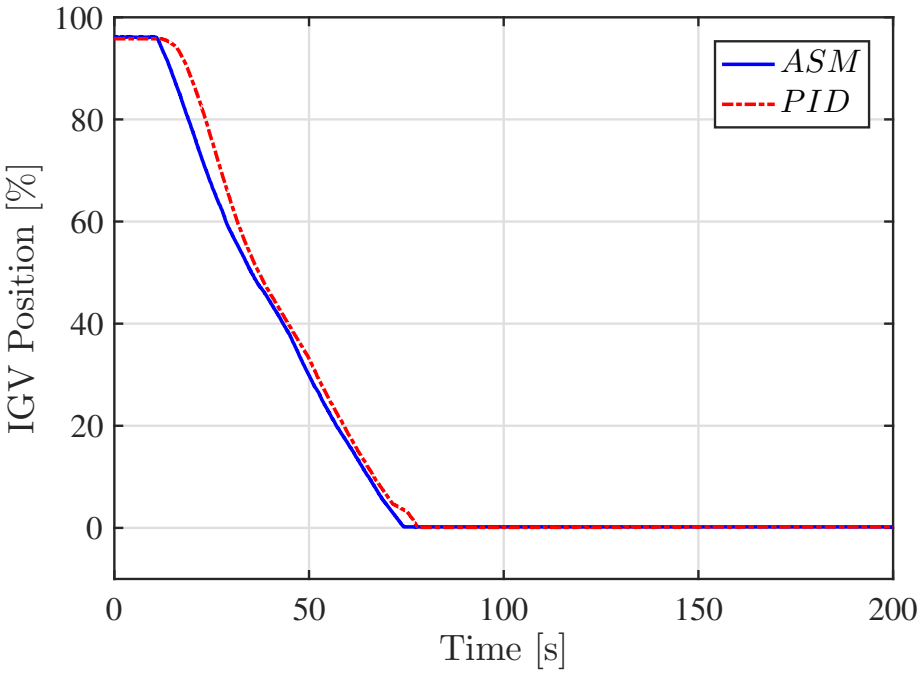

Figure 6.19: IGV position time profile.

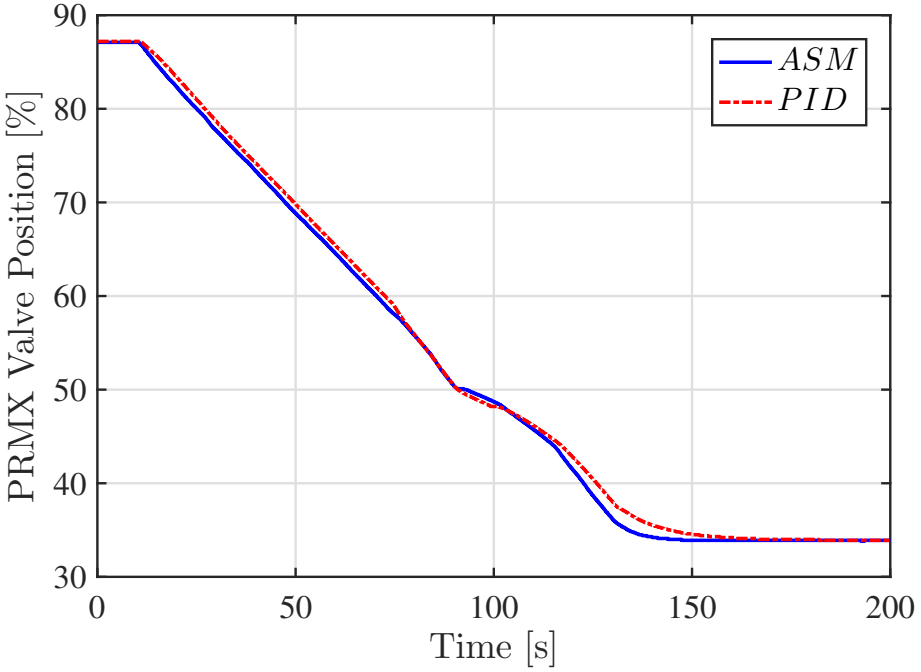

Figure 6.20: PRMX valve position time profile.

the air flow (see Fig.6.19). Again, obtaining a smooth transition between these two areas is an outstanding achievement as it proves once again the remarkable robustness of the controller. As a matter of fact, although it is designed on a MIMO system

(when the IGV are not saturated) it is able to perform greatly even when the system "degenerates" into a SISO one (when IGV are completely closed). Finally, for the sake of completeness, the PRMX valve position determined by both controllers is provided in Fig.6.20.

6.5.3 Robustness test in presence of noise on the electric power measurement

In this last test, a realistic GT power measurement is considered. Indeed, according to Ansaldo Energia the power measurement is affected by not negligible disturbances in field, giving rise to a noise characterized by 4MW amplitude peak to peak at maximum. For this reason, a white noise with this amplitude is introduced on the electrical power measurement to simulate a realistic field signal that the GT controller needs to process. The same reference variations of the previous testcases are provided here, leading to comparable results with respect to the previous real-time simulations. The same signal is also provided to the PID controller for a fair comparison between the two approaches.

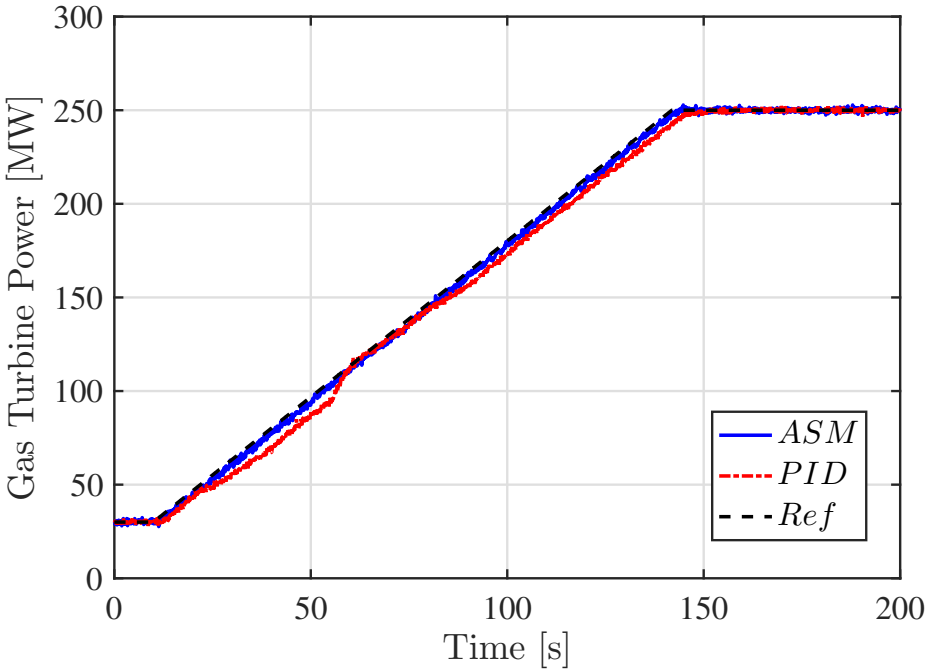

Figure 6.21: Gas turbine power time profile.

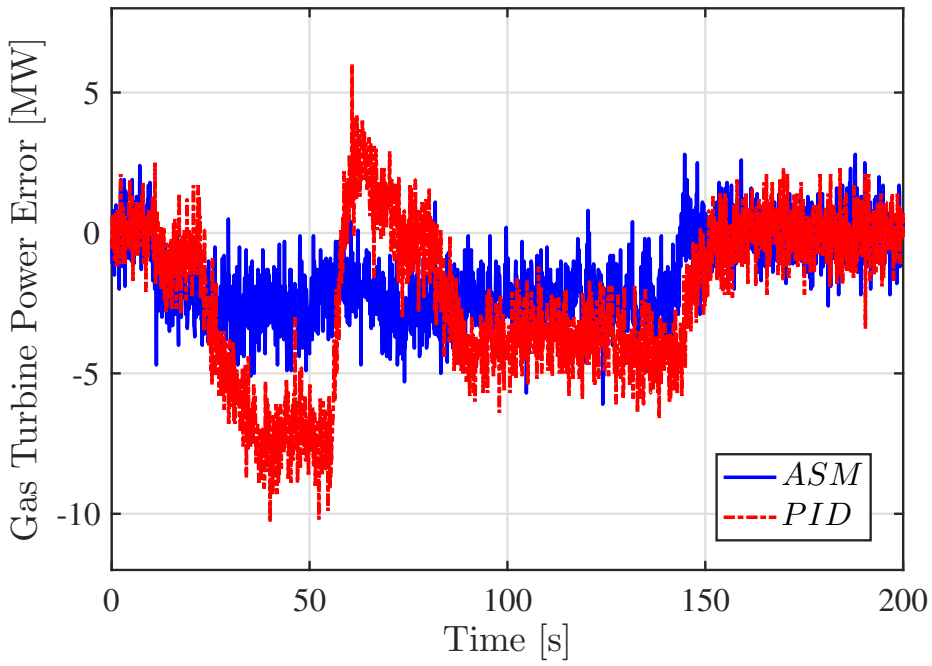

Figure 6.22: Power tracking error time profile.

The GT electric power is reported in Fig.6.21, while its tracking error is shown in Fig.6.22. As one can notice, the ASM controller performance are once again higher than the ones determined by the standard control system. Also the EGT profile shown in Fig.6.24 highlights that the noise on the power measurement deteriorates the performance of the PID EGT controller which is almost 1 °C higher than the case without the noisy measurement, leading to the intervention of the TETC control loop (see Fig.6.23). On the other hand, the EGT profile determined by the ASM controller remains the same as the one of the first simulation, showing the good decoupling between the two regulating channels. This has also a positive effect on the dynamics of the CCT (Fig.6.25).

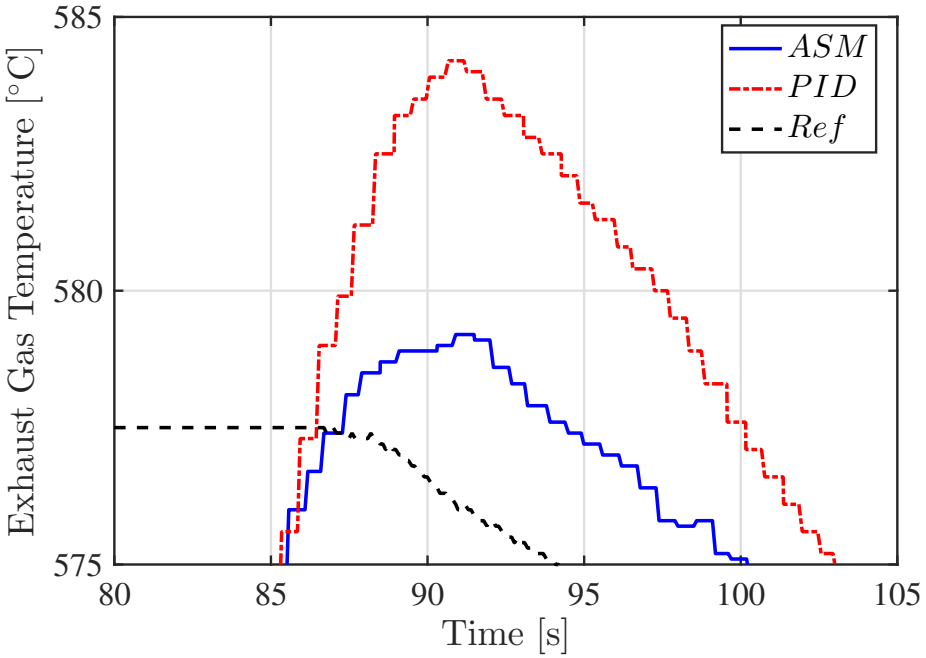

Figure 6.23: Exhaust gas temperature time profile - zoom.

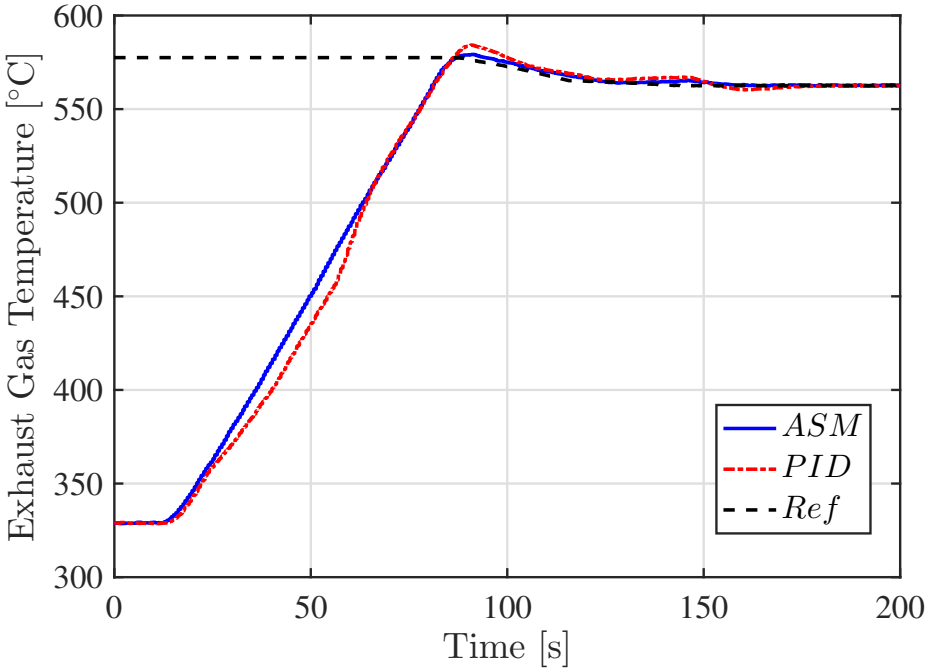

Figure 6.24: Exhaust gas temperature time profile.

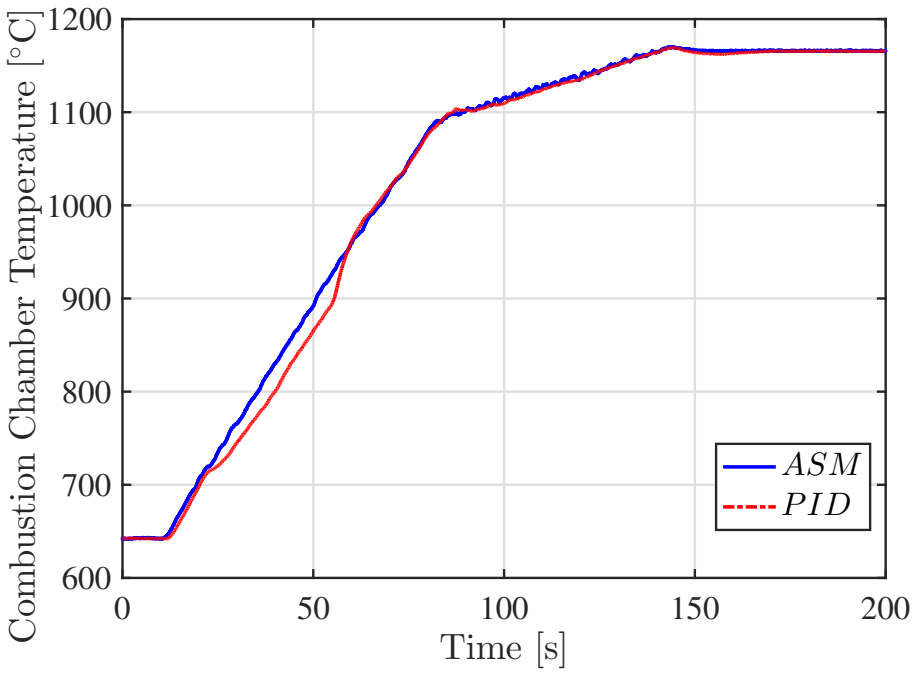

Figure 6.25: Combustion chamber temperature time profile.

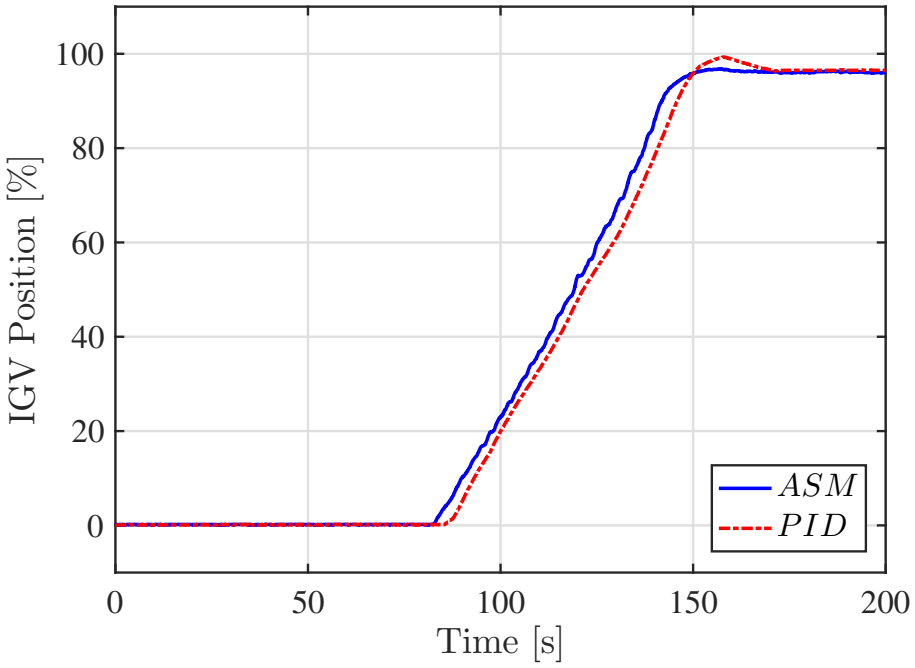

Figure 6.26: IGV position time profile.

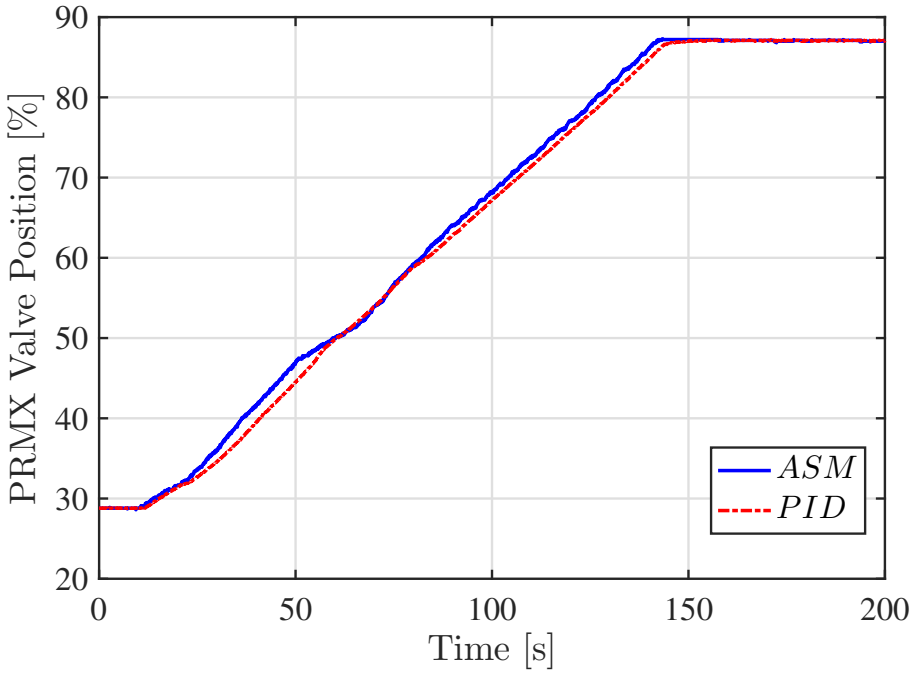

Figure 6.27: PRMX valve position time profile.

Then, Fig.6.26 and Fig.6.27 show the IGV and fuel valve position profiles in the considered test in order to stress the physical reproducibility of these profiles by the actuators.

Finally, for the sake of completeness, the results obtained for the decrease load robustness test are reported in Fig.6.28-6.33. Analogous considerations with the previous test can be made also in this case.

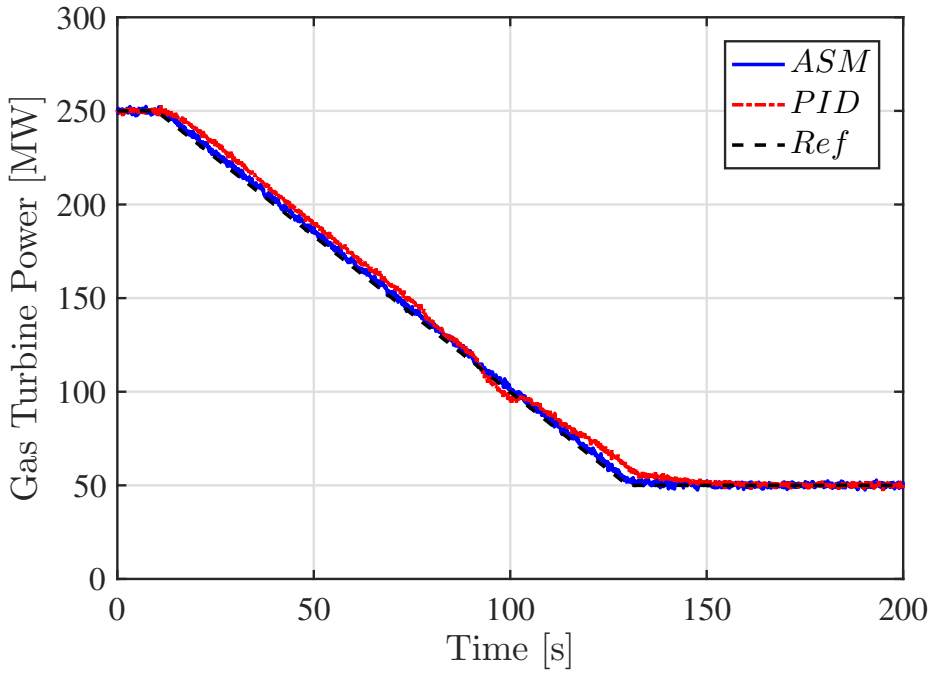

Figure 6.28: Gas turbine power time profile.

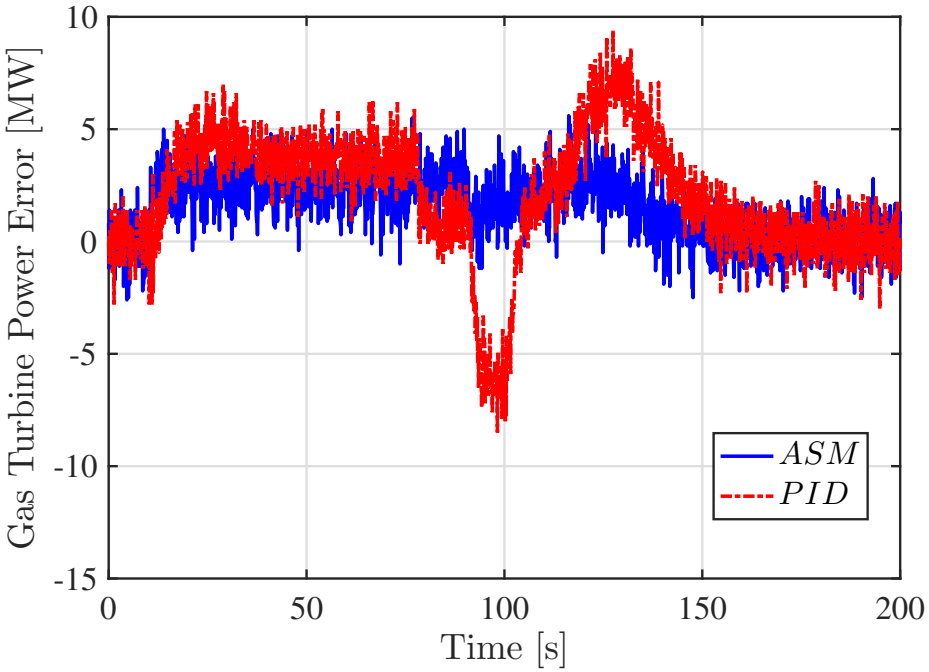

Figure 6.29: Power tracking error time profile.

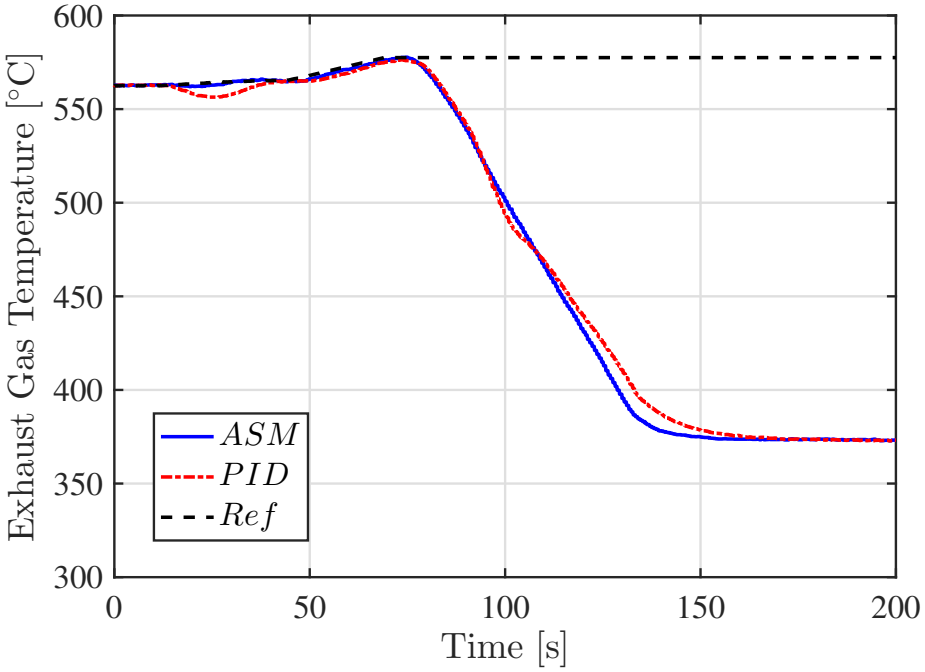

Figure 6.30: Exhaust gas temperature time profile.

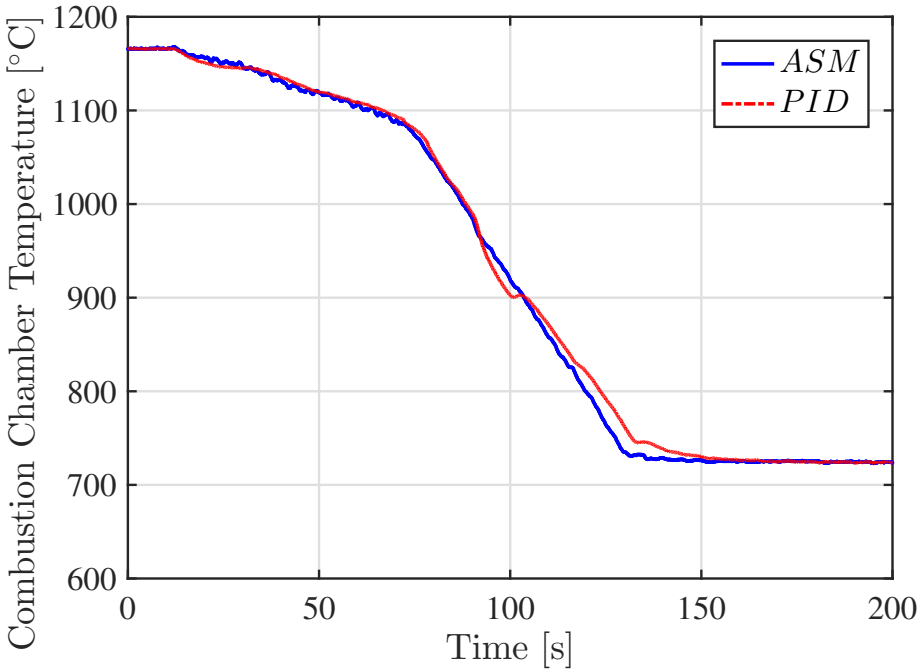

Figure 6.31: Combustion chamber temperature time profile.

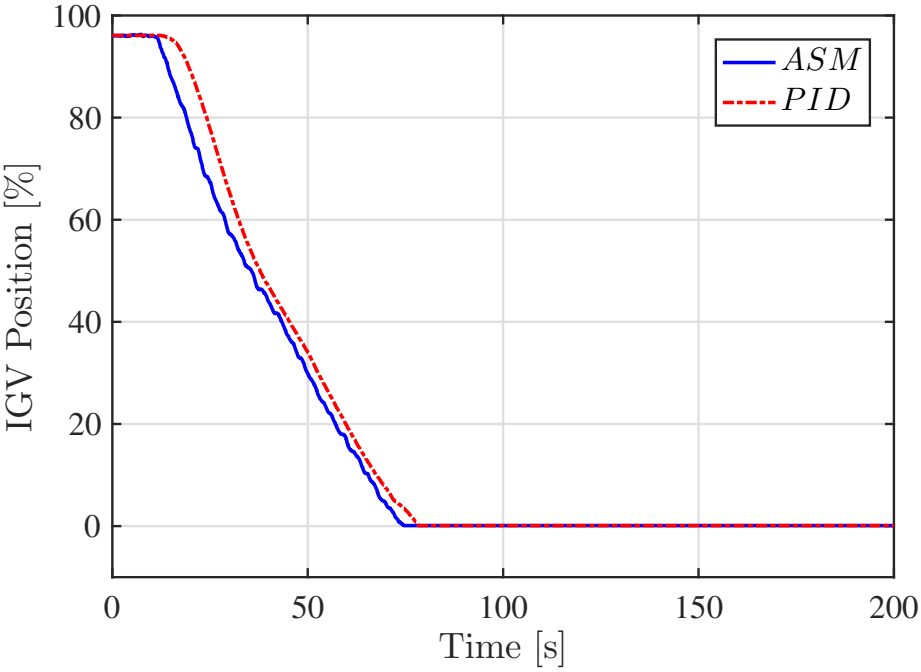

Figure 6.32: IGV position time profile.

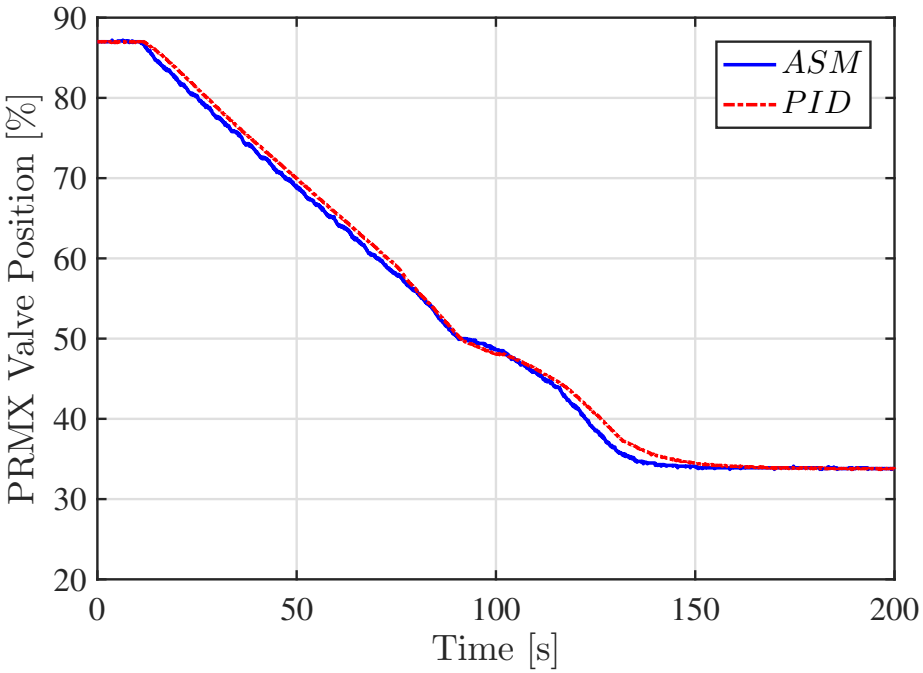

Figure 6.33: PRMX valve position time profile.

7. Conclusions

This thesis deals with the design of an advanced load controller for heavy-duty GTs and its experimental validation. In particular, the proposed work aimed at presenting an innovative sliding mode control system which can be effectively and systematically implemented in the heavy-duty GT industry. The need for developing this solution comes directly from the manufacturing company Ansaldo Energia S.p.A., in response to the increasing request of TSOs related to the ever-growing complex electrical power system, which has been dominated by an aggressive penetration of renewable energy sources.

Indeed, conventional PID based controllers, today employed in industrial solutions for GT control, provide low dynamic performance, since they deal with a strongly nonlinear system characterized by highly coupled dynamics. In such scenario, this PhD thesis describes the final advancements and achievements of a work started during the Master's thesis in 2016 which gave rise to two main publications [18],[20] on this subject. From the beginning of this work, the aim was to develop a reliable, effective and robust model-based controller capable of successfully replacing the PID load controller of current gas turbines manufactured by Ansaldo Energia.

This was a very important achievement since, usually, research activities achieve impacts characterized by low Technology Readiness Levels (TRLs). On the contrary, this thesis, begun with theoretical studies of the Sliding Mode technique, reaches in its final stage results which help filling the gaps from theory to an experimental validation of a final product on a realistic in-field application.

The entire work envisaged different phases:

1. Development of many different versions of controllers, all of them designed first on a theoretical basis.

2. Testing of these versions in a pure simulation environment (MATLAB&Simulink), leading to a progressive refinement and improvement of such controllers.

3. Identification of the best controller solution and its implementation in real ABB processors in the company's laboratories.

4. Interfacing of the new ASM controller on ABB processors with the Ansaldo Energia proprietary GT model thanks to real-time HIL simulators in the company's laboratories.

5. HIL comparison between the new ASM controller and the traditional PID controller, carrying out stress tests, robustness tests and sensitivity tests in the company's laboratories.

The results obtained in the experimental validation show a remarkable improvement in the load controller performance with respect to the traditional PID based approach. More in details the results of this research can be summarized as follows:

- The load increase and decrease analysis highlighted the superior ability of the ASM controller to keep the actual power closer to the desired profile, even under very demanding rates of change, i.e. 100 MW/min (please note that the maximum power reference rate of change usually required by TSOs varies between 20-30 MW/min). Indeed, the power tracking error determined by the ASM can be up to four times lower than to the one of the PID controller.

- The exhaust gas temperature profile becomes smoother thanks to the ASM controller, which, unlike the PID controller, is able to avoid the intervention of the combustion chamber temperature protection loop.

- The combustion chamber temperature keeps a safer profile, even for a rapid load increase, avoiding spikes and therefore dangerous temperature gradients, particularly critical in high temperature operating conditions.

In addition, the ASM controller also proved to be robust in many different off-design operating conditions, in case of structural variations and in presence of significant noise usually affecting the electrical power on field measurements.

8. Future Development

The future development of this research topic will rotate around the in-field validation of the proposed controller.

Even if the real-time simulations performed in the Ansaldo Energia S.P.A. laboratories represent a reliable and important field of testing, only the implementation in a real power plant would definetely prove the effectiveness of the proposed control strategy. Indeed, some aspects of the GT system, such as the combustion dynamics happening in the combustion chamber, cannot be neither simulated nor mathematically modeled and verified.

However, all the impressions derived from the large number of tests developed in the laboratories, make us quite confident about the implementation in the real power plant. Therefore, the next steps to be carried out in the future can be summarized as follows:

- Implementation of the proposed controller in an AE94.3A4 power plant owned by Ansaldo Energia S.P.A.
- Runnning of the ASM controller in parallel with the existing PID control system, in order to check the correct implementations of the command laws.
- Running of the ASM controller alone, making it regulate power and exhaust gas temperature, checking its correct operations and robustness.

Once the performance and effectiveness of the proposed solution are verified on the field, the improvement of the controllers implemented on the other machines will be performed. In particular, following the steps reported below:

- Mathematical modelling of the gas turbine to be considered.
- Calculation of the $\boldsymbol{D}$ matrix.
- Controller tuning by means of real time simulations in the company laboratories.
- Implementations in the real power plant as described previously.

References

[1] H. Ritchie and M. Roser, "Energy production & changing energy sources. 2018," *Tilgjengelig fra: https://ourworldindata. org/energy-production-and-changing-energy-sources,[Sist besøkt, 22.06. 2019]*, 2018.

[2] C. Lins, L. E. Williamson, S. Leitner, and S. Teske, "The first decade: 2004—2014: 10 years of renewable energy progress," *Renewable Energy Policy Network for the 21st Century.*, 2014.

[3] J. L. Sawin, F. Sverrisson, K. Seyboth, R. Adib, H. Murdock, C. Lins, *et al.*, *Renewables 2013: Global status report*. REN21, 2013.

[4] R. Verzijlbergh, L. De Vries, G. Dijkema, and P. Herder, "Institutional challenges caused by the integration of renewable energy sources in the european electricity sector," *Renewable and Sustainable Energy Reviews*, vol. 75, pp. 660–667, 2017.

[5] C. Simoglou, S. Vagropoulos, E. Bakirtzis, E. Kardakos, D. Chatzigiannis, P. Biskas, and A. Bakirtzis, "Large-scale res integration in electricity markets: Challenges and potential solutions," in *2015 50th International Universities Power Engineering Conference (UPEC)*, pp. 1–6, IEEE, 2015.

[6] A. Bonfiglio, M. Invernizzi, A. Labella, and R. Procopio, "Design and implementation of a variable synthetic inertia controller for wind turbine generators," *IEEE Transactions on Power Systems*, vol. 34, no. 1, pp. 754–764, 2018.

[7] D. McLarty, J. Brouwer, and S. Samuelsen, "Hybrid fuel cell gas turbine system design and optimization," *Journal of Fuel Cell Science and Technology*, vol. 10, no. 4, 2013.

[8] J. Lepers, W. Krebs, B. Prade, P. Flohr, G. Pollarolo, and A. Ferrante, "Investigation of thermoacoustic stability limits of an annular gas turbine combustor test-rig with and without helmholtz-resonators," in *ASME Turbo Expo 2005:*

Power for Land, Sea, and Air, pp. 177–189, American Society of Mechanical Engineers Digital Collection, 2005.

[9] T. C. Lieuwen and V. Yang, *Combustion instabilities in gas turbine engines: operational experience, fundamental mechanisms, and modeling*. American Institute of Aeronautics and Astronautics, 2005.

[10] E. Najimi and M. H. Ramezani, "Robust control of speed and temperature in a power plant gas turbine," *ISA transactions*, vol. 51, no. 2, pp. 304–308, 2012.

[11] H. Ghorbani, A. Ghaffari, and M. Rahnama, "Constrained model predictive control implementation for a heavy-duty gas turbine power plant," *WSEAS Transactions on Systems and Control*, vol. 3, no. 6, pp. 507–516, 2008.

[12] F. Jurado, M. Ortega, A. Cano, and J. Carpio, "Neuro-fuzzy controller for gas turbine in biomass-based electric power plant," *Electric Power Systems Research*, vol. 60, no. 3, pp. 123–135, 2002.

[13] W. I. Rowen, "Simplified mathematical representations of heavy-duty gas turbines," 1983.

[14] S. Camporeale, L. Dambrosio and, and B. Fortunato, "One-step-ahead adaptive control for gas turbine power plants," *J. Dyn. Sys., Meas., Control*, vol. 124, no. 2, pp. 341–348, 2002.

[15] V. I. Utkin, *Sliding modes in control and optimization*. Springer Science & Business Media, 2013.

[16] J. Zhu and K. Khayati, "Adaptive sliding mode control–convergence and gain boundedness revisited," *International Journal of Control*, vol. 89, no. 4, pp. 801–814, 2016.

[17] J.-J. E. Slotine, W. Li, *et al.*, *Applied nonlinear control*, vol. 199. Prentice hall Englewood Cliffs, NJ, 1991.

[18] A. Bonfiglio, S. Cacciacarne, M. Invernizzi, D. Lanzarotto, A. Palmieri, and R. Procopio, "A sliding mode control approach for gas turbine power generators," *IEEE Transactions on Energy Conversion*, vol. 34, no. 2, pp. 921–932, 2019.

[19] Ansaldo Energia S.P.A., "AE94.3A: The proven value." `https://www.ansaldoenergia.com/business-lines/new-units/gas-turbines/ae94-3a`.

[20] A. Palmieri, D. Lanzarotto, S. Cacciacarne, I. Torre, and A. Bonfiglio, "An innovative sliding mode load controller for gas turbine power generators: Design and experimental validation via real-time simulation," *Energy*, p. 119363, 2020.

[21] V. Utkin, "Variable structure systems with sliding modes," *IEEE Transactions on Automatic Control*, vol. 22, no. 2, pp. 212–222, 1977.

[22] C. Edwards and S. Spurgeon, *Sliding mode control: theory and applications*. Crc Press, 1998.

[23] A. Ferrara, G. P. Incremona, and M. Cucuzzella, *Advanced and optimization based sliding mode control: Theory and applications*. SIAM, 2019.

[24] I. Boiko, L. Fridman, A. Pisano, and E. Usai, "Analysis of chattering in systems with second-order sliding modes," *IEEE transactions on Automatic control*, vol. 52, no. 11, pp. 2085–2102, 2007.

[25] A. Levant, "Higher-order sliding modes, differentiation and output-feedback control," *International journal of Control*, vol. 76, no. 9-10, pp. 924–941, 2003.

[26] A. Levant, "Quasi-continuous high-order sliding-mode controllers," in *42nd IEEE International Conference on Decision and Control (IEEE Cat. No. 03CH37475)*, vol. 5, pp. 4605–4610, IEEE, 2003.

[27] J. A. Moreno and M. Osorio, "Strict lyapunov functions for the super-twisting algorithm," *IEEE transactions on automatic control*, vol. 57, no. 4, pp. 1035–1040, 2012.

[28] Y. B. Shtessel, J. A. Moreno, F. Plestan, L. M. Fridman, and A. S. Poznyak, "Super-twisting adaptive sliding mode control: A lyapunov design," in *49th IEEE conference on decision and control (CDC)*, pp. 5109–5113, IEEE, 2010.

[29] V. I. Utkin and A. S. Poznyak, "Adaptive sliding mode control with application to super-twist algorithm: Equivalent control method," *Automatica*, vol. 49, no. 1, pp. 39–47, 2013.

[30] V. Utkin and J. Shi, "Integral sliding mode in systems operating under uncertainty conditions," in *Proceedings of 35th IEEE Conference on Decision and Control*, vol. 4, pp. 4591–4596 vol.4, 1996.

[31] Y. Pan, C. Yang, L. Pan, and H. Yu, "Integral sliding mode control: Performance, modification, and improvement," *IEEE Transactions on Industrial Informatics*, vol. 14, no. 7, pp. 3087–3096, 2018.

[32] M. Rubagotti, A. Estrada, F. Castanos, A. Ferrara, and L. Fridman, "Integral sliding mode control for nonlinear systems with matched and unmatched perturbations," *IEEE Transactions on Automatic Control*, vol. 56, no. 11, pp. 2699–2704, 2011.

[33] I.-C. Baik, K.-H. Kim, and M.-J. Youn, "Robust nonlinear speed control of pm synchronous motor using boundary layer integral sliding mode control technique," *IEEE Transactions on Control Systems Technology*, vol. 8, no. 1, pp. 47–54, 2000.

[34] F. Plestan, Y. Shtessel, V. Bregeault, and A. Poznyak, "New methodologies for adaptive sliding mode control," *International journal of control*, vol. 83, no. 9, pp. 1907–1919, 2010.

[35] V. I. Utkin and A. S. Poznyak, "Adaptive sliding mode control," in *Advances in sliding mode control*, pp. 21–53, Springer, 2013.

[36] G. P. Incremona, M. Cucuzzella, and A. Ferrara, "Adaptive suboptimal second-order sliding mode control for microgrids," *International Journal of Control*, vol. 89, no. 9, pp. 1849–1867, 2016.

[37] Y.-J. Huang, T.-C. Kuo, and S.-H. Chang, "Adaptive sliding-mode control for nonlinearsystems with uncertain parameters," *IEEE Transactions on Systems, Man, and Cybernetics, Part B (Cybernetics)*, vol. 38, no. 2, pp. 534–539, 2008.

[38] H. I. Saravanamuttoo, G. F. C. Rogers, and H. Cohen, *Gas turbine theory*. Pearson Education, 2001.

[39] B. Pongrácz, P. Ailer, G. Szederkényi, and K. M. Hangos, "Nonlinear zero dynamics analysis and control of a low power gas turbine," in *5th International PhD Workshop on Systems and Control, Budapest, Hungary*, 2004.

[40] A. Levant, "Robust exact differentiation via sliding mode technique," *automatica*, vol. 34, no. 3, pp. 379–384, 1998.

[41] E. Cruz-Zavala, J. A. Moreno, and L. M. Fridman, "Uniform robust exact differentiator," *IEEE Transactions on Automatic Control*, vol. 56, no. 11, pp. 2727–2733, 2011.

[42] S.-N. Chow and J. K. Hale, *Methods of bifurcation theory*, vol. 251. Springer Science & Business Media, 2012.

[43] Y. A. Kuznetsov, "Elements of applied bifurcation theory," *Applied mathematical sciences*, vol. 112, p. 591, 1998.

[44] W. Govaerts, Y. A. Kuznetsov, and B. Sautois, "MATCONT," *Scholarpedia*, vol. 1, no. 9, p. 1375, 2006. revision #123862.

[45] ABB, "ABB HPC800 controller kit." `https://new.abb.com/products/HPC800K02/hpc800-controller-kit-redundant`.

[46] ABB, "Engineering - ABB Ability Symphony Plus." `https://new.abb.com/power-generation/systems/power-plant-automation/abb-ability-symphony-plus/engineering`.

[47] O. Huber, V. Acary, B. Brogliato, and F. Plestan, "Discrete-time twisting controller without numerical chattering: analysis and experimental results with an implicit method," in *53rd IEEE Conference on Decision and Control*, pp. 4373–4378, 2014.

[48] "Commission Regulation (EU) 2016/631 of 14 April 2016 establishing a network code on requirements for grid connection of generators (Text with EEA relevance).." `http://data.europa.eu/eli/reg/2016/631/oj`.